Volume 63C
Number 1
July–Sept. 1959

QC
1
.456
v.63C
no.1

Journal of Research

of the

NATIONAL BUREAU OF STANDARDS

C. ENGINEERING AND INSTRUMENTATION

UNIVERSITY OF MICHIGAN
GENERAL LIBRARY

Journal of Research
of the
National Bureau of Standards

C. Engineering and Instrumentation

JULY–SEPT. · 1959

VOLUME · 63C

NUMBER · 1

Editor: W. A. Wildhack

Associate Editors: G. F. Montgomery, R. B. Jacobs

Publication dates:
Aug. 15, Nov. 15, 1959

JOURNAL OF RESEARCH

The National Bureau of Standards Journal of Research reports research and development in the fields of activity shown at right. Also included from time to time are survey articles and compilations of information on topics closely related to the Bureau's scientific and technical program.

The Journal is published in four separate sections as follows:

A. Physics and Chemistry

Contains papers of interest primarily to scientists working in these fields. Issued six times a year. Annual subscriptions: domestic, $4.00; foreign, $4.75.

B. Mathematics and Mathematical Physics

Presents studies and compilations designed mainly for the mathematician and the theoretical physicist. Issued quarterly. Annual subscription: domestic, $2.25; foreign, $2.75.

C. Engineering and Instrumentation

Reports research and development results of interest chiefly to the engineer and the applied scientist. Issued quarterly. Annual subscription: domestic, $2.25; foreign, $2.75.

D. Radio Propagation

Reports work in radio propagation physics and upper atmospheric research. Issued six times a year. Annual subscription: domestic, $4.00; foreign, $4.75.

Functions and Activities

The functions of the National Bureau of Standards are set forth in the Act of Congress, March 3, 1901, as amended. These include the development and maintenance of the national standards of measurement and the provision of means and methods for making measurements consistent with these standards; the determination of physical constants and properties of materials; the development of methods and instruments for testing materials, devices, and structures; advisory services to government agencies on scientific and technical problems; invention and development of devices to serve special needs of the Government; and the development of standard practices, codes, and specifications. The work includes basic and applied research, development, engineering, instrumentation, testing, evaluation, calibration services, and various consultation and information services. The Bureau also serves as the Federal technical research center in a number of specialized fields. The scope of activities of the National Bureau of Standards is suggested in the following listing of the divisions and sections engaged in technical work.

Washington, D.C.

Electricity and Electronics. Resistance and Reactance. Electron Devices. Electrical Instruments. Magnetic Measurements. Dielectrics. Engineering Electronics. Electronic Instrumentation. Electrochemistry.

Optics and Metrology. Photometry and Colorimetry. Optical Instruments. Photographic Technology. Length. Engineering Metrology.

Heat. Temperature Physics. Thermodynamics. Cryogenic Physics. Rheology. Engine Fuels. Free Radicals Research.

Atomic and Radiation Physics. Spectroscopy. Radiometry. Mass Spectrometry. Solid State Physics. Electron Physics. Atomic Physics. Neutron Physics. Radiation Theory. Radioactivity. X-rays. High Energy Radiation. Nucleonic Instrumentation. Radiological Equipment.

Chemistry. Organic Coatings. Surface Chemistry. Organic Chemistry. Analytical Chemistry. Inorganic Chemistry. Electrodeposition. Molecular Structure and Properties of Gases. Physical Chemistry. Thermochemistry. Spectrochemistry. Pure Substances.

Mechanics. Sound. Mechanical Instruments. Fluid Mechanics. Engineering Mechanics. Mass and Scale. Capacity, Density, and Fluid Meters. Combustion Controls.

Organic and Fibrous Materials. Rubber. Textiles. Paper. Leather. Testing and Specifications. Polymer Structure. Plastics. Dental Research.

Metallurgy. Thermal Metallurgy. Chemical Metallurgy. Mechanical Metallurgy. Corrosion. Metal Physics.

Mineral Products. Engineering Ceramics. Glass. Refractories. Enameled Metals. Concreting Materials. Constitution and Microstructure.

Building Technology. Structural Engineering. Fire Protection. Air Conditioning, Heating, and Refrigeration. Floor, Roof, and Wall Coverings. Codes and Safety Standards. Heat Transfer.

Applied Mathematics. Numerical Analysis. Computation. Statistical Engineering. Mathematical Physics.

Data Processing Systems. SEAC Engineering Group. Components and Techniques. Digital Circuitry. Digital Systems. Analog Systems. Application Engineering.

• Office of Basic Instrumentation. • Office of Weights and Measures.

Boulder, Colorado

Cryogenic Engineering. Cryogenic Equipment. Cryogenic Processes. Properties of Materials. Gas Liquefaction.

Radio Propagation Physics. Upper Atmosphere Research. Ionospheric Research. Regular Propagation Services. Sun-Earth Relationships. VHF Research. Radio Warning Services. Airglow and Aurora. Radio Astronomy and Arctic Propagation.

Radio Propagation Engineering. Data Reduction Instrumentation. Modulation Systems. Radio Noise. Tropospheric Measurements. Tropospheric Analysis. Radio Systems Application Engineering. Radio-Meteorology. Lower Atmosphere Physics.

Radio Standards. High Frequency Electrical Standards. Radio Broadcast Service. High Frequency Impedance Standards. Electronic Calibration Center. Microwave Physics. Microwave Circuit Standards.

Radio Communication and Systems. Low Frequency and Very Low Frequency Research. High Frequency and Very High Frequency Research. Ultra High Frequency and Super High Frequency Research. Modulation Research. Antenna Research. Navigation Systems. Systems Analysis. Field Operations.

U.S. DEPARTMENT OF COMMERCE
Frederick H. Mueller, Acting Secretary

NATIONAL BUREAU OF STANDARDS
A. V. Astin, Director

Order all publications from the Superintendent of Documents
U.S. Government Printing Office, Washington 25, D.C.

Use of funds for printing this publication approved by the Director of the Bureau of the Budget (June 24, 1958).

U.S. DEPARTMENT OF COMMERCE
NATIONAL BUREAU OF STANDARDS

Frederick H. Mueller, Secretary
A. V. Astin, Director

THE UNIVERSITY OF MICHIGAN
MAY 3 1960
LIBRARY

QC
1
.U56
Vol. 63-C
T.P. + Conf.

JOURNAL OF RESEARCH

of the

NATIONAL BUREAU OF STANDARDS

Section C

ENGINEERING AND INSTRUMENTATION

Volume 63C—July to December 1959

Papers 63C1–1 to 63C2–17

For sale by the Superintendent of Documents, U.S. Government Printing Office
Washington 25, D.C.

Corrections to be noted in Volume 63 of the JOURNAL OF RESEARCH of the National Bureau of Standards—C. Engineering and Instrumentation

Page	Column	Line	Now reads in part	Should read
49	2	13 from bottom	error of the piston	area of the piston
83	2	11 from bottom	MTT–6, 333	MTT–6, 333
88	1	eq. 1	$E \cdot \eta = E =$	$E \cdot \eta = E =$
	2	4	when σ is a	when σ, the surface charge density, is a
100	2	1	chang	change
	2	2	no	not
122	5	6	3	3.5
	6	6	9	30

DEPOSITED BY THE
UNITED STATES OF AMERICA

CONTENTS OF VOLUME 63C

Volume 63C—No. 1—July–September

Page

Creep of cold-drawn nickel. William D. Jenkins and Carl R. Johnson 1
Friction and endurance of prelubricated and unlubricated ball bearings at high speeds and extreme temperatures. Hobart S. White 19
Effect of light and water on the degradation of asphalt. L. R. Kleinschmidt and H. R. Snoke 31
Current and potential relations for the cathodic protection of steel in a high resistivity environment. W. J. Schwerdtfeger 37
A tilting air-lubricated piston gage for pressures below one-half inch of mercury. U. O. Hutton 47
Compact multi-anvil wedge-type high pressure apparatus. E. C. Lloyd, U. O. Hutton, and D. P. Johnson 59
A coulometric-titration coulometer. Stanley W. Smith and John K. Taylor 65
Electron beam magnetometer. L. Marton, Lewis B. Leder, J. W. Coleman, and D. C. Schubert 69
A refined X-band microwave microcalorimeter. Glenn F. Engen 77

Volume 63C—No. 2—October–December

Page

Conical coaxial capacitors and their advantages. M. C. Selby 87
A photoelectric followup and recording system, and its application to remote observations of the beam in high-precision balances. H. A. Bowman and L. B. Macurdy 91
A stroboscopic vibration analyzer. S. Edelman, R. Brooks, S. Saito, E. Jones, and E. R. Smith 97
Evaluation of lens distortion by the inverse nodal slide. Francis E. Washer and Walter R. Darling 105
Evaluation of lens distortion by the modified goniometric method. Francis E. Washer and Walter R. Darling 113
Proposed criteria for defining load failure of beams, floors, and roof constructions during fire tests. J. V. Ryan and A. F. Robertson 121
Conductive flooring for hospital operating rooms. Thomas H. Boone, Francis L. Hermach, Edgar H. MacArthur, and Rita C. McAuliff 125
Measurement of the aging of rubber vulcanizates. J. Mandel, F. L. Roth, M. N. Steel, and R. D. Stiehler 141
Index to volume 63C (July to December 1959, Papers 63C1–1 to 63C2–17) 153

DEPOSITED BY THE
UNITED STATES OF AMERICA

Foreword

More effective dissemination of scientific and technical information is the primary objective in subdividing the Journal of Research of the National Bureau of Standards into four separate sections (effective July 1, 1959). In the past, the Journal has reported results of Bureau research in most fields of the physical sciences and engineering. Subdividing the Journal by subject matter should make it more valuable to the individual scientist or engineer.

With this objective in mind, the editors of the Section on Engineering and Instrumentation plan to present material of interest chiefly to the applied scientist and the engineer. Within the broad field of instrumentation, emphasis will be placed on papers dealing with standards, measurement methods, individual instruments, and instrument systems. It is believed that papers of this type will be of general interest to all readers of this section. Engineering reports will be concerned mainly with the properties of materials and structures and with general engineering devices and techniques. Papers in these areas should find a large, though somewhat more specialized, audience.

In addition to reports on research and development, there may be occasional review articles, tables of useful data, and compilations of information on subjects closely related to the Bureau's program. Thus, Section C is planned to include some of the material which heretofore the Bureau has been publishing in its nonperiodical series of publications. A complete listing, with selected abstracts, of NBS nonperiodical publications and of articles by the Bureau staff in professional journals will also be a regular feature.

It is hoped that this editorial policy will result in a journal sufficiently defined in scope to be valuable to specific groups of readers. However, if a large volume of material develops in both engineering and instrumentation, consideration may be given to dividing Section C into two separate sections, each devoted exclusively to one of these fields.

W. A. Wildhack, *Editor*,
Section C, Engineering and Instrumentation.

Journal of Research of the National Bureau of Standards—C. Engineering and Instrumentation
Vol. 63C, No. 1, July–September 1959

Creep of Cold-Drawn Nickel

William D. Jenkins and Carl R. Johnson

(March 18, 1959)

Creep tests were made in tension under constant loads at temperatures of 300°, 700°, 900°, and 1,200° F on specimens of nickel initially cold-drawn to 40-percent reduction in area. None of the equations for defining the strain-time relationship proposed by other investigators was found to be suitable to express or predict the creep-test results of this investigation with high accuracy because these equations inadequately describe the changes in structure accompanying the creep processes. However, conformance to the parabolic strain-time law was obtained over limited ranges of stresses and strains. The effects of cold-drawing on the creep properties are discussed. Certain etching techniques were employed that gave evidence of the presence and movement of dislocations in the structure.

1. Introduction

During the past few years, a number of theories have been proposed to describe the creep behavior of metal specimens subjected to constant applied stress at constant temperature. The degree of success in the application of the theories to experimental creep data depends on the reality of the models used. Generally, it is accepted that the rate-determining factor during creep is the motion of defects (primarily dislocations) through the crystal lattice by thermal activiation under the action of an applied stress. As more accurate data are accumulated, the role of the instantaneous structure of metals during creep appears to become increasingly important.

An extensive review of the current literature on theories of creep has been presented in a recent symposium [9].[1] Therefore, only selected references, pertinent to the present data, will be made in this paper, with a discussion of the results obtained in this investigation.

A comprehensive investigation designed to evaluate the influence of stress, strain, strain rate, temperature, and structure on the rheological properties of nickel, copper, and nickel-copper alloys has been in progress at the Bureau and the results have been published in several papers [1 to 8]. The present phase of the study was made to evaluate the influence of stress and cold-drawing to 40-percent reduction in area (hereafter referred to as "cold-drawn") on the creep characteristics of nickel at 300°, 700°, 900°, and 1,200° F. The selected temperatures are 0.24, 0.37, 0.44, and 0.53, respectively, of the melting temperature (1,726° K) of nickel. Data derived from previously published values for annealed nickel [5] are included for purposes of comparison with the data for the cold-drawn metal.

2. Material and Procedures

The nickel used in this study was prepared by induction melting, and all bars were processed from one 14- by 14- by 60-in. ingot. This ingot was milled, then forged to 8- by 8-in. blooms, and hot-rolled to 2½-in.-square billets. The material was then hot-rolled to $1\frac{5}{32}$-in.-diam bars and annealed for 16 hr at 1,100° F plus 8 hr at 1,000° F to produce the desired grain size. The nickel was then centerless ground to 1⅛-in. diam and cold-drawn to ⅞-in. diam. Chemical, spectrochemical, and vacuum-fusion analyses made on this ingot of nickel gave the following impurities (percentage by weight): 0.009 Cu, 0.04 Fe, 0.03 Mn, 0.11 Si, 0.007 C, 0.002 S, $<$0.01 Co, 0.001 O_2, 0.001 N_2, and 0.0002 H_2.

All specimens were made from the same bar of nickel that was cold-drawn to 40-percent reduction in area by the manufacturer. This bar was from the same ingot of nickel from which specimens were obtained for evaluating its high-temperature tensile properties [7] and creep properties of the annealed stock [5]. Creep specimens were machined to a 0.505-in. diameter over a 2-in. reduced section. Each creep specimen was heated in air to the desired temperature before loading to the required stress in increments equivalent to a stress of 5,333 lb/in.[2] applied at 1-hr intervals.

The temperatures of the creep furnaces were controlled within ±1° F of the desired values over the specimen length, and the probable error in measuring the extension increments was less than 0.00002 in. Contours of the specimens after testing were determined by measuring the diameters at various distances from the fracture. Rockwell hardness determinations were made along the longitudinal axis of the fractured specimens according to procedures adopted in reference [1].

Recommended procedures were used for preparation of specimens by mechanical means for metallographic examination. However, several special etching techniques, described later in this paper, were also used.

The test data are summarized in table 1 and plotted in figures 1 to 13, inclusive.

[1] Figures in brackets indicate the literature references at the end of this paper.

TABLE 1. *Test conditions and results of creep tests on high-purity nickel, initially cold-drawn to 40-percent reduction in area*

Specimen No.	Test temperature	Creep stress	Plastic strain		Average creep rate, second stage	Beginning of third stage		End of test					Remarks
			1 hour after application of load	Intercept at zero time		Time	Plastic strain	Time	Elongation	Reduction of area	True strain at fracture	True stress at fracture	
	°F	lb/in.²	%	%	%/1,000 hr	hr	%	hr	%	%	$\log_e(A_o/A)$	P/in.²	
A-17	300	72,000	0.15	0.46	0			2,297	[a] 0.46	[b] 0.4			Test stopped in second stage.
A-19	300	75,000	.47	.37	75	2.5	0.61	3.2	18.5	76.4	1.442	317,000	Tested to complete fracture.
A-20	300	75,600		.13	1,270	0.15	.32	0.25	18	78.1	1.518	345,000	Do.
A-10	700	42,670	0	.07	0.42	425	.25	2,091	26.8	82.1	1.722	238,000	Do.
A-4	700	48,000	.11	.17	4.12	80	.5	164.3	23.0	83.4	1.793	288,000	Do.
A-18	700	51,500	.26	.23	21.4	14	.56	27.8	22	87.8	2.064	300,000	Do.
A-8	700	53,330	2.01	.15	670	0.6	.55	1.2	23.5	83.6	1.808	325,000	Do.
A-15	900	24,000	0.01	.19	0.67	1,320	1.08	3,546	42	84.5	1.863	154,000	Do.
A-12	900	26,670	.06	.31	1.66	800	1.62	1,746	30.0	82.2	1.721	149,000	Do.
A-9	900	32,000	.11	.17	6.55	165	1.25	452	30.3	85.0	1.901	213,000	Do.
A-5	900	37,330	.35	.30	61	9	0.85	44.5	33.5	89.5	2.219	343,000	Do.
A-16	900	40,000	.51	.29	200	3.2	.93	7.5	24.5	82.8	1.761	232,000	Do.
A-11	1,200	2,665	.15	1.2	1.24	2,100	3.8	4,853	[a] 8.5	[b] 7.5			Test stopped in third stage.
A-6	1,200	4,010	.40	1.75	7.9	500	5.7	3,825	74.5	78.8	1.554	19,000	Tested to complete fracture.
A-7	1,200	6,670	1.88	4.15	72.6	58.5	8.4	86	97.3	97.6	3.745	281,000	Do.
A-14	1,200	9,330	6.72	7.6	632	21.2	21	28.3	62.5	97.8	3.839	433,000	Do.

[a] These values are for plastic strain as the specimens did not break.
[b] These values are for contraction of area as the specimens did not break.

3. Results and Discussion

3.1. Effect of Stress and Temperature on Strain-Time Relations

Hazlett and Parker [10] indicated that creep curves for high-purity nickel specimens, tested at constant stress within the temperature range 550° to 700° C, contained no region of constant creep rate and could be represented over a temperature range by the equation

$$\epsilon - \epsilon_0 = Bt^b e^{-Q/RT} \qquad (1)$$

where

ϵ = total true strain,
ϵ_0 = instantaneous true strain at loading,
B and b = parameters, varying with grain size and other metallurgical factors,
t = time,
Q = activation energy,
R = gas constant, and
T = absolute temperature in degrees Kelvin.

Conrad and Robertson [11] have recently reviewed the work of the above authors and applied this parabolic time law to other data obtained on close-packed hexagonal metals. They concluded that a recovery mechanism, occurring above 0.4 the melting temperature, was associated with this law. Below this temperature, the negative curvature of some of the log strain-log time plots for magnesium specimens necessitated the use of a negative value of ϵ_0. From a physical standpoint, a negative strain on loading has no significance.

Strain-time data for the specimens of the cold-drawn nickel used in the present investigation were plotted on a linear scale. These curves (not shown) were similar to those previously given [1, 2, 5, 8] and indicated the existence of a first, second, and third stage of creep; however, the stages were more clearly defined in the tests conducted at high temperatures than at low temperatures. Values derived from the data are summarized in table 1. The relation between log plastic strain [2] and log time is shown in figure 1. Although small portions of the curves appear to be linear, the general trend is a positive curvature. Only one curve of this family showed a negative curvature (the specimen tested at 300° F with a stress of 72,000 lb/in.²). A linear relation could not be established in all the curves of figure 1 by any selection of ϵ_0 values.

Andrade [12] pointed out that there were many points of similarity between creep curves obtained under various test conditions and that it would be possible by simple transposition to derive the creep curve of one metal from data obtained on another metal at the same fraction of their melting temperatures. In order to ascertain the degree of similarity between strain-time curves of long and short duration, several methods were used for evaluating the behaviour of the cold-drawn nickel. The data for some of the specimens are plotted using plastic strain as a function of the ratio of time to fracture time (fig. 2) and the ratio of plastic strain to elongation at fracture as a function of the ratio of time to fracture time (fig. 3). It is apparent that no appreciable coincidence was obtained for the curves for specimens of nickel tested at the same temperature at different stresses or at different temperatures and stresses when the data were evaluated in this manner. The curvatures and the relative positions

[2] The values for plastic strain were taken as equal to the total strain minus the elastic strain as derived from the modulus of elasticity and the stress.

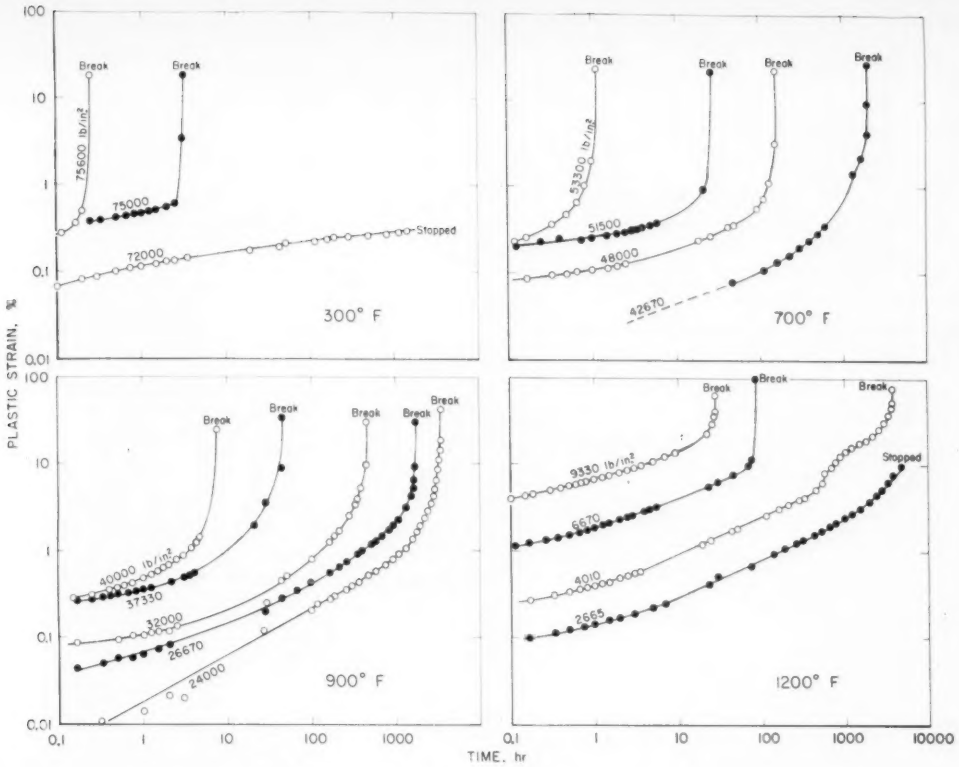

FIGURE 1. *Strain-time curves for the initially cold-drawn nickel specimens tested in creep.*

of the curves, however, can be related to the structural changes occurring during the creep test and to the ductility resulting from the action of the applied stress on the motion of the lattice defects. At 700° F, where the predominating mechanism for creep was assumed to be the intersection of dislocations threading the glide plane [11], the curves merge more nearly than at 1,200° F where both recovery and recrystallization occur.

3.2. Effect of Temperature and Stress on Second-Stage Creep Rate

McVetty [13] concluded that the second-stage creep rate varies linearly with the hyperbolic sine of the stress. Thus for large values of stress, the log creep rate becomes proportional to the stress. A similar relation was proposed by Dushman and collaborators [14]. The equation was of the form

$$\log_e(\dot{\epsilon}/T)=(-A/T)-C+K\sigma, \qquad (2)$$

where
$\dot{\epsilon}$ represents the second-stage creep rate,
T is absolute temperature in degrees Kelvin,
σ is stress,
A and C are constants, and
K is a parameter dependent on temperature.
Therefore, at constant temperature,

$$\log \dot{\epsilon}=C_1+C_2\sigma, \qquad (2a)$$

where C_1 and C_2 are constants. This is the logarithmic rate law often used for the presentation of creep data.

The relation between stress and logarithm of the second-stage creep rate of the cold-drawn nickel specimens used in the present investigation is shown in figure 4. At test temperatures of 700° and 900° F a negative curvature is observed; whereas, at 1,200° F, within the same range of creep rates, a positive curvature exists. A positive curvature of the stress-creep rate curve is interpreted as a confirmation of the generally accepted theory that creep at relatively high temperatures takes place by a diffusion-controlled mechanism.

For engineering applications, it is common practice to describe the applied creep stress in relation to the short-time tensile strength at the designated temperatures. This ratio was plotted against the second-stage creep rate for both the cold-drawn and annealed nickel used in a previous investigation [5] and the results are shown in figure 5. The two families of curves are of the same general shape as those shown in figure 4 for the cold-drawn metal and for the annealed metal. At 700° or 900° F, the curves for the cold-drawn material are significantly above the corresponding curves for the annealed nickel although the two curves for specimens tested at 700° F tend to converge at the higher creep rates. At 1,200° F, however, the strengthening effect of cold-drawing is removed and the curves are quite similar for each of the initial conditions. This is to be expected, as 1,200° F is above the recrystalliza-

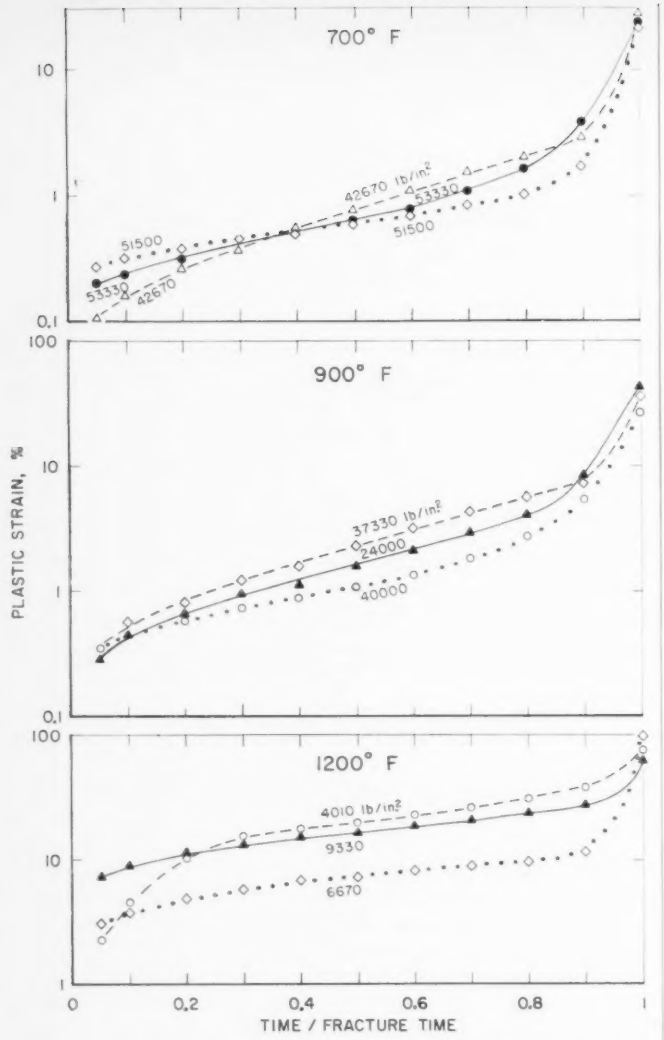

FIGURE 2. *Relation of plastic strain to the time-fracture time ratio for the cold-drawn nickel.*

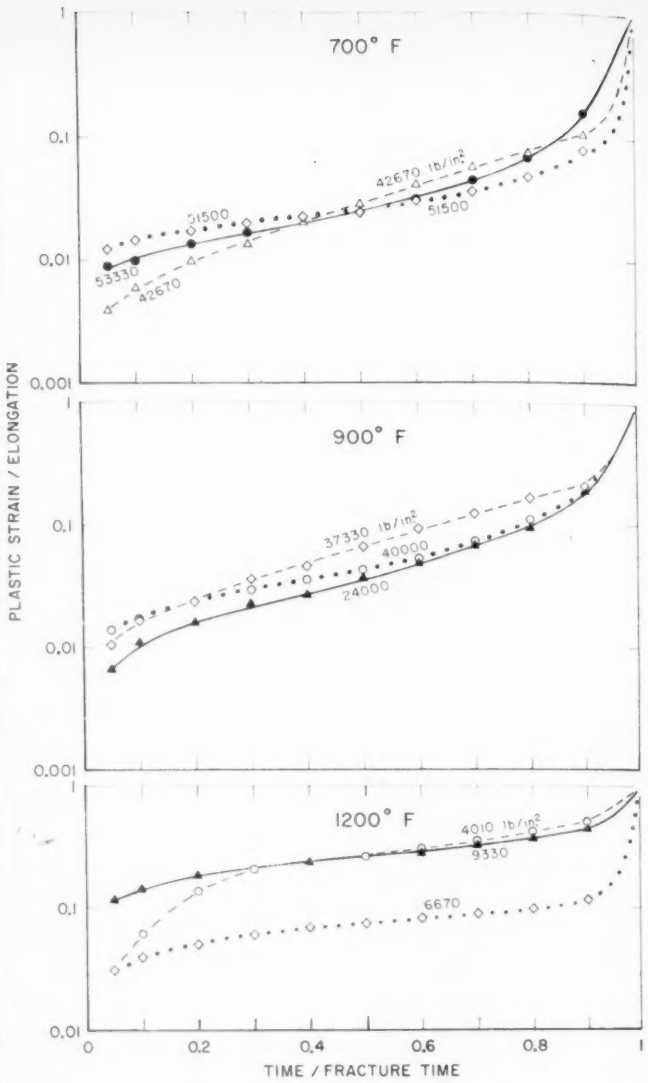

FIGURE 3. *Relation of the plastic strain-elongation ratio to the time-fracture time ratio for the cold-drawn nickel.*

tion temperature of the cold-drawn nickel. Sufficient tests were not made at 300° F on the annealed nickel to definitely establish the trend, but apparently cold-drawing had no material effect on the magnitude of the ratio. It is noteworthy that the curve for the cold-drawn nickel at 900° F and for the annealed nickel at 700° F nearly coincide.

A linear relation is obtained when the logarithm of the stress is plotted against the logarithm of the second-stage creep rate for a number of materials. Using this relation Lubahn [15] proposed the following equation:

$$n=\left[\frac{\partial \log \sigma}{\partial \log \dot{\epsilon}}\right]_T \tag{3}$$

where n="rate sensitivity", σ=stress, and $\dot{\epsilon}$=second-stage creep rate at temperature, T.

The quantity, n, for Lubahn's data appeared to be strongly dependent on the test temperature. Approximately linear relations (curves not shown) were obtained when the logarithm of the creep stress was plotted against the logarithm of the second-stage creep rate for the specimens used in the present investigation. Rate sensitivities were obtained from the slopes of the curves.

The effect of temperature on the rate sensitivity for both the annealed and cold-drawn nickel is shown in figure 6. It is apparent that the rate sensitivity of the nickel decreases with decrease in test temperature and with cold-drawing. The greatest decrease due to cold-drawing appears to exist in the region of 700° F.

The relation between stress and temperature to produce selected constant creep rates of 1, 10, or 100 percent per 1,000 hr at different temperatures for cold-drawn nickel is shown in figure 7. The tendency is for the curves to converge at 300° F to a single value equal almost to the short-time tensile strength at this temperature. Within the limits of the creep data shown, the greatest divergence of the curves is observed at 900° F.

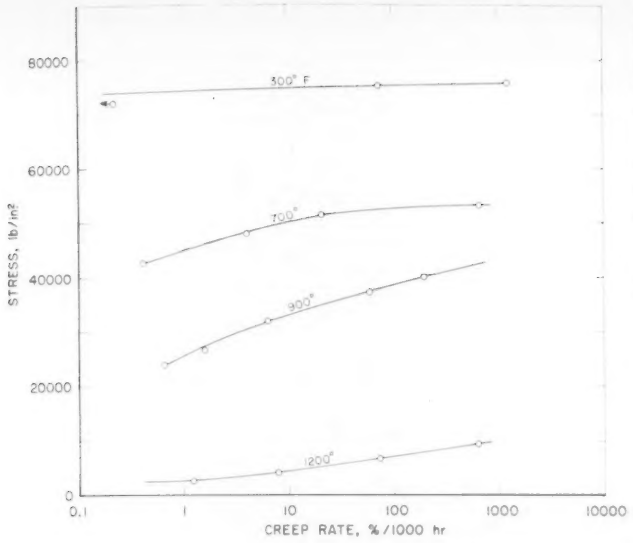

FIGURE 4. *Effect of stress on the average second-stage creep rate of the cold-drawn nickel.*

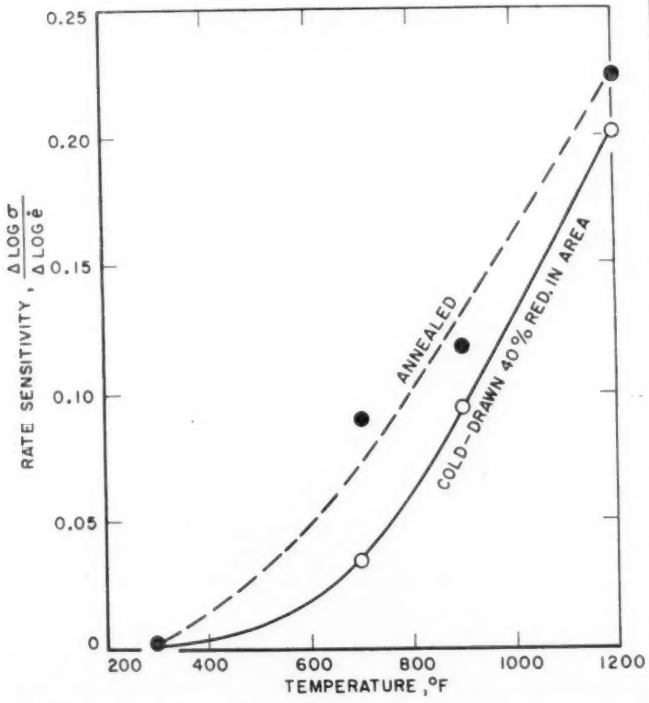

FIGURE 6. *Relation of temperature to the rate sensitivity of annealed and cold-drawn nickel.*

3.3. Effect of Stress, Temperature and Creep Rate on Fracture Time

The relation between stress and fracture time for the cold-drawn nickel is shown in figure 8. The breaks in the curves, such as those occurring for specimens tested at 900° and 1,200° F, are generally interpreted as an indication of an abrupt change in the mode of fracture. Transcrystalline fractures

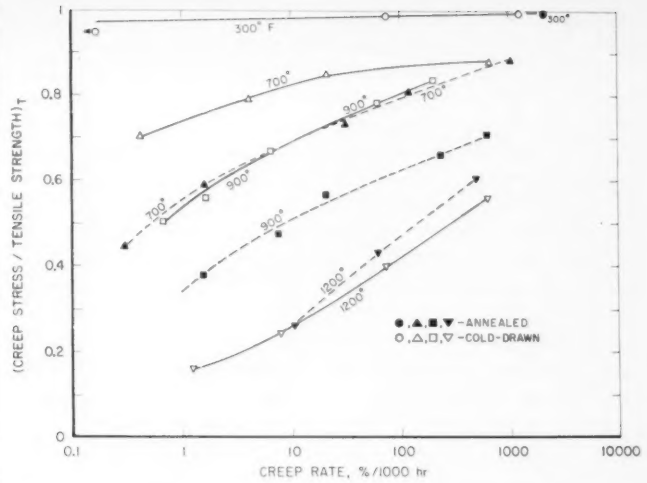

FIGURE 5. *Relation of creep stress-tensile strength ratio (at temperature T) to the average second-stage creep rate of annealed and cold-drawn nickel.*

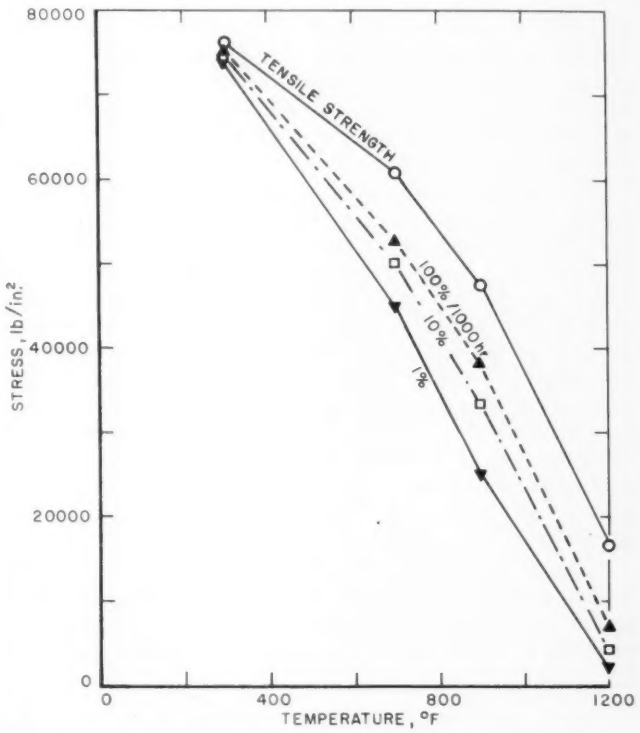

FIGURE 7. *Variation of stress with temperature required to produce second-stage creep rates in the cold-drawn nickel.*

The effect of temperature on the tensile strength is also shown.

were associated with the relatively short fracture times and intercrystalline fractures with longer fracture times.

Monkman and Grant [16] have proposed that the relation between "rupture life" and "minimum creep rate" could be expressed by an equation of the form:

$$\log t_r + m \log \dot{e} = K_1 \qquad (4)$$

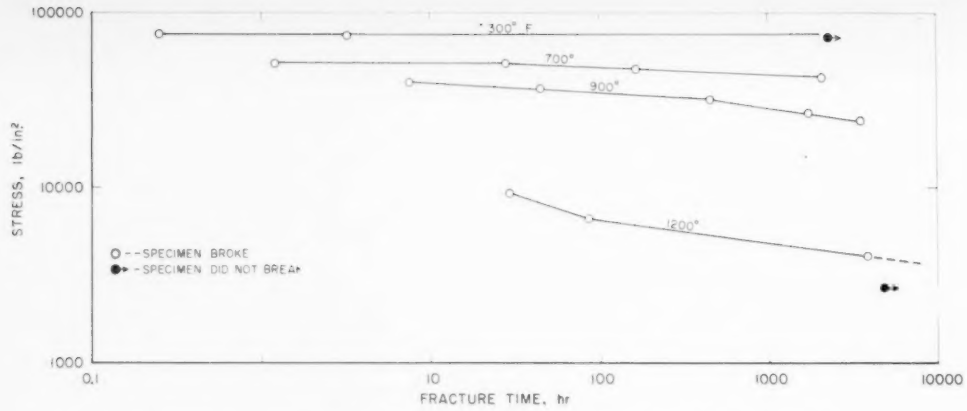

FIGURE 8. *Relation of stress to fracture time for the cold-drawn nickel.*

where t_r=rupture life (fracture time), $\dot{e}$=minimum creep rate (creep rate, second stage), and m and K_1=constants.

Within experimental error the equation was conidered to be independent of testing temperature, stress, chemical composition, hardness or structure; however, the ductility (elongation or reduction of area values) at fracture appeared to affect this relationship.

The effect of temperature on the relation between log fracture time and log second-stage creep rate for both the annealed and the cold-drawn nickel is shown in figure 9. With the exception of the data for the specimens tested at 1,200° F and one specimen tested at 900° F at a fast creep rate, the slopes of the linear portion of these curves appear to be independent of temperature and of cold-drawing. The curvature of the curves for the cold drawn and the annealed specimens tested at 1,200° F are similar in shape and give evidence of the effect of simultaneous creep and recrystallization on this relationship. Due to its greater ductility, the curves for the annealed nickel are above those of the cold-drawn nickel.

Numbers of parameters have been proposed to describe the relation of stress to temperature and either fracture time or creep rate. Two of the first of these were proposed by Larson and Miller [17] and are of the form:

$$(T_R)(a+\log t)=f(\sigma), \tag{5}$$

or

$$(T_R)(a-\log r)=f_1(\sigma), \tag{6}$$

where

$f(\sigma)$ and $f_1(\sigma)$ are functions of the stress,
T_R is absolute temperature in degrees Rankine,
a is a constant (20),
t is rupture time (fracture time) in hours, and
r is creep rate in percent per hour.

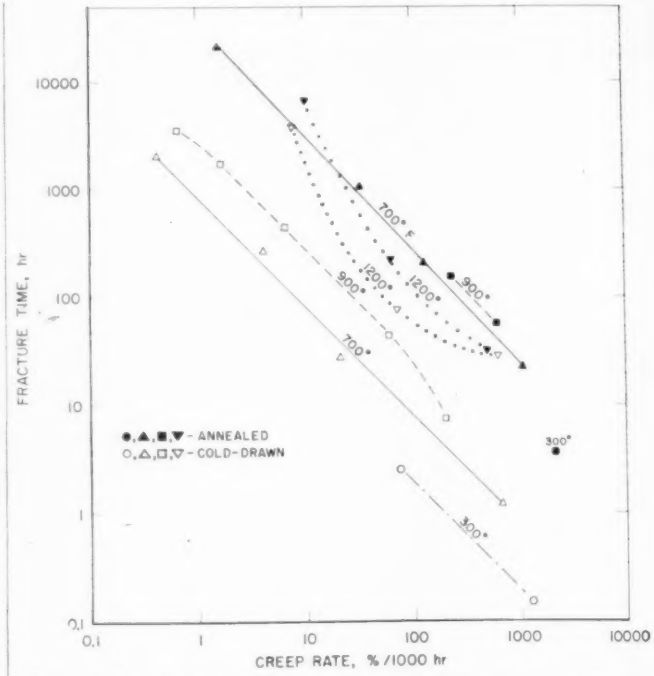

FIGURE 9. *Relation of fracture time to the average second-stage creep rate of annealed [5] and cold-drawn nickel.*

Although the validity of the proposed parameters has been questioned, it appears that this is a useful means of cataloging engineering data and for interpolation. However, usage in extrapolation over wide ranges of stresses and temperatures may involve large errors.

The effects of cold-drawing on these stress-parameter relations are shown in figure 10. The curves for the cold-drawn nickel are above those of the annealed nickel at the low temperatures (low parameter values). However, an approximate coincidence of the two curves is observed for specimens tested at 1,200° F. This occurred for values of 35×10^3 or greater for the parameter involving fracture time (fig. 10A) and 27×10^3 for the parameter involving creep rate (fig. 10B).

3.4. Effect of Temperature and Creep Rate on Ductility and Fracturing Characteristics

The relation between second-stage creep rate and elongation and reduction of area values of annealed and cold-drawn specimens of the nickel tested to fracture at 700°, 900°, and 1,200° F is shown in figure 11. Insufficient data were available to evaluate this relation at 300° F. Cold-drawing reduced the elongation markedly and the reduction of area slightly at 700° and 900° F, whereas at 1,200° F no consistent relation was observed. Moreover, the elongation and reduction of area values appear, with few exceptions, to be less dependent on the creep rate than on the temperature.

The relation between true stress and true strain at fracture for cold-drawn specimens tested at different temperatures is shown in figure 12. These values were calculated on the basis of the minimum diameter of the specimens at room temperature and after fracture. Although some scatter is apparent, the general trend, with one major exception, is for the true strain at constant temperature to increase only slightly with an increase in true stress. However, at a constant stress, increase in strain with temperature is apparent. These results are in agreement with those found previously for the annealed nickel [5].

Some of the processes occurring during the third stage of creep preceding fracture of the initially-annealed nickel were previously discussed [8]. It was also pointed out that the necking characteristics and hardness of the specimens were influenced by the test temperature, creep rate, and rate of loading. The effects of temperature and creep rate in the second stage on the specimen contours and on the room-temperature post-test hardness values for some of the cold-drawn nickel specimens are shown in figure 13. Specimens 8, 10, and 16 exhibited the greatest tendency toward the formation of an acute neck whereas the least tendency toward this phenomenon was shown by specimen 6 (fig. 13A). The former specimens were tested at 700° or 900° F, whereas the latter specimen was fractured at 1,200° F with a slow creep rate. It may also be observed that the tendency toward localized

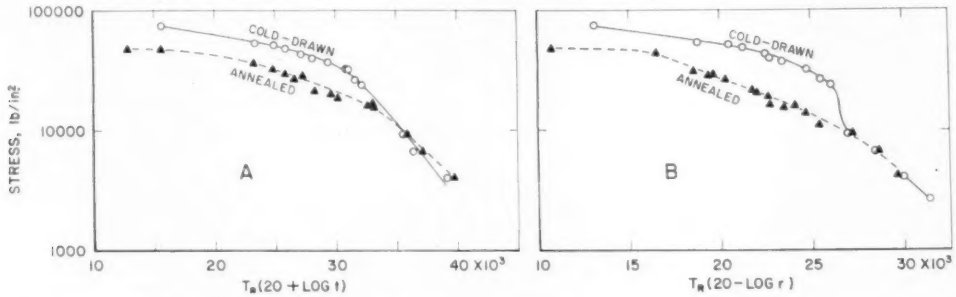

FIGURE 10. *Relation of creep stress to fracture-time or creep-rate parameters for the annealed [5] and cold-drawn nickel.*

t=fracture time (hr), T_R=temperature (°R), and r=second-stage creep rate (%/hr)

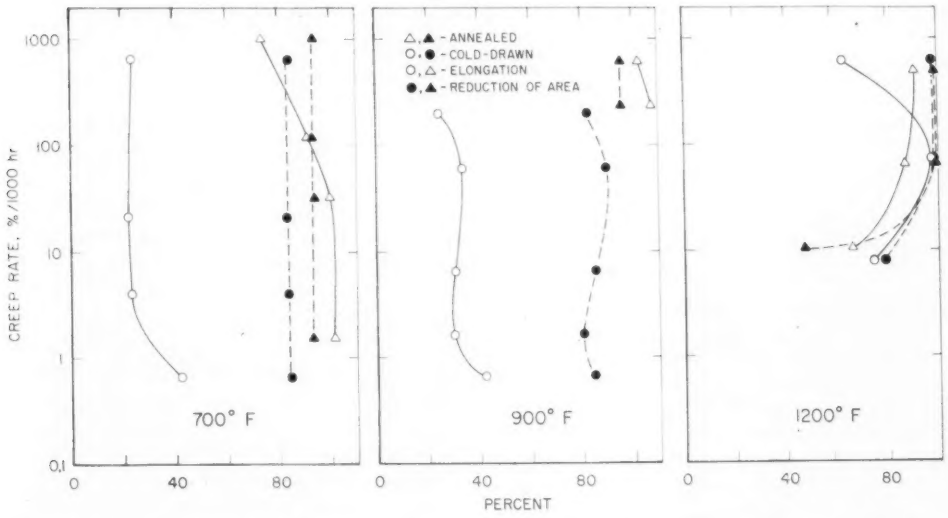

FIGURE 11. *Relations of second-stage creep rate and elongation and reduction of area for the annealed [5] and cold-drawn nickel.*

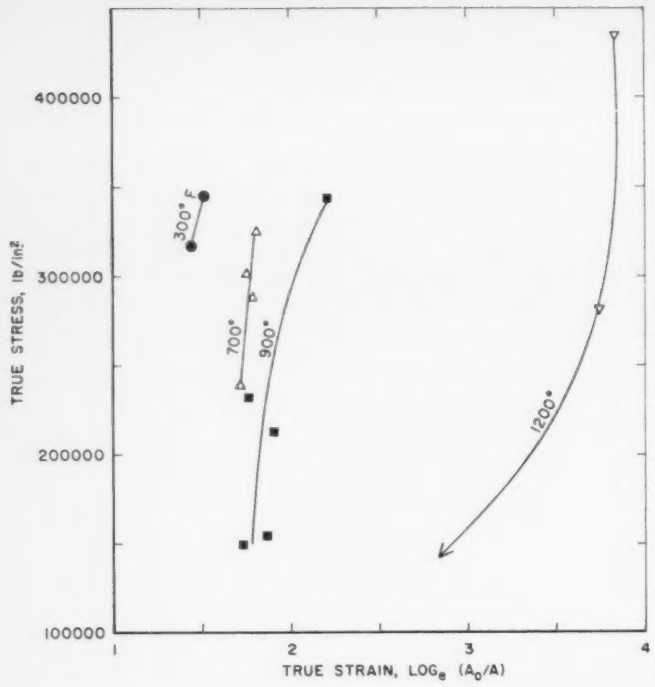

FIGURE 12. *Relation of true stress to true strain of the cold-drawn nickel.*

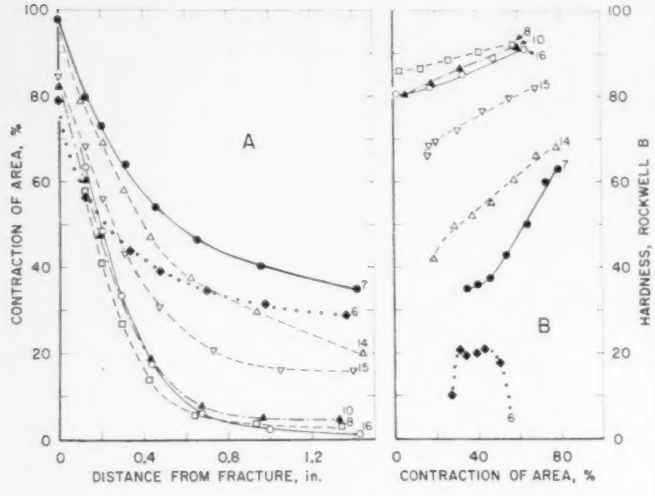

FIGURE 13. *Contour and hardness distribution of fractured specimens of cold-drawn nickel.*

Specimen number	Temperature	Creep rate second stage
	° F	%/1,000 hr
10	700	0.42
8	700	670.
15	900	0.67
16	900	200.
6	1,200	7.9
7	1,200	72.6
14	1,200	632.

necking decreased with increase in temperature or with decrease in creep rate (at constant temperature). The influence of creep rate on necking characteristics of the specimens is less pronounced at the low test temperature.

All the specimens, except number 6, exhibited a tendency toward an increase in hardness with increase in contraction of area values (fig. 13B). As will be shown later, specimen 6 also showed a marked tendency toward recrystallization and grain growth accompanying deformation. Furthermore, for any constant value of contraction of area, the hardness decreased with increase in test temperature and with decrease in creep rate. The difference in hardness values of the specimens tested at the lower temperatures was less than the corresponding differences at the higher temperatures.

3.5. Effect of Creep Conditions on Structures

Limited surface cracking and extensive elongation of the grains in the direction of straining were evident for all the cold-drawn specimens tested at 300°, 700°, or 900° F. This was also observed for the annealed nickel [5]. High ductility accompanied by extensive surface cracking was observed for the cold-drawn specimens tested to fracture at 1,200° F, as shown in figure 14. The extent of the cracking decreased as the creep rate was increased. The structure near the axis adjacent to the fracture of these three specimens is shown in figure 15. Extensive grain elongation is evident in the specimen tested at the fastest rate (fig. 15A) whereas small equiaxed recrystallized grains were predominant in the specimen tested at a slower rate (fig. 15B). Complete recrystallization, accompanied by grain growth and intercrystalline cracking, is evident in the specimen tested to fracture at a much slower rate (fig. 15C).

These three specimens were selected for a detailed metallographic examination. In addition, another creep specimen tested into the third stage of creep at 1,200° F for 4,853 hr without complete fracture (table 1) was examined. Several other unstressed specimens were annealed at different temperatures to ascertain the influence of temperature only on the structures.

By varying the etchants and the etching or photographic techniques, several characteristic features of the nickel were observed. These features and the etching procedures were as follows:

(1) Grain size and intercrystalline cracks were revealed by moderately-deep etching (about 1 min) in six parts concentrated nitric acid and four parts glacial acetic acid.

(2) Etch pits and subgrain boundaries were revealed by deep etching for about 6 min in the above solution.

(3) "Etch figures" of tertiary and quaternary symmetry were revealed by etching first in the above solution for 3 min; second, in a solution of six parts concentrated nitric acid and four parts amyl acetate for 2 min; and third, in a solution of five parts con-

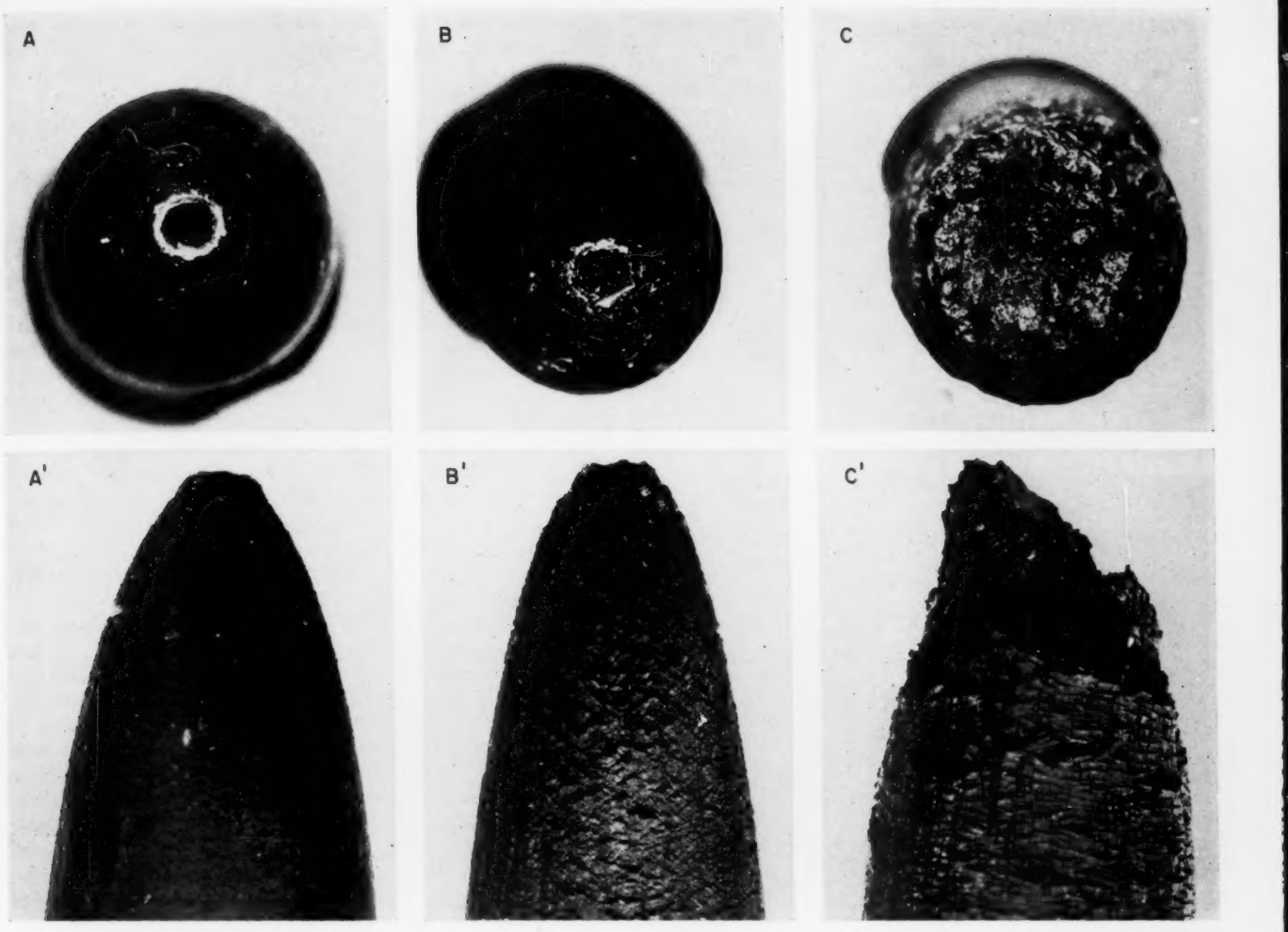

FIGURE 14. *Appearance of specimens of cold-drawn nickel fractured at 1,200° F at different rates.* (× 5)

	Creep rate, second stage	Elongation in 2 in.	Reduction of area
	%/1,000 hr	%	%
A, A'	632.	62.5	97.8
B, B'	72.6	97.3	97.6
C, C'	7.9	74.5	78.8

centrated nitric acid and five parts glacial acetic acid for 5 min. This procedure is hereafter termed "triple etch."

Triangular and square etch figures, produced by etching the nickel after testing in creep at 1,200° F under different stresses, are shown in figure 16. Lacombe and Beaujard [18] have shown that the equilateral triangular figures in aluminum were associated with the surface parallel to the (111) plane and the square figures were associated with the surface parallel to the (100) plane. More recently Wernick et al. [19] indicated that triangular etch pits could be produced and randomly dispersed on the (111) plane and that the pits were formed at dislocation sites. There was a predominance of triangular etch figures produced in the specimens examined in the present investigation. The largest size of the triangular figures (etching times and procedures constant) increased with increase in test time or decrease in creep rate. This is in accordance with known relations between slip-band spacing and creep rate and is probably associated with the ability of the atmospheres to move with the dislocations.

In order to ascertain the effect of temperature, in the absence of an applied stress, on the size of the etch figures, specimens were annealed at several

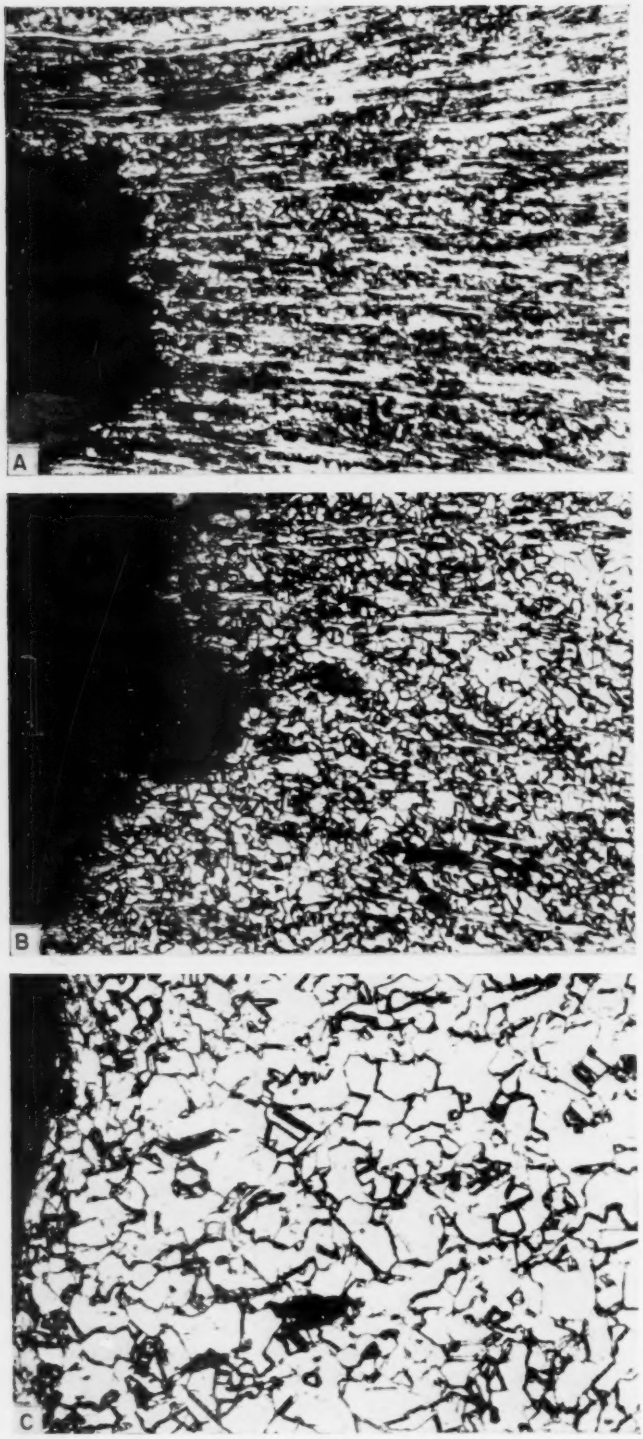

FIGURE 15. *Structure of the cold-drawn nickel after fracturing in creep at 1,200° F.*

Longitudinal sections at fracture surface near axis; etched in 6 parts of HNO_3 (conc.) and 4 parts of glacial acetic acid. (× 100)

	Creep rate	Elongation in 2 in.	Reduction of area
	%/1,000 hr	*%*	*%*
A	632	62.5	97.8
B	72.6	97.3	97.6
C	7.9	74.5	78.8

temperatures for one hour, polished and etched. Microstructures of these specimens are shown in figure 17 A, B and C. An etch figure produced on the surface of a single crystal of nickel [3] is shown, for comparison, in figure 17D. The size of the largest etch figures increased with increase in annealing temperature or grain size and decreased with increasing hardness.

It was observed in high-purity copper [1] that, at low stresses or high temperatures, cracking was often initiated at the surface and progressed toward the axis during the third stage of creep. Intercrystalline cracking near the surface of two specimens of high-purity nickel, tested at 1,200° F, is shown in figure 18. One of the specimens (fig. 18A) was tested in creep into the third stage; the other specimen (fig. 18B) was tested to complete fracture. Although the time at temperature for the former specimen was longer (4,853 hr) than the latter (3,825 hr), the cracking in the latter specimen had progressed much farther into the interior of the specimen. This observation indicates that the extent of intercrystalline cracking is a function of the total strain as well as of the strain rate.

One consequence of high-temperature creep appears to be that high-angle (high-energy) grain boundaries are less evident at the high temperature as shown for some of the adjacent grains with the triangular etch figures in figure 19. Boundaries of this type are considered to be less effective barriers to the motion of dislocations, and thus contribute more to the weakness of the metal, than the high-angle boundaries observed after creep at the lower temperatures. The neighboring grains, separated by low-angle grain boundaries, are less susceptible to intercrystalline cracking (fig. 20 A and B) than those separated by the high-angle grain boundaries (fig. 20 C and D). The grain boundary (fig. 20D) may have acted as a barrier to the continued motion of the dislocations, or the crack may have acted as a source for the concentration of etch figures near the intercrystalline crack. This phenomenon is practically nonexistent in the structures shown in figures 19 and 20 A and B.

Subgrains within the parent grains of high-purity nickel have been observed for a number of years [20, 21]. The nature and the distribution of etch pits within the subgrains and at the subgrain boundaries, as a consequence of high temperature annealing, was recently discussed by Feltham [22]. Parker and Hazlett [23] suggested that the dislocation types of substructure boundaries sometimes have a more marked effect on strengthening than does solution-hardening. The distribution of subgrains and etch pits in a specimen of cold-drawn nickel, tested into the third stage of creep (4,853 hr) at 1,200° F, is shown in figure 21. A general estimation of etch pit density was impossible as the number appeared to very from grain to grain and even within different areas of the same grain. Part of a grain that is densely populated with etch pits and contains small subgrains having dislocation boundaries

[3] The crystal was produced for another project in this laboratory and possessed approximately the same composition as the material used in this investigation

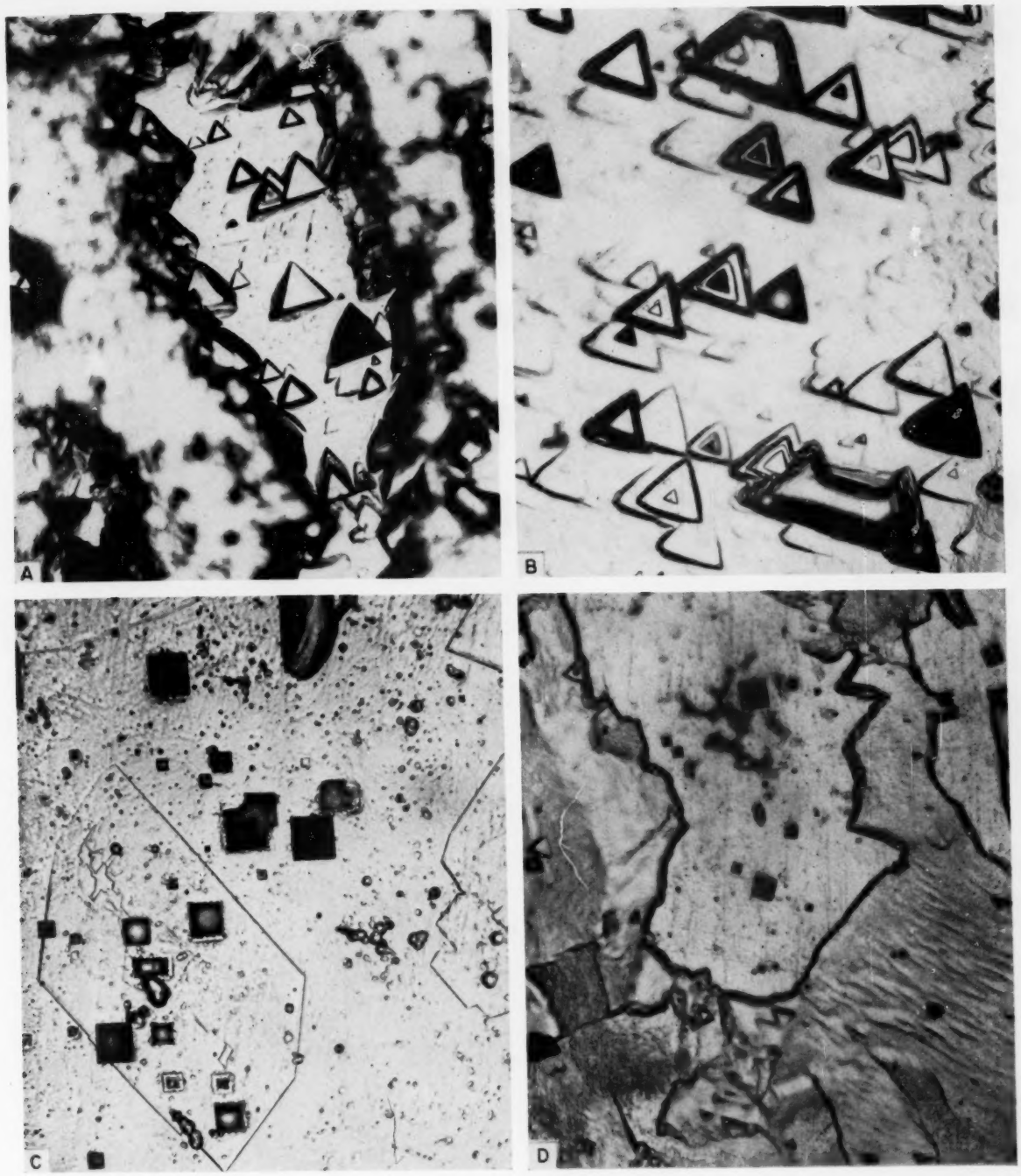

FIGURE 16. *Etch figures in the cold-drawn nickel after creep-testing in tension at 1,200° F for various times at different stresses.*

Cross section, "triple etch". (× 500).

	Stress	Creep rate, second stage	Time
	lb/in.²	*%/1,000 hr*	*hr*
A	9,330	632	28.3
B	2,665	1.24	4,853
C	2,665	1.24	4,853
D	6,670	72.6	86

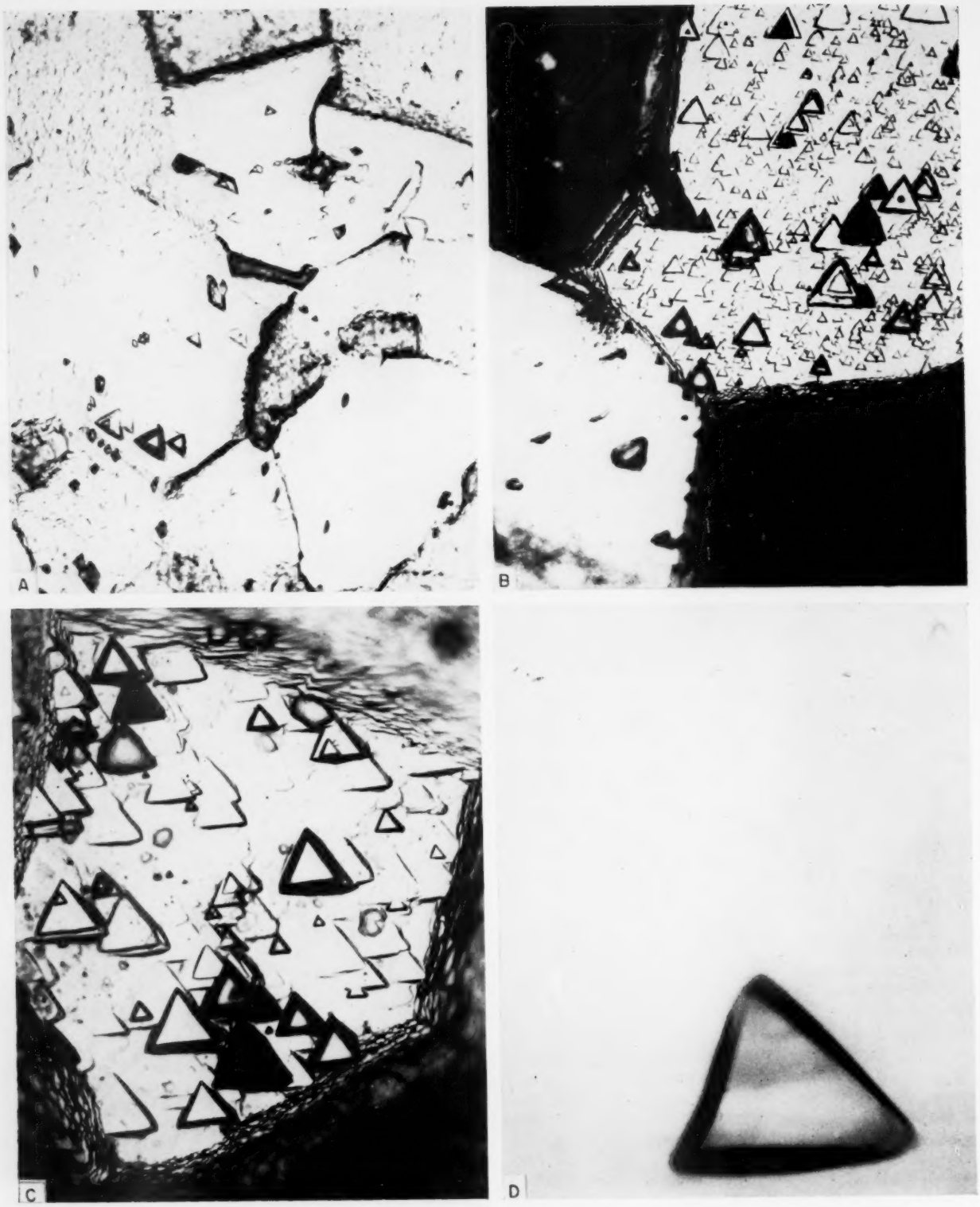

FIGURE 17. *Effect of annealing temperature or grain size on the size of etch figures in nickel.*

Longitudinal sections, "triple etch". (× 500).
A, 1,100° F; B, 1,500° F; C, 1,800° F; D, single crystal, produced from a different lot of high-purity nickel.

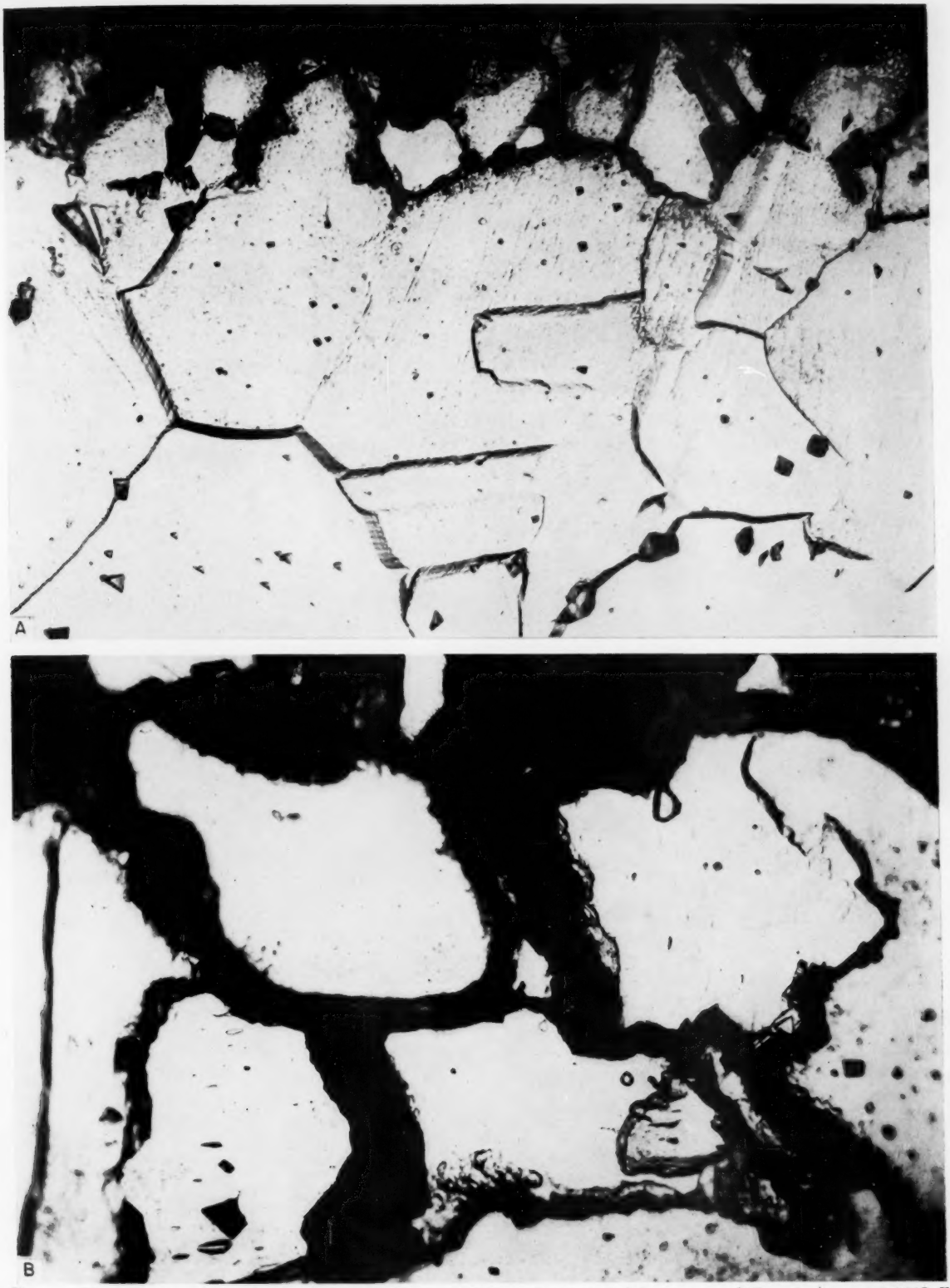

FIGURE 18. *Structure, near surface, of cold-drawn nickel specimens tested in creep at different rates at 1,200° F.*
Longitudinal sections, etched in 6 parts HNO_3 (conc.) and 4 parts glacial acetic acid. (× 500).

	Stress	Creep rate, second stage	Time	Remarks
	lb/in.²	*%/1,000 hr*	*hr*	
A	2,665	1.24	4,853	Stopped in 3rd stage.
B	4,010	7.9	3,825	Complete fracture.

UNIVERSITY OF MICHIGAN LIBRARIES

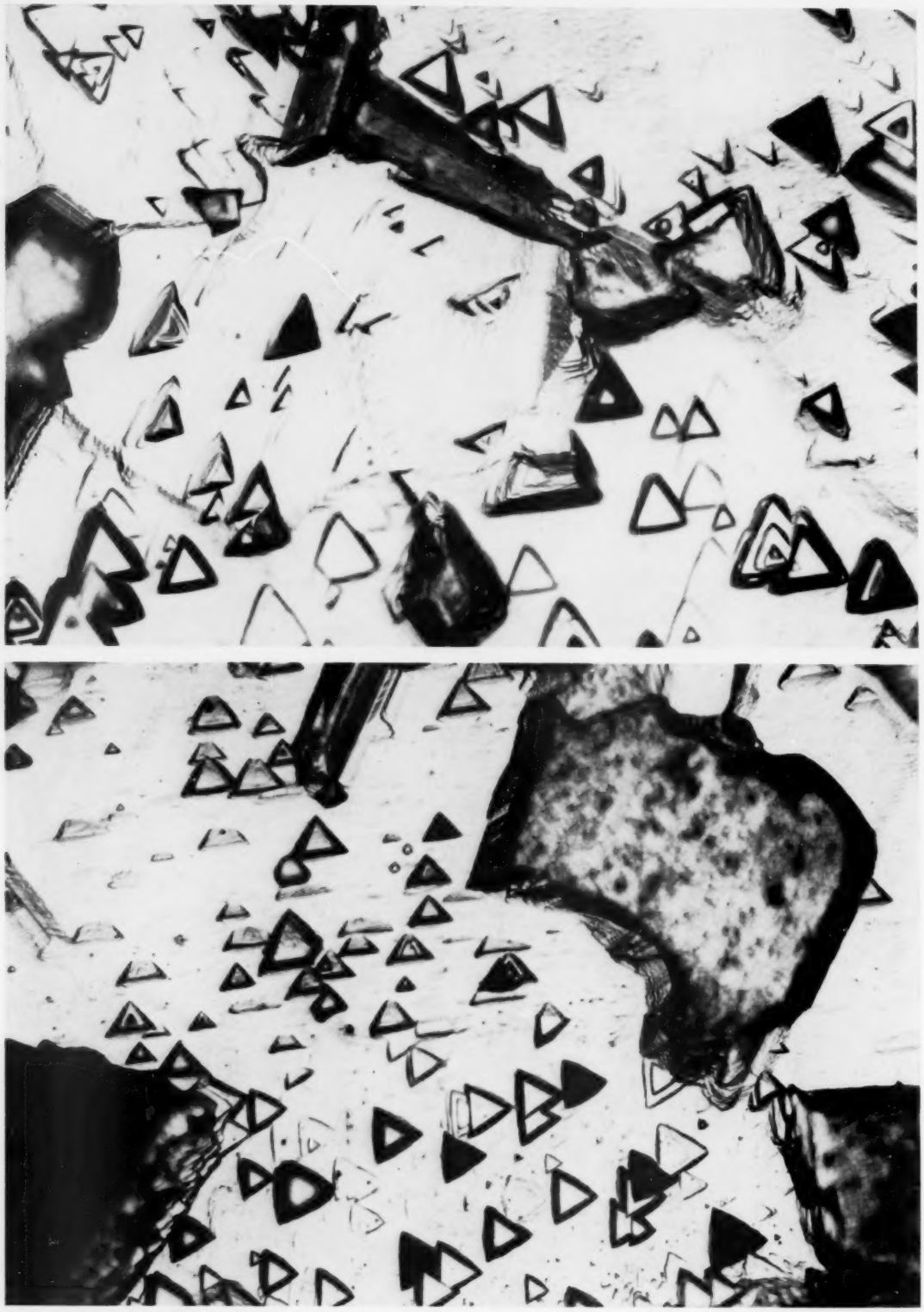

FIGURE 19. *Etch figures in cold-drawn nickel after testing in creep for different times and rates at 1,200° F.*

Longitudinal sections of the same specimen shown in figure 18, "triple etch". (× 500).

	Stress	Creep rate, second stage	Time	Remarks
	lb/in.²	*%/1,000 hr*	*hr*	
A	2,665	1.24	4,853	Stopped in 3rd stage.
B	4,010	7.9	3,825	Complete fracture.

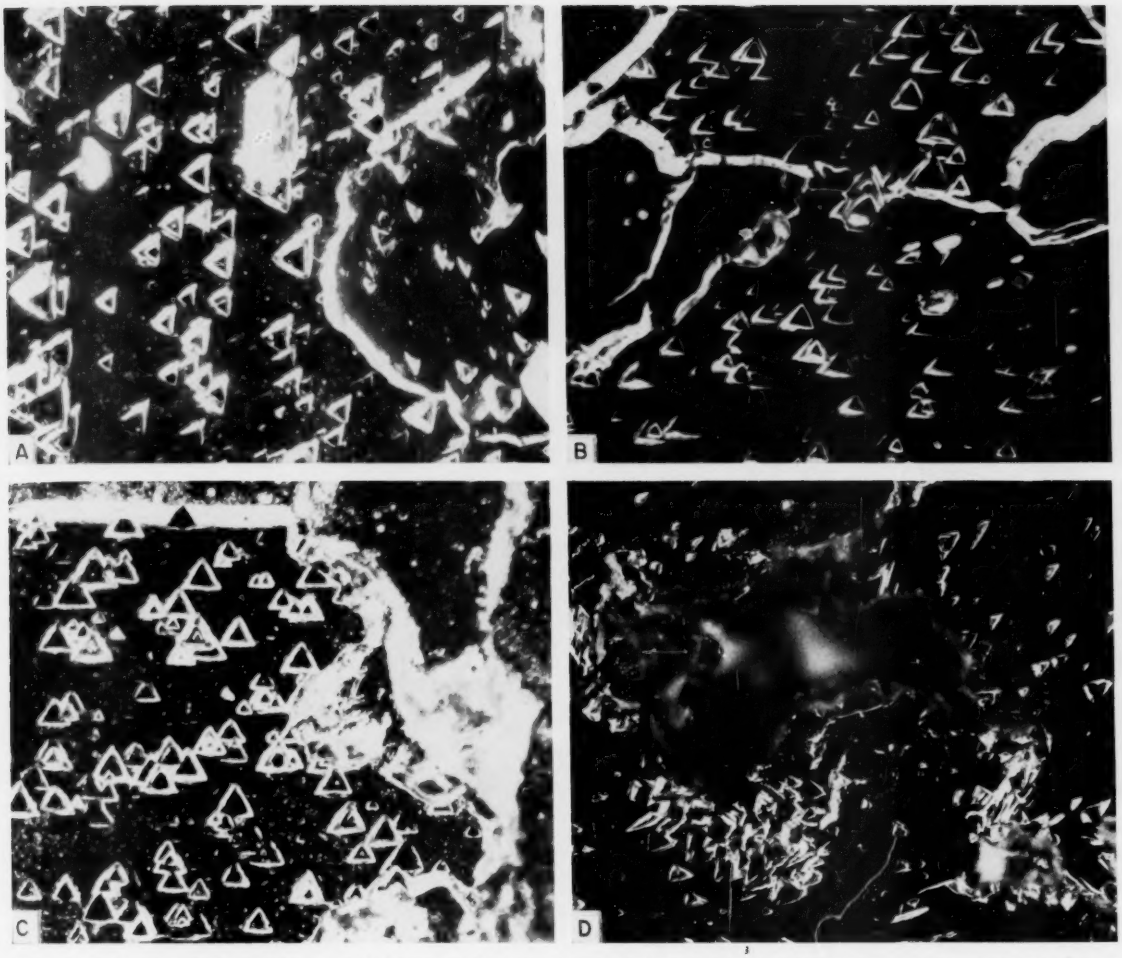

FIGURE 20. *Etch figures in a cold-drawn nickel specimen tested to complete fracture in creep in 3,825 hr at 1,200° F under stress of 4010 lb/in.².*

Cross section of same specimen as B in figures 18 and 19. 0.25 in. from fracture. A and B illustrate low-angle boundaries; C and D illustrate high-angle boundaries; "Triple etch", dark-field illumination. (× 250).

is shown in figure 21A. Two grains separated by a relatively low-energy grain boundary are shown in figure 21B. Small subgrains are evident in each parent grain and the etch-pit density is greater near the grain boundary for the grain on the left than for the grain on the right. Larger subgrains and fewer etch pits are evident in the grain shown in figure 21C. Portions of two grains separated by a high-energy boundary are shown in figure 21D. No subgrains were observed in one grain while the other grain appeared to be densely populated with them. The size of these subgrains appears to increase with increasing distance from the grain boundary.

Several attempts to reveal subgrains in the nickel by annealing in the absence of stress proved unsuccessful, as illustrated by the structures reproduced in figure 22. Rather, recrystallization of the cold-drawn nickel into large grains accompanied by profuse twinning occurred. Etch pits were more easily delineated at or near the grain or twin boundaries than in the interior of the grains. The density of the pits appear to be related both to the orientation of the adjacent grains and to the differences in energy along a specific boundary. Apparently, cold-drawing followed by annealing was less effective for promoting the formation of subgrains and more effective for promoting the formation of annealing twins than creep deformation of nickel at high temperatures.

4. Summary

Creep tests were made in tension under constant loads at temperatures of 300°, 700°, 900°, and 1,200° F on specimens of nickel initially cold-drawn to 40-percent reduction in area.

None of the equations proposed for defining the strain-time relationship conformed to the data for specimens tested under various conditions although conformance to the parabolic strain-time law was obtained over limited ranges of stresses and strains. This lack of conformance was attributed to the structural changes that occurred at the different temperatures and stresses.

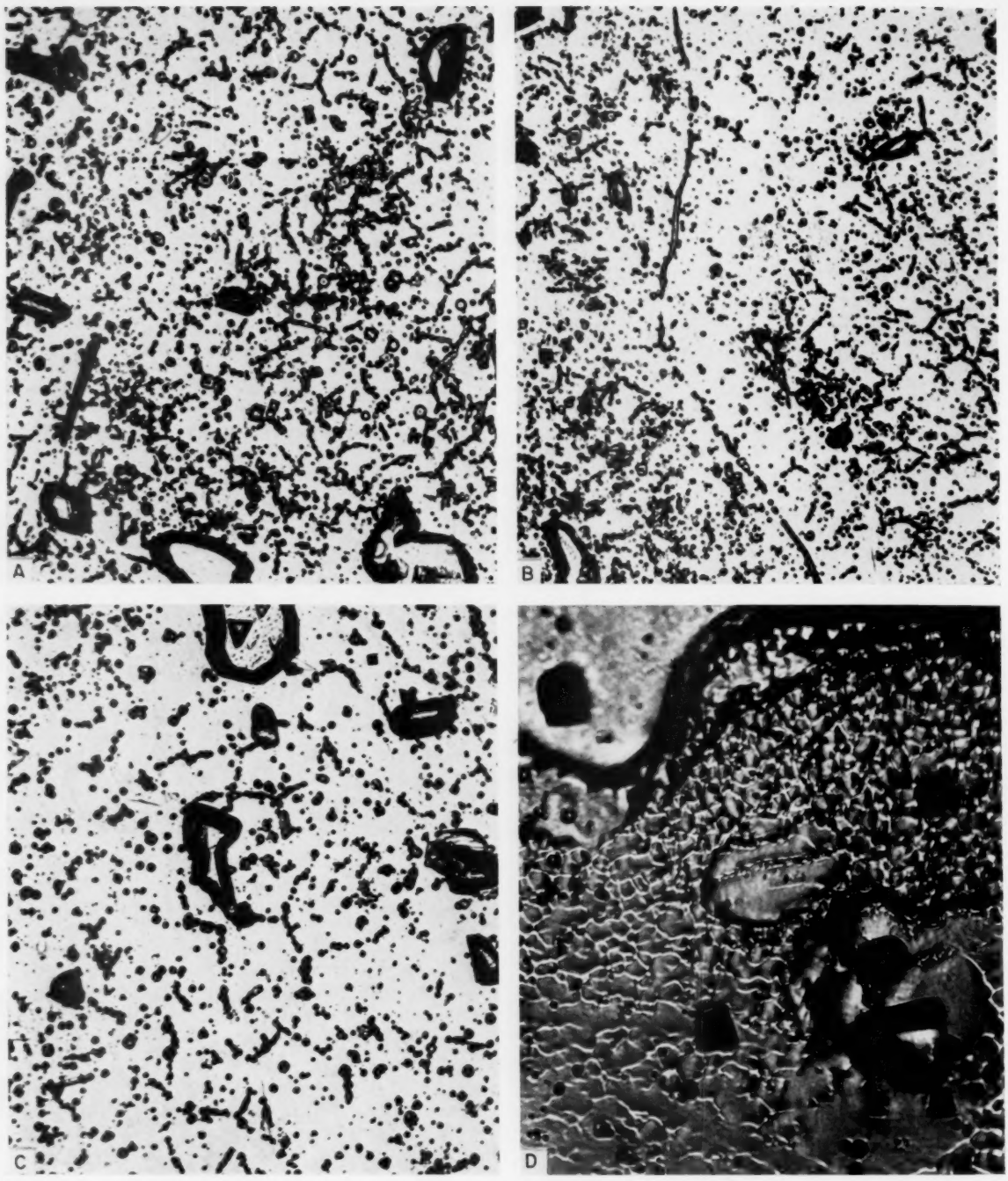

FIGURE 21. *Subgrains and etch pits in a cold-drawn nickel specimen, tested in creep under a stress of 2,665 lb/in.² at 1,200° F and stopped in the third stage after 4,853 hr and 8.5 percent plastic strain.*

Longitudinal sections of same specimen as figure 18A. Etched in 6 parts HNO_3 (conc.) and 4 parts of glacial acetic acid. (× 250). A, B, and C, vertical illumination, and D, oblique illumination.

The "rate sensitivity" of the nickel increased with increase in test temperature. At constant temperature, this value was lower for cold-drawn than for annealed nickel.

The dependence of fracture time on creep stress increased with increase in test temperature. However, in the absence of extensive recovery, the log fracture time varied linearly with log creep rate for both the annealed and the cold-drawn metal.

An evaluation of temperature-time and temperature-creep rate parameters showed that, at equal parameters, the stress values were higher for the cold-drawn than for the annealed nickel at the lower creep temperatures but the stress values coincided at 1,200° F. Thus, the resistance of the nickel to creep at temperatures below about 900° F was significantly increased by cold-drawing, whereas the strengthening effect of cold drawing was eradi-

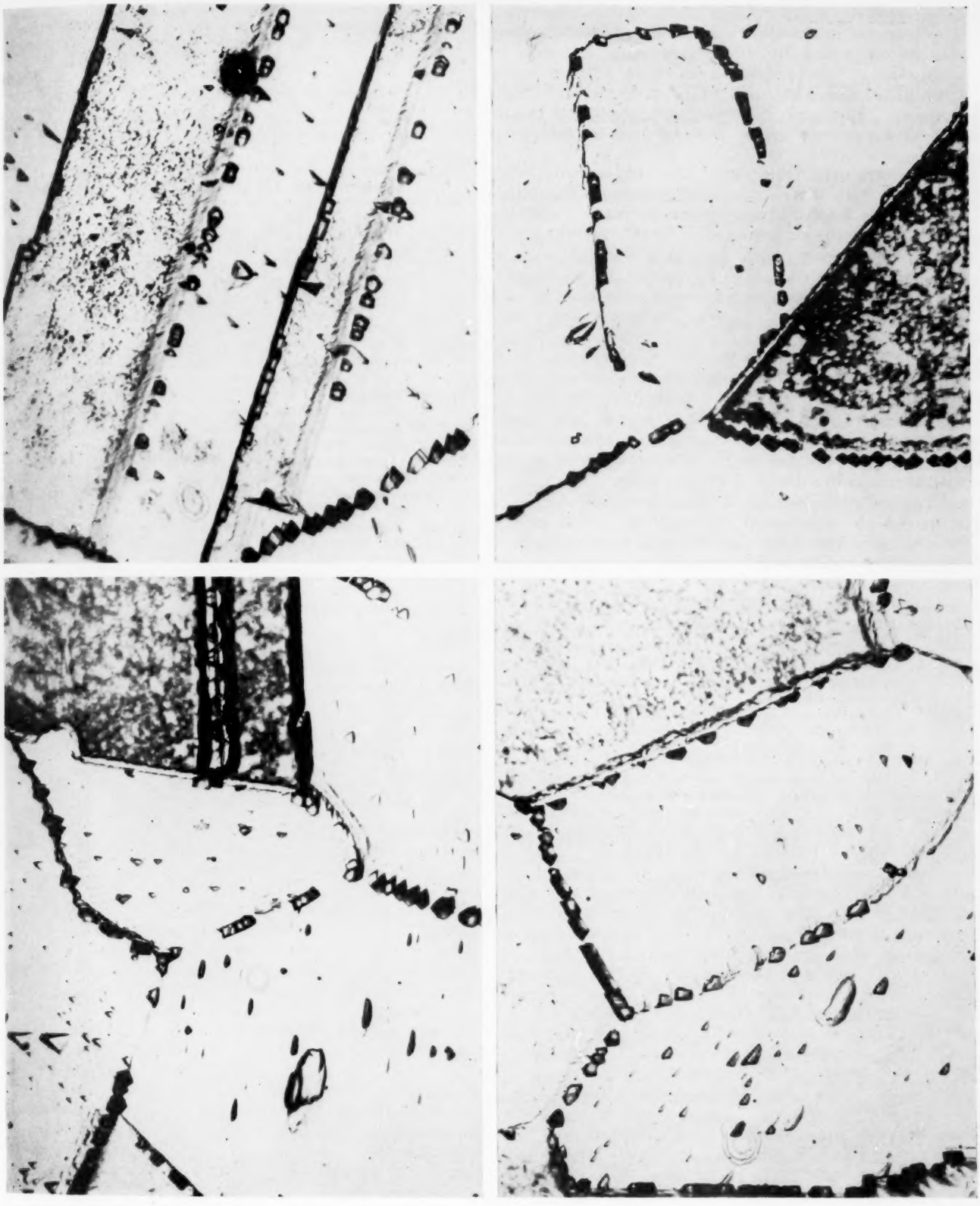

FIGURE 22. *Etch-pit distribution in a nickel specimen, annealed at 1,800° F.*

Longitudinal sections. Etched in 6 parts HNO_3 (Conc.) and 4 parts of glacial acetic acid. (× 500).

cated at creep temperatures above recrystallization. The increase in resistance to creep by cold-drawing was accompanied by a corresponding decrease in elongation. The reduction of area of the creep specimens was not materially changed by cold-drawing. However, both the elongation and reduction of area were nearly independent of the creep rate.

True strain at fracture of the cold-drawn nickel increased with increase in temperature. The hardness of the fractured specimens decreased with increase in temperature and decrease in creep rate.

The tendency to neck decreased with increase in temperature and decrease in creep rate; moreover, the tendency to form intercrystalline cracks at the surface increased with increase in temperature and decrease in creep rate. Furthermore, the intercrystalline cracking was generally initiated at high angle boundaries. The extent of the intercrystalline cracking increased with the increase in strain.

The size of etch figures of tertiary or quaternary symmetry increased with decrease in creep rate at constant temperature or, in the absence of stress, with increase in annealing temperature.

The size and density of stress-induced subgrains appeared to be affected by the orientation of the individual grains and the relative orientations of neighboring grains.

5. References

[1] W. D. Jenkins and T. G. Digges, Creep of high-purity copper, J. Research NBS **45,** 153 (1950) RP2121.

[2] W. D. Jenkins and T. G. Digges, Creep of annealed and cold-drawn high-purity copper, J. Research NBS **47,** 272 (1951) RP2254.

[3] W. D. Jenkins and T. G. Digges, Effect of temperature on the tensile properties of high-purity nickel, J. Research NBS **48,** 313 (1952) RP2317.

[4] W. D. Jenkins and T. G. Digges, Influence of prior strain history on the tensile properties and structures of high-purity copper, J. Research NBS **49,** 167 (1952) RP2354.

[5] W. D. Jenkins, T. G. Digges, and C. R. Johnson, Creep of high-purity nickel, J. Research NBS **53,** 329 (1954) RP2551.

[6] W. D. Jenkins, T. G. Digges, and C. R. Johnson, Effect of temperature on the tensile properties of a commercial and a high-purity 70-percent-nickel-30-percent-copper alloy, J. Research NBS **54,** 21 (1955) RP2561.

[7] W. D. Jenkins, T. G. Digges, and C. R. Johnson, Tensile properties of copper, nickel, and 70-percent-copper-30-percent-nickel and 30-percent-copper-70-percent-nickel alloys at high temperatures, J. Research NBS **58,** 201 (1957) RP2753.

[8] W. D. Jenkins and C. R. Johnson, Creep of annealed nickel, copper, and two nickel-copper alloys, J. Research NBS **60,** 173 (1958) RP2836.

[9] Seminar on creep and recovery of metals, Trans. Am. Soc. Metals **49A** (1957).

[10] T. H. Hazlett and E. R. Parker, Nature of the creep curve, Trans. AIME **197,** 318 (1953).

[11] H. Conrad and W. D. Robertson, Creep characteristics of magnesium single crystals from 78° to 364° K, Trans. Met. Soc. AIME **212,** 536 (1958).

[12] E. N. da C. Andrade, The concept of creep, Trans. Am. Soc. Metals **49A,** 176 (1957).

[13] P. G. McVetty, Creep of metals at elevated temperatures. The hyperbolic-sine relation between stress and creep rate, Trans. Am. Soc. Mech. Engrs. **65,** 761 (1943).

[14] S. Dushman, L. W. Dunbar, and H. Huthsteiner, Creep of metals, J. Appl. Phys. **15,** 108 (1944).

[15] J. D. Lubahn, Simultaneous aging and deformation in metals, Trans. AIME **185,** 702 (1949).

[16] F. C. Monkman and N. J. Grant, An empirical relationship between rupture life and minimum creep rate in creep-rupture tests, Am. Soc. Testing Materials, Proc. **56,** 593 (1956).

[17] F. R. Larson and J. Miller, A time-temperature relationship for rupture and creep stresses, Trans. Am. Soc. Mech. Engrs. **74,** 765 (1952).

[18] P. Lacombe and L. Beaujard, The application of etch figures on pure aluminum (99.99%) to the study of some micrographic problems, J. Inst. Metals **74,** 1 (1948).

[19] J. H. Wernick, J. N. Hobstetter, L. C. Lovell, and D. Dorsi, Dislocation etch pits in antimony, J. Appl. Phys. **29,** 1013 (1958).

[20] L. Northcott, Veining or sub-boundary structures, J. Iron Steel Inst. (London) **126,** 267 (1932).

[21] L. Northcott, Veining and sub-boundary structures in metals, J. Inst. Metals **59,** 225 (1936).

[22] P. Feltham, Intragranular substructures in high-purity nickel, J. Inst. Metals **86,** 237 (1957–58).

[23] E. R. Parker and T. H. Hazlett, Principles of solution hardening, Trans. ASM **46A,** 30 (1954).

WASHINGTON, D.C.

(Paper 63C1–1)

Journal of Research of the National Bureau of Standards—C. Engineering and Instrumentation
Vol. 63C, No. 1, July–September 1959

Friction and Endurance of Prelubricated and Unlubricated Ball Bearings at High Speeds and Extreme Temperatures

Hobart S. White

(April 23, 1959)

Endurance tests were made with 20-millimeter bore prelubricated ball bearings, at 10,000 revolutions per minute, using polyester felt rings saturated with di(2-ethylhexyl) sebacate containing appropriate additives, at ambient temperatures ranging from 80° to 400° F. Tests were made with greases for comparative purposes. Results indicate that endurance with these oil-soaked pads is comparable with the high-temperature performance of MIL–G–3278 [1] [1] grease at 250° F and MIL–L–3545 [2] grease at 300° F. Some endurance tests were made with special bearings (20-millimeter bore) made of high-speed tool steel, prelubricated at 450° F ambient temperature, and unlubricated at 650° F ambient temperature (5,000 revolutions per minute at 650° F). Experiments were made with greased bearings and with felt-pad oiled bearings in gyros and small high-speed direct-current motors at high temperatures. With oiled bearings and with unlubricated bearings, wearing or breaking of separators (ball cages) was the most common cause of failure. Compared to low-temperature greases MIL–G–3278 [1] and MIL–G–7421 [3], with oiled bearings starting friction was low and running friction was about one-tenth that of greased bearings at −75° F ambient temperature.

1. Introduction

In aircraft accessory equipment, such as gyros, motors, and inverters, it is highly desirable that the ball bearings be prelubricated in such a manner that no further lubrication is required during their useful life. At ordinary temperatures, ball bearings prepacked with suitable greases may be operated several thousand hours satisfactorily. However, accessory equipment in modern aircraft is subjected to temperatures ranging from −65° to +300° F, and in some cases to 450° F or higher. In many such applications, conventional and even special greases are not satisfactory because of excessive friction at low temperatures and short endurance life at high temperature.

One of the chief difficulties with greases has been that the soaps or other thickeners cause high friction at low temperatures and are not chemically stable at high temperatures. Although much progress has been made in the development of greases suitable for prelubrication at high temperatures, not much progress has been made in developing a grease suitable for use at both extremes of temperature. Some previous work [4] at the National Bureau of Standards indicated that instead of thickeners as used in greases, a feltlike material could be used to hold a supply of suitable oil and bleed it slowly to the races of the ball bearings.

The wool felt used in the previous work charred badly at 325° F. More recently, synthetic felts which will withstand much higher temperatures than wool felt have become available. Accordingly, further work (sponsored by the Bureau of Aeronautics, Department of the Navy) was started in December of 1955, with polyester felt rings incorporated in size 204K ball bearings which have a nominal width of 0.8125 in. instead of the more conventional width of 0.5512 in.

The main objective of this work was to investigate the performance with the oil-soaked felt-pad method of prelubrication for comparison with grease prelubrication in high-speed applications requiring low friction at low temperatures and long-endurance life at high temperatures. However, some experiments were made with unlubricated bearings.

2. Apparatus

2.1. Endurance Test Machines

Four machines were built for making endurance tests at high temperatures. Each shaft and housing was made to accommodate 20-mm bore test bearings having a nominal width of 0.8125 in. (such as Fafnir 204KTT), and provided with spacers such that the more conventional size 204K (SAE No. 20BC02) having a nominal width of 0.5512 in. could be tested also. The test bearing is mounted outboard on a steel spindle which is supported by two self-alining oil-lubricated pillow block ball bearings with 1 3/16-in. bores. Test bearing seats on the shafts were made 0.7872 in. ±0.0002 in. in diam and the housing bores were made 1.8504 in. ±0.0002 in. A nut is used to secure the inner race to each shaft, and removable plates which act as bearing shields are used on each end of the housing to secure the outer race.

A compression spring is used to apply a 5-lb axial load, and a weight at the lower end of a torque arm attached to the bearing housing adds to the weight of the housing to provide a 3-lb radial load. A leaf-actuated microswitch is located under the base of each machine such that a torque of about 3,000 g-cm causes the torque arm to operate the microswitch which adds a 600-w heater load on the motor

[1] Figures in brackets indicate the literature references at the end of this paper.

circuit and causes quick operation of the overload breaker in each motor circuit.

Two electric heaters in series are mounted below the bearing housing. The heaters and bearing housing assembly are enclosed in an aluminum alloy chamber. Figure 1 shows a machine with the chamber in place and another with the chamber removed. The temperature is controlled by a bimetallic regulator, and measured by a thermocouple almost contacting the outer race of the test bearing and another in the air near the bearing housing. The thermocouples are electrically insulated to avoid interconnection and pickup of small stray voltages.

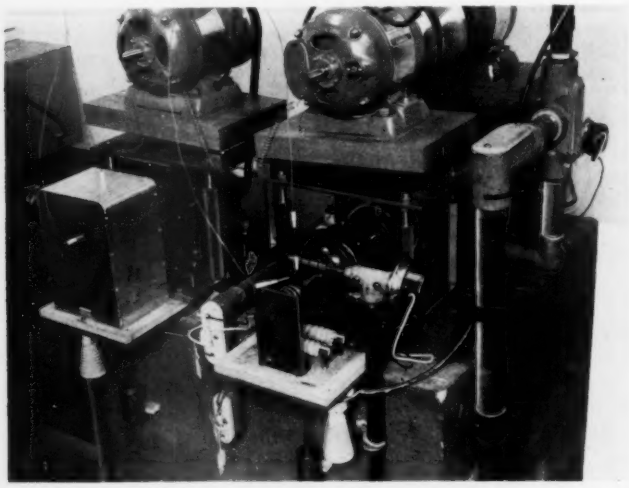

FIGURE 1. *High-temperature ball bearing endurance testing machines.*

For operation at 10,000 rpm, each spindle is driven by a ½-hp, 3,450-rpm, 115-v, capacitor-type motor through a 1-in. wide flat fabric belt, with a 2-in. diam pulley on the spindle and a 5⅞-in. diam pulley on the motor. The pillow block ball bearings supporting each spindle are lubricated with a MIL–L–7808 type of synthetic oil containing a viscosity index improver and a rust inhibitor.

2.2. Friction Test Machine

The test shaft for the friction testing machine is similar to the endurance test shafts except that it is longer to allow for the outboard portion to extend through the wall of an insulated box. The shaft and test-bearing housing were made of type 303 stainless steel, to prevent rusting from condensation which occurs after low-temperature tests. A cast iron ring fitted around the housing provides additional load. A pendulum consists of an aluminum alloy tube, a small bob, and a pointer which measures displacement from the zero line on a horizontal scale. The test-bearing-housing assembly is mounted in an insulated box, which has an internal compartment containing a blower and space for dry ice. The front is removable, and has an observation window. Either of two brass weights can be placed on the bob for higher ranges of torque. The pendulum was calibrated with the bob and with each of the brass weights in place, so that three ranges of torque capacity are available. The load on the bearing is in the range from 3.6 to 4.3 lb, depending on the use of the brass weights for the desired torque range. Since the torque to be investigated is mostly that resulting from shearing of the lubricant, this variation in loading is not considered important. The lower end of the pendulum tubing dips into a damping fluid in an open pan back of the scale, for minimizing fluctuations. The test spindle may be driven at speeds ranging from 10 to 10,000 rpm, by motorized drives back of the insulated box.

2.3. Miscellaneous Apparatus

A modified air-driven gyro and a preheating coil for the compressed air were mounted in a conventional laboratory oven. The modified gyro is similar to those tried by a Coordinating Research Council Sub-Panel for testing lubricants in miniature ball bearings at 20,000 rpm at high temperature.

Several small motors, 26-v, d-c, 11,000 rpm, 1/20-hp, were used for testing prelubricated instrument bearings. A 26-v, d-c, 11,000-rpm, 1/12-hp motor was modified to act as a generator to load the above motors in some tests.

3. Materials

3.1. Test Bearings

Ball bearings which were used in the tests on the endurance machines and on the friction machine included the conventional size 204K (20-mm bore, 0.5512-in. width) and the extra wide size 204KTT (0.8125-in. width), having rings and balls made of SAE No. 52100 steel (or possibly SAE No. 51100 in some cases for the balls), with pressed steel separators.

Special bearings made of high-speed tool steel were used for tests at temperatures above 400° F. Some of these, including the separators, were made of AISI type M–2 tool steel, and a few were made of type M–10 steel with silver-plated beryllium-copper separators. Tungsten-carbide balls were used in a few tests. Experimental separators made of temperature-resistant, nonmetallic compositions were tried in a few tests.

The size 8502 (15-mm bore, 0.500-in. width) ball bearings in one of the ½-hp, 3,450-rpm, driving motors were replaced with size 202KTT bearings (0.656-in. width) fitted with oil-soaked felt rings.

N.D. 5, S34–5–SS, and 34–5B ball bearings (5-mm bore, 16-mm o.d.) were used in tests with the air-driven gyro.

SS77034 and Q34 ball bearings (4-mm bore, 16-mm o.d.) were used in tests with the high speed d-c motors. Tests with a magnet and with nitric acid indicated the separators in the SS77034 bearings were not stainless steel although the rings were stainless (presumably SAE No. 51440C). The Q34 bearings were made of conventional ball bearing steel, but fitted with phenolic-fabric nonmetallic separators.

3.2. Felts and Shields

The polyester felt used for the data given in this paper has a nominal thickness of 0.130 in. and is described by the manufacturer as 3 denier, ST54, 1.25 lb/yd.^{2} When heated in an oven at 350° F for 500 hr it remained pliable and tough; wool felt under the same conditions was charred and crumbly.

Teflon felt, having a nominal thickness of 0.125 in. and weighing 2.8 lb/yd,^{2} was used for tests at ambient temperatures above 350° F. Layers of glass paper were used as felt in some tests.

The commercial extra wide 204K ball bearings (such as Fafnir 204KTT) use felt rings between two metal shields to retain grease and exclude dirt. For the oil-soaked felt ring installations, new inner steel shields were made at NBS, with the depth increased from about 0.062 in. to about 0.102 in. This, with the 0.25-in. depth of the commercial outer steel shield, provides about 0.127-in. space for the oiled felt. Small holes (1/16-in. diam) were drilled at the outer edge of the depression in the inner shields to facilitate creeping of the oil to the outer race of the bearing. For most of the tests a steel inner band was fitted to the inner shield to prevent stray felt fibers from touching the inner race of the bearing. In most of the tests a Teflon gasket (0.015-in. thick) was used between the felt and the outer steel shield. In figure 2, at the top, a bearing is shown before installation of the felt and shields and another with the outer shield staked in place; at the bottom, going from right to left is a bearing with an inner shield in place, a felt ring, a Teflon gasket, and the outer shield. There are only 4 holes in the inner shield shown, but shields with 16 holes were used for some of the tests.

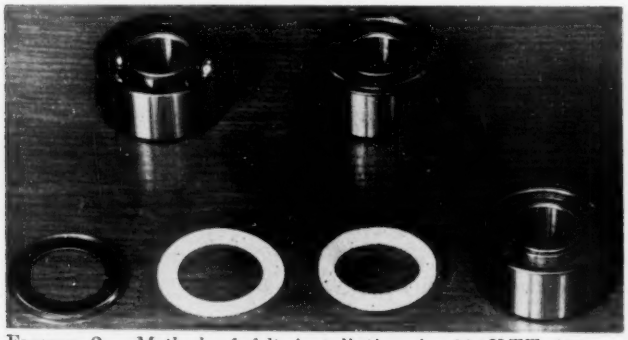

FIGURE 2. *Method of felt installation in 204KTT (20-mm bore) ball bearings.*

The steel inner shields for the 202KTT ball bearings were proportionately smaller than the shields described above for 204KTT bearings, and were made in one piece instead of being fitted with separate inner bands.

3.3. Lubricants

The lubricants used in the tests covered by this paper are described in table 1. Sample SO–15 is the oil which was investigated for use in the temperature range from −75° to +350° F; most of the other oils were tried for a higher range of temperature. Tests with the greases were for comparative purposes.

TABLE 1. *Lubricants*

Sample	Description
G–6	Ball and roller bearing grease, 14L3c (same product now MIL–G–18709) [6].
G–7	Ball and roller bearing grease, 14L3c [6].
G–8	Grease; Aircraft and Instruments (for Low and High Temperatures), MIL–G–3278 [1].
G–9	Grease, MIL–G–3278 type [1].
G–10	Grease, high temperature, MIL–L–3545 type [2].
G–11	ASTM TG–III–29 grease.
G–12	ASTM TG–III–31 grease.
G–13	Arylurea-silicone grease, MLG–9305.
G–14	Silicone grease, low temperature (consistency not known).
G–14a	Silicone grease, low temperature, medium.
G–15	Grease, extreme low temperature, MIL–G–7421 [3].
SO–10	Di(2-ethylhexyl) sebacate.
SO–14	(Di(2-ethylhexyl) sebacate 86% Acrylic viscosity-index improver 8% Tricresyl phosphate 5% Acid phosphate type additive 0.5% Phenothiazine 0.5% Silicone antifoam 0.001% Viscosity: 43 cs at 100°F; 10.0 cs at 210°F. (Same as SO–14 in previous paper. [4].)
SO–15	(Di (2-ethylhexyl) sebacate 91.5% Tricresyl phosphate 5.0% Barium mahogany sulfonate 3.0% Phenothiazine 0.5% Silicone antifoam 0.001% Viscosity: 14.8 cs at 100°F; 3.6 cs at 210°F.
SO–16	Diester plus 3% tricresyl phosphate and other additives.
SO–17	Silicone fluid. Viscosity: about 50 cs at 100°F; about 3,500 cs at −76°F.
SO–18	SO–15 plus 5% additional tricresyl phosphate.
SO–19	Silicone fluid, SO–17 type plus oxidation inhibitor.

4. Tests and Results

4.1. Endurance Machine Tests and Results

a. Conventional Steel Bearings

Endurance tests with prelubricated 20-mm bore ball bearings were run at 10,000 rpm, at ambient temperatures ranging from 80° to 400° F, with 3-lb radial and 5-lb axial load. Dry cleaning solvent and benzene were used for cleaning the bearings before the prelubrication. The commercial bearing containing grease G–7 was used as received; with the other greases 3.0 g was used in each bearing. The motors and heaters were started at the same time, and sufficient heat was applied to raise the ambient to the selected test temperature within 1 hr; in general, the bearing temperature (outer race) was near or considerably beyond the ambient within the hour. After 22 hr of operation each machine was stopped and allowed to cool for 2 hr or more (occasionally stopped over weekends). Each test was continued with 22-hr periods of operation until the bearing failed, as evidenced by excessive torque which operated the overload device or caused the belt to slip or throw off from the pulleys in cases of sudden seizure.

Most of these endurance tests were run for evaluating the performance of the ball bearings over a wide range of temperature when prelubricated with SO–15 oil in polyester felts incorporated in the bearings. However, a few tests were run with a variety of greases for comparative purposes, and a few tests were run with other synthetic oils.

Data for the endurance tests are given in table 2. The test with grease G–6 was for comparison with data obtained on previous machines [4] which did not provide the 5-lb axial load. In the previous tests, at 325°F bearing temperature, the endurance runs for this grease ranged from 178 to 330 hr; with the added 5–lb axial load and 325°F ambient instead of bearing temperature, the endurance of 198 hr is compatible with the data for the previous tests. It is believed that a lubricant which causes a bearing to operate at temperatures abnormally higher than the ambient temperature should not be favored by reducing the ambient to lower the bearing temperature. Accordingly, the ambient temperature was used as the controlled temperature in this later work.

TABLE 2.—*Ball bearing endurance tests, at 10,000 rpm, with 3-lb radial and 5-lb axial loads, 20-mm bore, 52100-type steel*

Lubricant	Bearing		Type of shield [c]	Ambient temperature	Hours run before failure	Separator broken
	Size [a]	Stabilized [b]				
				°F		
G–6	204 K	Yes	1	325	198	No.
G–7	204 KTT	No	2	325	76	No.
G–8	204 K	Yes	1	325	32	Yes.
G–9	204 K	Yes	1	325	66	No.
G–10	204 K	Yes	1	325	85	Yes.
G–13	204 K	Yes	1	325	3,300+	No.
G–14a	204 K	Yes	1	325	339	No.
G–14a	204 K	Yes	1	325	1,011	Yes.
SO–10	204 KTT	Yes	3	325	26	Yes.
SO–15	204 KTT	Yes	3	325	1,012	Yes.
SO–15	204 KTT	Yes	3	325	1,618	No.
SO–15	204 KTT	Yes	3 [a]	325	750	Yes.
SO–15	204 KTT	Yes	3 [b]	325	248	Yes.
SO–15	204 KTT	Yes	3 [b]	325	486	Yes.
SO–15	204 KTT	Yes	3 [b]	325	1,119	Yes.
SO–15	204 KTT	Yes	3 [c]	325	484	Yes.
SO–15	204 KTT	Yes	3 [c]	325	484	Yes.
SO–15	204KTT	No	4	80	1,590	Yes.
SO–15	204KTT	No	4	80	3,300+	Yes.
SO–15	204KTT	No	4	250	708	Yes.
SO–15	205KTT	No	4	250	1,430	Yes.
SO–15	204KTT	Yes	4	250	3,300+	No.
SO–15	204KTT	No	4	300	440	Yes.
SO–15	204KTT	No	4	300	462	Yes.
SO–15	204KTT	No	4	300	508	Yes.
SO–15	204KTT	No	4	300	594	No.
SO–15	204KTT	No	4	300	924	No.
SO–15	204KTT	Yes	4	300	812	Yes.
SO–15	204KTT	Yes	4	300	930	Yes.
SO–15	204KTT	Yes	4	300	1,075	No.
SO–15	204KTT	Yes	4	325	424	Yes.
SO–15	204KTT	Yes	4	325	571	Yes.
SO–15	204KTT	Yes	4	325	708	No.
SO–15	204KTT	Yes	4	350	195	No.
SO–14	204KTT	Yes	4	400	21	Yes.
SO–16	204KTT	Yes	4	325	99	Yes.
SO–16	204KTT	Yes	4	400	25	No.
SO–18	204KTT	Yes	4	300	281	Yes.

[a] Nominal bearing width: 204K=0.5512 in.; 204KTT=0.8125 in.

[b] Stabilized bearings were heat stabilized during manufacture to minimize dimensional changes at high temperature during use.

[c] Types of shields:

1. No shield in bearing; side plates of housing act as shields.
2. Commercial inner and outer steel shields with felt between.
3. NBS inner steel shields, 16 holes, polyester felts, commercial outer steel shields not staked in place.

3a. Same as No. 3, with outer shields staked in place.

3b. Same as No. 3a, except with narrow Teflon gaskets.

3c Same as No. 3b, except with inner band.

4. NBS inner steel shields, 4 holes, inner band, polyester felt (Teflon felt at 400° F), wide Teflon gaskets, commercial outer steel shields staked in place.

The test with grease G–7 was with a commercially obtained extra wide 204K bearing as prelubricated at the factory with a 14L3c [6] grease believed to be similar to grease G–5 in the previous paper [4].

Grease G–8 is a well-known MIL–G–3278 [1] grease obtained commercially. Grease G–9 is a sample tested by another laboratory for high-temperature performance in accordance with MIL–G–3278; at 250°F bearing temperature and 10,000 rpm the endurance life was 1,385, 1,361, 1,281, and 1,767 hr, with an average of 1,449 hr (1,000 hr required).

Grease G–10 is a sample tested by another laboratory for high-temperature performance in accordance with MIL–L–3545; at 300° F bearing temperature and 10,000 rpm the endurance life was 1,477, 2,146, 1,231, and 1,521, with an average of 1,594 hr (600 hr required).

Although greases G–7 and G–8 are satisfactory at 212° and 250° F respectively, and greases G–9 and G–10 exceed the specification requirements at 250° and 300° F respectively, the endurance life with each at 325° F ambient temperature and 10,000 rpm is very short (less than 100 hr).

Grease G–13 (MLG–9305) was tested at Wright Air Development Center in accordance with CRC Method L–35 (specified in MIL–G–25013 [7]) on the Navy-type spindle; with high-speed tool steel bearings, at 450° F and 10,000 rpm, the endurance life was 368 and 596 hr, with an average of 482 hr. A test with this grease in a heat stabilized 52100–type bearing was ended at 3,300 hr without failure, at 325° F. However, this grease gives excessive torque at low temperatures (see section 4.2).

Grease 14a is recommended (on the container) for operating temperatures from −100° to +300° F. The average of 675 hr for 2 tests at 325° F ambient temperature and the low torque at −75° F (see section 4.2) are in agreement with the recommendation. Tests with grease 14 were conducted at another laboratory several years ago at 250° and 300° F, with results averaging 2,473 and 1,741 hr, respectively. However, this grease is not qualified under any military specification.

The test with oil SO–10 was for comparison with data obtained on a previous machine [4] which did not provide the 5-lb axial load. In the previous test at 325° F bearing temperature, the endurance of 48 hr is compatible with the endurance of 26 hr in the test at 325° F ambient temperature with a 5-lb axial load.

In two tests with SO–15 oil, NBS inner shields were used and commercial outer shields were held in place with spacers between the shields and the housing side plates. Both of these tests exceeded 1,000 hr in duration at 325° F. However, this type of shield installation (type 3 in table 2) was considered undesirable because it would require installation of felts and fitting with spacers in service installation of bearings. Accordingly, a test was made with the outer shields staked in place in the same manner (type 3a) used for commercial 204KTT ball

bearings, and in this test failure occurred at 750 hr at 325° F. In these three tests there was an undesirable amount of oil seepage from the bearings during the first hour of operation. Accordingly, other methods (see 3b, 3c, and 4 at end of table 2) of shield installation were tried.

In most of the endurance tests, NBS inner shields with 4 holes each (see fig. 2) were used with an inner band to prevent stray felt fibers from touching the inner race, and a Teflon gasket was used between each felt and outer shield to prevent oil seepage from the bearing. The data for the tests with SO–15 oil and polyester felt, at 10,000 rpm, are shown in figure 3, with solid points for the type 4 shields, and open circles for the other types of shielding. The straight line in this figure is based on 1,000 hr at 250° F and 600 hr at 300° F, which are the requirements in MIL–G–3278 [1] and MIL–L–3545 [2] respectively, except that these grease specifications use bearing temperatures instead of ambient temperatures. This line may be represented by the equation $L=3{,}000-8T$, where L represents the endurance life in hours and T represents the temperature in degrees Fahrenheit. The averages of endurance data for these tests at 80°, 250°, 300°, and 325° F ambient temperatures are above the line in each case.

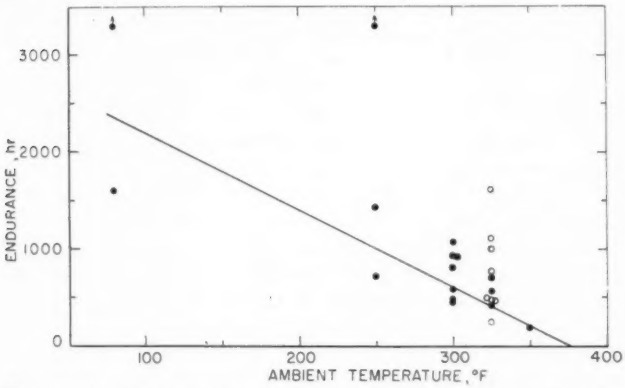

FIGURE 3. *Effect of temperature on endurance tests with 20-mm bore ball bearings, at 10,000 rpm, prelubricated with SO–15 oil in polyester felt pads.*

The straight line is based on 1,000 hr at 250° F and 600 hr at 300° F, the requirements in MIL–G–3278 and MIL–L–3545, respectively.

Exploratory tests with lubricants SO–14 and SO–16 indicated they were not suitable for prelubrication at 400° F. Also, a test with lubricant SO–18 at 300° F did not indicate any advantage in adding more tricresyl phosphate to lubricant SO–15.

As shown in table 2, broken separators caused the failures in most of the tests with oil-prelubricated bearings, apparently by jamming the balls in the races. However, in one test at 80° F the bearing was in operating condition at the end of 3,300 hr although a small segment was broken from the separator. At the end of the tests at high temperature with SO–15 oil varnishlike films were observed on the races and balls. These films were not continuous but were broken and uneven in thickness. In some cases (especially at 300° F) failures resulted from these films causing binding (no clearance). On the other hand, it is probable that the formation of the film is the mechanism whereby the SO–15 oil provides satisfactory operation at temperatures up to 325° F for many hours after the supply of oil is exhausted.

b. High-Speed Tool Steel Bearings at 10,000 rpm

Endurance tests were made with high-speed tool steel ball bearings (20-mm bore) at 10,000 rpm and 450° F ambient temperature. The data for these tests are given in table 3. In these tests the machined and riveted M–2 steel separators did not leave sufficient space in the size 204KTT (0.8125 in. width) bearings for installing the special NBS inner steel shields; accordingly, the commercial inner shields were used after drilling 16 holes in each shield (similar to type 3 in table 2 except for depth). With the size 204K (0.5512 in. width) bearings, the felts were installed in rings on each side of the bearings as described in the previous paper [4].

In two tests with unhardened M–2 steel separators the separators broke in 16 and 15 hr. In addition to the breaks, several cracks were present in the separators at the ball pockets. It is believed that, after the lubricant was exhausted, vibration from "stick-slip" of the land-riding separators stressed the unhardened steel beyond its elastic limit and quickly induced fatigue cracks.

In the tests with hardened M–2 steel separators no breaks or fractures were observed. However, in general, the bearings became noisy and the friction became excessively high after exhaustion of the lubricant; but in some cases the bearings and separators were found to be in good condition after being cleaned and examined at the end of the tests.

Tests with the SO–15 oil indicated that at 450° F ambient temperature it did not form a varnishlike film which would provide satisfactory operation after the oil was exhausted; and its volatility at 450° F caused exhaustion of the oil in the bearings in a relatively short time.

Tests with the less volatile oils SO–16, SO–17, and SO–19 indicated they were not suitable for prelubrication at 450° F ambient temperature although they lasted somewhat longer than the SO–15 oil.

The silver-plated beryllium-copper separators (currently being used for grease prelubricated bearings at 450° F) appeared to be the most suitable of the separators tried in these tests, with 52 hr of operation with SO–15 oil and 155 hr of operation with SO–19 oil. It is believed that a large part of this operation occurred after the supply of oil was exhausted in each case.

A separator made of asbestos-fiber reinforced high-temperature phenolic composition failed at 116 hr of operation because of excessive wear and breakage after the supply of SO–19 oil was exhausted by evaporation. A separator made of oriented glass-fiber reinforced composition rovings failed in 9 hr because of breaking into halves in the plane of the ball centers.

Endurance (16 hr) with an M–2 steel ball bearing

TABLE 3. *Ball bearing endurance tests, at 10,000 rpm, at 450° F ambient temperature, with 3-lb radial and 5-lb axial loads, 20-mm bore, high-speed tool steel*

Lubricant	Bearing		Separator		Sulfurized	Felt	Hours run before failure	Separator broken
	Size	Steel	Material	Hardened				
SO–15	204 KTT	M–2	M–2	Yes	Yes	Teflon	9	No.
SO–15	204 K	M–10	(1)		No	Teflon	52	Yes.
SO–15	204 KTT	M–2	(2)		No	Teflon	6	
SO–16	204 KTT	M–2	M–2	No	No	Teflon	16	Yes.
SO–16	204 KTT	M–2	M–2	Yes	No	Teflon	13	No.
SO–17	204 KTT	M–2	M–2	No	No	Teflon	15	Yes.
SO–17	204 KTT	M–2	M–2	Yes	Yes	Teflon	33	No.
SO–19	204 KTT	M–2	M–2	Yes	No	Glass	8	No.
SO–19	204 KTT	M–2	M–2	Yes	Yes	Glass	12	No.
SO–19	204 K	M–2	M–2	Yes	No	Teflon	42	No.
SO–19	204 K	M–10	(1)		No	Teflon	155	Yes.
SO–19	204 KTT	(3)	(3)		No	Teflon	44	
SO–19	204 K	M–2	(4)		No	Teflon	30	No.
SO–19	204 KTT	M–2	(5)		No	Teflon	9	Yes.
SO–19	204 K	M–2	(6)		No	Teflon	116	Yes.
MoS_2	204 KTT	M–2	M–2	Yes	Yes	None	16	No.
None	204 KTT	M–2	M–2	Yes	Yes	None	88	No.
None	204 KTT	M–2	M–2	Yes	No	None	12	No.

[1] Silver-plated beryllium-copper separator.
[2] Balls as separators, 9/32-in. diam, type 52100.
[3] M–2 steel rings with tungsten-carbide balls; 7 balls 5/16-in. diam for load, 7 balls 9/32-in. diam for spacing.
[4] Silver-plated hardened M–2 steel separator.
[5] Glass-fiber reinforced high-temperature molded composition.
[6] Asbestos-fiber reinforced high-temperature phenolic composition.

prelubricated with molybdenum disulfide powder was not significantly better than with an unlubricated bearing which failed in 12 hr. A sulfurized unlubricated bearing continued in operation 88 hr when failure occurred with broken rivets in the separator; the balls, races, and separator were worn excessively and, even before final failure, the bearing would not have been satisfactory in applications where large radial play of the shaft could not be tolerated.

c. High-Speed Tool Steel Bearings at 5,000 rpm

Three endurance tests were made with high-speed tool steel ball bearings (20-mm bore) at 5,000 rpm and 650° F ambient temperature.

One test was made with M–2 steel rings fitted with tungsten carbide balls; 7 balls 5/16 in. in diam for supporting the load and 7 balls 9/32 in. in diam for spacing the load balls. A coating of SO–15 oil was applied to the bearing and it was operated 22 hr at room temperature for "run-in" before testing at 650° F. No oil-soaked felt was used, and it is probable that all the oil in the bearing evaporated during the first hour while being heated to 650° F. The thermocouple nearly touching the outer ring reached 750° F with the 650° F ambient temperature, and it is probable that the ball and race temperatures were much higher than 750° F. One of the lands of the inner ring had been ground to a smaller diameter to make this a separable bearing to permit installing the balls to fill the raceway; failure occurred after 88 hr of operation at 650° F ambient temperature when two of the spacer balls escaped the raceway. The races were worn considerably and "spalling" was observed on the balls when examined with a 10-power stereomicroscope.

Two tests were made with sulfurized M–2 steel bearings and separators (hardened) at 650° F ambient temperature and 5,000 rpm, without lubrication. One of these bearings, sulfurized after assembly, failed after 10 hr of operation, because of high torque. It was worn excessively. The other bearing, sulfurized before assembly, was inspected after 550 hr of operation. The balls, races, and separator were worn excessively, and the separator rivets were broken. Apparently, the inner race had been sliding on some of the balls, with the bearing no longer functioning as a ball bearing. Although the bearing was operating in the endurance machine without excessive torque at the end of 550 hr, the condition of the bearing was such that it would not have been satisfactory in applications where large radial play of the shaft could not be tolerated.

4.2. Friction Machine Tests and Results

Frictional torque and bearing temperature rise above the ambient were investigated with two greases and with SO–15 oil in felt rings, at speeds ranging from 10 to 8,500 rpm. The data for these tests with grease G–8 are given in table 4. A clean 204K bearing was lubricated with 3.0 g of grease in the conventional manner, with rotation by hand to ensure the presence of grease in the races. Starting at 10 rpm, the torque in gram-centimeters and the temperature rise above the ambient were determined near the end of the first and the tenth minute, at room temperature (80° F nominal). Then the speed was increased in steps to 100, 500, 1,000, 2,000, 4,900, and 8,500 rpm, with 10 min of operation at each speed, and readings were taken for the first and tenth minute at each speed. With the same bearing, with-

TABLE 4. *Frictional torque and bearing temperature rise above ambient for a 20-mm bore ball bearing lubricated with 3.0 g of G–8 grease, with 4-lb nominal radial load*

Speed	Time at each speed	Nominal ambient temperature, ° F							
		80		−40		−75, blower on		80	
		Torque	ΔT	Torque	ΔT	Torque	ΔT	Torque	ΔT
rpm	*min*	*g-cm*	*° F*	*g-cm*	*° F*	*g-cm*	*° F*	*g-cm*	*° F*
10	1	99	0	25	10	403	1	45	0
10	10	45	0	25	10	252	1	41	0
100	1	72	0	113	10	113	1	34	0
100	10	29	0	113	10	88	1	26	0
500	1	48	0	277	11	113	1	48	0
500	10	32	0	202	12	101	1	40	0
1,000	1	64	0	277	12	88	1	68	0
1,000	10	48	0	101	13	50	1	68	0
2,000	1	90	0	151	13	50	1	113	0
2,000	10	90	1	202	13	38	1	99	1
4,900	1	378	4	328	14	277	2	378	4
4,900	10	328	13	328	29	126	3	328	12
8,500	1	504	17	882	38	2,520	27	504	18
8,500	10	227	27	757	80	1,310	102	227	27

out repacking, similar tests were made at an ambient temperature of −40° F (−40° C) with no forced air circulation, at −75° F (−59.4° C) with forced air circulation (except when reading torque), and at 80° F (26.7° C), respectively. In each case, the bearing stood overnight between tests at the different ambient temperatures.

Similarly, data obtained with grease G–9 are given in table 5. With each of the two greases, at −75° F ambient temperature, the bearing temperature rise exceeded 100° F after 10 min of operation at 8,500 rpm with forced air circulation, and the torque exceeded 1,000 g-cm.

Torque and temperature-rise data were obtained in a similar manner with extra wide 204K ball bearings prelubricated with polyester felt rings soaked in SO–15 oil. Data are given in table 6, for a bearing fitted with inner shields having 4 holes each and

TABLE 5. *Frictional torque and bearing temperature rise above ambient for a 20-mm bore ball bearing lubricated with 3.0 g of G–9 grease, with 4-lb nominal radial load*

Speed	Time at each speed	Nominal ambient temperature, ° F							
		80		−40		−75, blower on		80	
		Torque	ΔT	Torque	ΔT	Torque	ΔT	Torque	ΔT
rpm	*min*	*g-cm*	*° F*	*g-cm*	*° F*	*g-cm*	*° F*	*g-cm*	*° F*
10	1	203	0	302	10	1,560	2	158	0
10	10	203	0	302	10	1,760	2	181	0
100	1	203	0	630	11	1,060	2	136	0
100	10	172	0	630	11	882	2	118	0
500	1	217	0	1,460	12	1,260	2	140	0
500	10	212	1	1,080	18	958	3	145	1
1,000	1	271	1	1,260	20	958	4	194	1
1,000	10	253	3	504	23	832	10	185	2
2,000	1	316	3	479	24	882	12	217	3
2,000	10	217	5	353	27	857	19	190	4
4,900	1	504	9	1,510	35	2,520	43	302	6
4,900	10	353	20	932	70	1,640	84	227	14
8,500	1	605	24	1,080	78	1,510	94	454	20
8,500	10	466	48	756	100	1,010	109	353	36

TABLE 6.—*Frictional torque and bearing temperature rise above ambient for a 20-mm bore ball bearing lubricated with polyester felt rings soaked in SO–15 oil, with 4-pound nominal radial load*

Speed	Time at each speed	Nominal ambient temperature, ° F							
		80		−40		−75, blower on		80	
		Torque	ΔT	Torque	ΔT	Torque	ΔT	Torque	ΔT
rpm	*min*	*g-cm*	*° F*	*g-cm*	*° F*	*g-cm*	*° F*	*g-cm*	*° F*
10	1	8	0	4	10	54	1	8	0
10	10	8	0	4	10	54	1	8	0
100	1	10	0	14	10	108	1	6	0
100	10	8	0	14	10	113	1	6	0
500	1	18	0	50	10	63	1	10	0
500	10	18	0	50	11	50	1	10	0
1,000	1	32	0	108	11	41	1	13	0
1,000	10	32	1	100	12	36	1	13	0
2,000	1	67	1	136	11	27	1	26	0
2,000	10	67	1	127	12	23	1	26	0
4,900	1	145	1	362	14	122	1	51	0
4,900	10	131	6	325	23	118	2	51	2
8,500	1	99	6	158	24	46	3	80	3
8,500	10	77	7	127	24	36	3	64	4

NOTE: Oil in bearing and felt; at start = 2.93 g; at end of testing = 2.13 g.

inner bands, but without the Teflon gaskets. The torque and the temperature rise at −75° F and 8,500 rpm are very low in comparison with the data for the greased bearings. However, there was an undesirable loss of oil from the bearing (see table 6) during the friction testing. Accordingly, a similar test was made with Teflon gaskets (0.015-in. thick) used between the felts and the outer shields, and these data are given in table 7. The gaskets reduced the loss of oil, and it is assumed that the greater amount of oil remaining in the races caused the torque at −75° F ambient temperature to be higher than in the previous test in which more oil was lost.

The loss of oil from the bearings is undesirable.

TABLE 7.—*Friction torque and bearing temperature rise above ambient for a 20-mm bore ball bearing lubricated with polyester felt rings soaked in SO–15 oil, with teflon gaskets, with 4-lb nominal radial load*

Speed	Time at each speed	Nominal ambient temperature, ° F							
		80		−40		−75, blower on		80	
		Torque	ΔT	Torque	ΔT	Torque	ΔT	Torque	ΔT
rpm	*min*	*g-cm*	*° F*	*g-cm*	*° F*	*g-cm*	*° F*	*g-cm*	*° F*
10	1	10	0	4	10	86	1	10	0
10	10	10	0	4	10	86	1	10	0
100	1	11	0	3	10	212	1	8	0
100	10	10	0	3	10	212	1	8	0
500	1	21	0	126	10	244	1	13	0
500	10	21	0	122	11	226	1	13	0
1,000	1	35	0	217	12	253	1	21	0
1,000	10	35	0	208	12	240	1	21	0
2,000	1	72	0	294	12	230	1	37	0
2,000	10	67	1	221	13	212	3	37	0
4,900	1	149	2	452	16	248	4	145	1
4,900	10	136	5	352	23	235	9	126	4
8,500	1	95	5	181	25	122	9	81	4
8,500	10	81	7	158	25	122	10	68	6

NOTE: Oil in bearing and felt; at start = 2.77 g; at end of testing = 2.40 g.

However, there was some loss of oil by bleeding from the greases in the friction testing; adherence of grease to the side plates at the end of the tests made it impractical to estimate the loss from the greased bearings. Also, in the high-temperature endurance tests there was excessive loss of grease from the bearings at the start of each test, evidenced by grease on the torque arms and smoking from the heaters.

With data taken from tables 5 and 7, the effect of speed on frictional torque and bearing temperature rise at −75° F (−59.4° C) is shown in figure 4, on logarithmic scales. At the lower and the higher speeds the torque with the grease is about 10 times greater than with the oil, but at intermediate speeds it is only about 4 times greater than with the oil. Under the conditions of these tests (see tables 4 to 7), at −75° F ambient temperature with forced air circulation and 8,500 rpm, it is of interest to note that the torque in gram-centimeters is approximately 10 times the temperature rise in ° F.

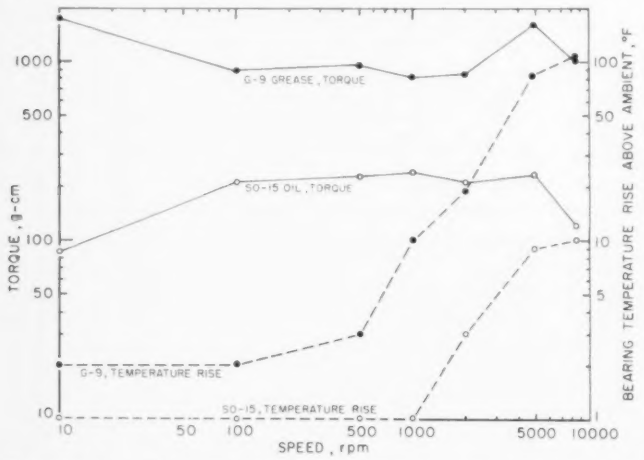

FIGURE 4. *Effect of speed on frictional torque and bearing temperature rise at −75° F ambient temperature, with 20-mm bore ball bearings.*

With size 204K ball bearings freshly packed with 3.0 g of grease G–8 and grease G–9, and an extra wide 204K bearing freshly oiled with SO–15 oil in the same manner as described for the data in table 7, data were obtained with operation at 10,000 rpm in an ambient temperature of −75° F (−59.4° C) with forced air circulation. A ½-hp, capacitor-type, 3,450-rpm, motor was connected to the spindle (behind the cold box) through a vee belt. In each test, the bearing was cooled to −75° F before starting the motor. With grease G–8 the motor "hummed and groaned" but started without stopping from overloading of the built-in overload protector. With grease G–9 the overload protector stopped the motor 10 times during attempted starts even with manual help applied to the pulley, but got up to nearly normal speed on the 11th start. With the SO–15 oil the motor started with no difficulty. After starting, each run was continued for 2 hr. With the greases the torque immediately after starting was beyond the capacity of the torque measuring apparatus with the large brass weight on the bob (beyond 2,850 g-cm). The torque data for grease G–9 and oil SO–15 are given in figure 5.

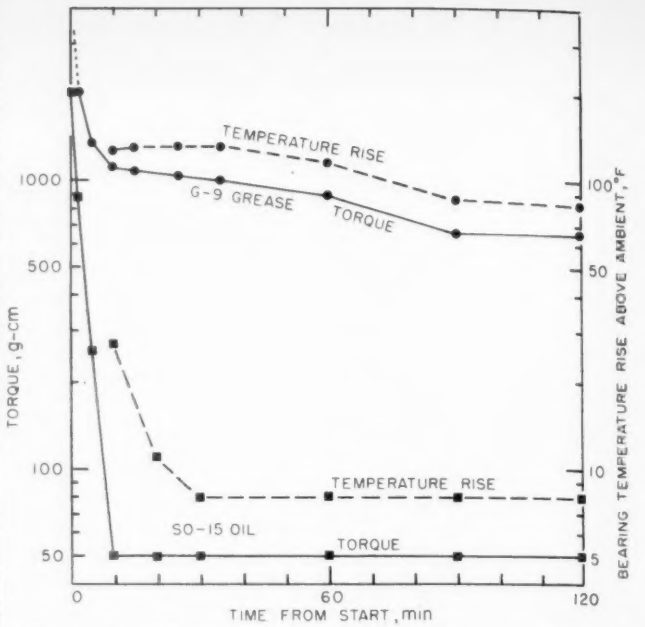

FIGURE 5. *Effect of time on frictional torque and bearing temperature rise, at −75° F ambient temperature for a MIL–G–3278-type grease and SO–15 oil, with 20-mm bore ball bearings, at 10,000 rpm.*

The temperature rise data for each bearing (not including data for the very rapid rise occurring during the first few minutes) are given also in figure 5. After 2 hr of operation the torque with grease G–9 was about 13 times greater than the torque with oil SO–15. Except for starting with less difficulty, the torque with grease G–8 was similar to that for G–9 during the first hour, at 90 min it varied from 353 to 2,270 g-cm, and at the end of 2 hr it was 1,010 g-cm.

Torque and temperature rise data were obtained in a similar manner at 10,000 rpm with greases G–11, G–12, G–14a, and G–15. These data for G–11 and G–12 (ASTM greases used in ASTM study of slow-speed torque at −65° F) and for G–14a (a commercial low-temperature silicone grease) are given in figure 6. The data obtained with sample G–15 (MIL–G–7421) were very similar to the curves given for G–11. After 2 hr of operation at 10,000 rpm for greases G–8, G–9, G–11, G–12, and G–15, at −75° F ambient temperature the values of torque were in the range from 630 to 1,010 g-cm; but with grease G–14a the torque of 63 g-cm was nearly as low as the 50 g-cm obtained with SO–15 oil under these conditions (see fig. 5).

With grease G–13 the bearing could not be turned by hand at −75° F without bending the torque arm, and at −50° F the ½-hp motor could not start because of the high friction. The motor started the bearing at −10° F and during the first 20 min the torque at −10° F ambient temperature was similar to that for sample G–12 at −75° F ambient (in fig. 6), at 10,000 rpm; but after an hour of operation the torque dropped to 88 g-cm. After standing overnight, the bearing started easily at −10° F and during the next half-hour of operation the torque varied in the range from 88 to 252 g-cm.

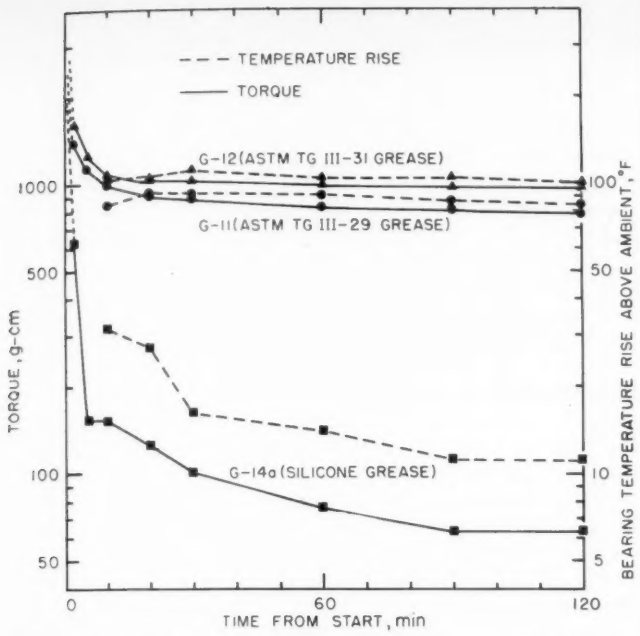

FIGURE 6. *Effect of time on frictional torque and bearing temperature rise, at −75° F ambient temperature for 2 ASTM greases and a silicone grease, with 20-mm bore ball bearings, at 10,000 rpm.*

In connection with investigating the effect of the sulfurizing treatment of the M–2 high-speed tool steel bearings, frictional data were obtained with two unlubricated sulfurized bearings and with untreated dry bearings made of M–2 steel and 52100-type steel. These data were obtained in the manner described for the data in tables 4 to 7, at room ambient temperature. The friction data for these unlubricated bearings are given in table 8, which includes some data from tables 4 and 7 for lubricated bearings for comparison. At speeds up to 1,000 rpm with this low load (4 lb) the friction with the sulfurized bearing is higher than with the greased bearing and much higher than with the oiled bearing and the dry untreated bearing.

Examination with a 10-power stereomicroscope indicated that the surfaces of the sulfurized balls and races were rougher than the untreated balls and races, and this probably accounts for the relatively high friction. This is in agreement with the paragraph under table III of U.S. Patent No. 2,707,159, covering sulfurizing processes. In table 4, the bearing which gave excessive torque after 8 min at 4,900 rpm had been sulfurized before assembly of the balls and separator. The other sulfurized bearing was treated after it had been assembled.

4.3. Miscellaneous Tests and Results

a. Air-Driven Gyro Tests

Tests were made with the modified air-driven gyro, with 10-in. Hg air pressure, in an oven at controlled temperatures, with filtered air going through a coil of copper tubing for preheating the air. Tests with an air-driven gyro at high temperatures are more severe than with an electric motor, because of the greater evaporation and oxidation of the lubricant,

TABLE 8. *Frictional torque for 20-mm bore ball bearings, with 4-lb radial load, 80° F nominal ambient temperature*

Speed	Time at each speed	Torque, g-cm						
		52100-type steel bearings				M–2 tool steel bearings		
		Synthetic oil	MIL-G-3278 Grease	Dry		Dry	Dry, sulfurized	
rpm	*min*							
10	1	10	99	12	16	12	32	32
10	10	10	45	12	16	12	32	32
100	1	11	72	12	16	14	40	48
100	10	10	29	12	16	16	48	56
500	1	21	48	10	16	16	54	59
500	10	21	32	10	16	16	63	68
1,000	1	35	64	12	21	18	68	68
1,000	10	35	48	12	32	27	72	68
2,000	1	72	90	18	45	32	90	101
2,000	10	67	90	18	504	36	99	101
4,900	1	149	378	36	------	90	202	252
4,900	10	136	328	36	------	252	227	[b]
8,500	1	95	504	68	------	378	302	--------
8,500	10	81	227	[a]	------	428	353	--------
10,000	1	----------	----------	------	------	504	378	--------
10,000	10	----------	----------	------	------	630	504	--------

[a] Seized in 7 min, severely scuffed, broke torque arm.
[b] Very high torque in 8 min; no scuffing observed, bent torque arm.

resulting from the large volume of hot air blown past the bearings. In this gyro, the shaft is fixed and the bearing outer races rotate with the rotor. An aluminum alloy cage was made such that it enclosed a felt pad wrapped around the shaft, and two small holes at each end of the cage allowed oil to bleed to the inner races of the bearings. Tests were made with 22-hr runs and shutdown periods as described for the tests on the endurance testing machines. Polyester felt pads were used, saturated with about 1.0 g of oil. In one test the alloy cage was omitted and the felt was fitted inside the brass sleeve used for spacing the outer ball races and hence rotated with the rotor.

The data for the tests with the air-driven gyro are summarized in table 9. At 250° F the endurance

TABLE 9. *Ball bearing endurance tests in air-driven gyro, 20,000 rpm nominal speed, 5-mm bore*

Ambient temperature	Lubricant	Bearing	Separator material	Hours run before failure
° *F*				
250	G–9	S34–5–SS	Stainless steel	220
250	SO–15	S34–5–SS	Stainless steel	22
250	SO–15	N.D. 5	Chrome-plated brass	23
250	SO–15	N.D. 5	Chrome-plated brass	94
250	SO–15	N.D. 5	Teflon-coated brass	20
250	SO–15	N.D. 5	No. 220 filled Teflon [a]	22
250	SO–15	N.D. 5	No. 206 filled Teflon [a]	110
250	SO–15	N.D. 5	10 balls filled raceway	66
250	SO–15	34–5B	Phenolic composition	378
250	SO–15	34–5B	Phenolic composition	[b] 307
250	SO–17	N.D. 5	Teflon-coated brass	7
325	SO–15	N.D. 5	Teflon	22
325	SO–16	N.D. 5	No. 206 filled Teflon [a]	22
325	SO–17	N.D. 5	Asbestos-phenolic	22
325	SO–17	34–5B	Phenolic composition	33

[a] See reference [8] for descriptions of No. 206 and No. 220 filled Teflon.
[b] The oil-soaked felt was installed in the rotating brass sleeve used for spacing the outer ball races instead of in the stationary alloy cage used in the other tests.

(378 hr) with the commercial phenolic composition separator was much better than with any of the other separator materials in the oil-prelubricated bearings. With the stainless steel separators the endurance with grease G–9 (220 hr) was much better than with SO–15 oil (22 hr). In the 4 tests at 325° F, the endurances (33 hr maximum) were very short with the lubricants and separators that were tried.

b. Small Direct-Current Motor Tests

Endurance tests were made with bearings in the 27-v, d-c, 11,000-rpm motors. Three tests were made with motors having their shafts connected to shafts of other motors modified to act as generators, with a resistor connected to the generator lead wires adjusted to load the driving motors to a nominal speed of 11,000 rpm. During the tests each motor-generator unit was installed in an aluminum box, 6 in. by 6 in. by 12 in., with a transite base and a clear plastic front, to simulate installation in a closed compartment. No heat was provided except that from the test units, and no provision was made for controlling the temperature. After warm-up during the first hour of each 22-hr period of operation, in general the air temperature inside the box ranged from 150° to 200° F and the temperature inside the motor case ranged from 200° to 250° F. Failure to restart or continue running with a 5-amp fuse in the circuit was used as a criterion for a bearing failure; ordinarily, the motors started and continued running with a 3-amp fuse.

In test DCMG–1, the original SS77034 bearings as received, prelubricated with G–14 silicone grease, were tested in a motor-generator unit in the box. After 245 hr of operation the bearing at the brush end of the generator failed by seizure.

In test DCMG–2, one of the metal shields was removed from each of the SS77034 bearings and the bearings were cleaned with solvents. The motors were modified slightly at each end to accommodate aluminum alloy cups containing oil-soaked polyester felt pads. SO–15 oil was used in the felts and bearings. After 61 hr of operation the bearing at the brush end of the generator failed because of excessive wear of the separator.

In test DCMG–3, operation of the motor used in test DCMG–2 was continued. The generator was fitted with new Q34 ball bearings having phenolic-fabric separators, with SO–15 oil in the felts and bearings. After 780 hr (including 61 hr in previous test) the SS77034 bearing at the brush end of the motor failed because of a worn and broken steel separator. The Q34 bearings in the generator with 719 hr of operation did not fail, although under similar conditions the SS77034 bearing with the steel separator at the brush end of the generator failed in 61 hr.

Five tests were made with the 27-v, d-c, 11,000-rpm motors under no load conditions, at a nominal speed of 16,000 rpm. The motors were operated in the enclosed box described for the motor-generator tests.

In test DCM–1 with the original SS77034 bearings as received, prelubricated with G–14 silicone grease, the bearing at the shaft (output) end failed by seizure after 84 hr of operation.

In test DCM–2, a motor was fitted with Q34 bearings having phenolic-fabric separators, with SO–15 oil in the felts and bearings. The bearings did not seize, but inspection at 2,237 hr of operation disclosed excessive wear of the separators.

In test DCM–3 with the original SS77034 bearings as received, prelubricated with G–14 silicone grease, the bearing at the shaft end failed and caused stoppage because of very high friction after 173 hr of operation.

In test DCM–4, as received (same as in tests DCM–1 and DCM–3), the bearing at the shaft end caused stoppage after 264 hr of operation.

In test DCM–5, Q34 bearings were fitted and lubricated as in test DCM–2. They were inspected after 1,743 hr of operation. The separators were worn and the test was discontinued, but probably operation could have been continued to a total of 2,000 hr.

In these tests with d-c motors, the operation was interrupted frequently because of difficulties other than bearing failure. These difficulties included brush wear, brushes sticking in holders, brush "pigtail" wire stiffness preventing brush movement to compensate for wear, breaking of "pigtail" wires, and melting of solder joints.

Starting tests were made with the 27-v, d-c motors in a low-temperature cabinet, at −76° F (−60° C), after storage for 18 hr and again after storage for 42 hr.

With a motor as received, factory prelubricated with G–14 silicone grease, there was no difficulty in starting at −76° F with a 3-amp fuse.

With the motor used in test DCM–2, prelubricated with SO–15 oil, after 500 hr of operation (in test DCM–2), there was no difficulty in starting at −76° F with a 3-amp fuse.

A motor freshly prelubricated with SO–15 oil (later used in test DCM–5) would not start after 18 hr at −76° F with a 3-amp fuse, but started with a 5-amp fuse. After 24 more hr (42 hr total) at −76° F the motor started with a 3-amp fuse. However, after running 3 hr at room temperature, the results of a test after 18 hr at −76° F were the same as before the 3-hr run-in at room temperature.

c. Service Test in ½-hp Motor

Size 202KTT bearings fitted with polyester felt rings, prelubricated with SO–15 oil, were installed in a ½-hp, 3,450-rpm motor used for driving one of the endurance testing machines. These bearings were functioning normally after 4,200 hr of operation at the conclusion of the project.

5. Conclusions

Polyester felt pads saturated with SO–15 oil (see table 1 for composition) may be incorporated in prelubricated ball bearings to provide satisfactory operation in the temperature range from −75° to

+325° F, with type 204KTT bearings and probably with bearings having bores ranging from 10 to 35 mm. Endurance with bearings prelubricated in the above manner is comparable with the high-temperature performance of MIL–G–3278 [1] grease at 250° F and MIL–L–3545 [2] grease at 300° F. Compared to MIL–G–3278 and MIL–G–7421 [3] greases, with the oiled bearings starting friction is low and running friction is about one-tenth of that of greased bearings.

Although it is not feasible to incorporate oiled felt pads in small instrument bearings (less than 10-mm bore) of conventional width, oiled pads may be installed in instruments (or motors) to provide oil prelubrication for the bearings.

Although Teflon felt may be used for ambient temperatures up to 450° F and glass felt may be used for much higher temperatures, none of the high temperature oils were satisfactory for prelubrication at 450° F ambient temperature.

Excessive wear occurred with unlubricated high-speed tool steel bearings when operated at 5,000 rpm in a 650° F ambient temperature, but operation with these unlubricated bearings could be satisfactory for very short periods in special applications.

The major cause of failure in endurance tests with the bearings prelubricated with oil-soaked felt pads was breakage or wear of the separators. Improvements in separators could greatly increase the endurance life of oil-prelubricated ball bearings.

The modified air-driven gyro may be useful for evaluating lubricants for high-speed instrument ball bearings at high temperatures. It is being tried by other laboratories for this purpose in connection with efforts of the Coordinating Research Council to develop a test method for instrument-bearing lubricants. Advantages are the ease of detection of bearing failure (indicated by stoppage or reduced speed) and the absence of other components which may fail, especially at high temperatures. The high air velocity increases the evaporation and oxidation of the lubricant. While this shortens the test, the air environment is not typical of enclosed ball bearings in most service applications.

Low-temperature torques of ball bearing greases determined for starting and running at 1 rpm as in ASTM Tentative Method D1478–57T are not significant in predicting the starting and running torques at 10,000 rpm at −75° F ambient temperature. This conclusion is based, partly on data for the ASTM greases TG–III–29 and TG–III–31; from other laboratories the torque with TG–III–31 was nearly four times greater than with TG–III–29 by the ASTM method, but in figure 6 the torque data for these greases soon after starting at 10,000 rpm do not differ greatly. Also, data [9] from another laboratory show no correlation between results of torque tests by the ASTM method and the results of tests on actual aircraft accessory equipment.

The author is grateful for information and/or material samples received from the following:

The Fafnir Bearing Company
Bendix Aviation Corp. (Eclipse-Pioneer Div.)
E. I. duPont de Nemours and Company
Lehigh Chemical Company
Western Felt Works
Lubri-Case, Incorporated
The Drever Company
Continental-Diamond Fibre Corporation
Hooker Electrochemical Co. (Durez Plastics Div.)
General Electric Company
American Felt Company
Kearfott Company, Inc.
Industrial Tectonics, Inc.
Coordinating Research Council
Wright Air Development Center
U.S. Naval Engineering Experiment Station
Naval Research Laboratory

6. References

[1] MIL–G–3278 Military Specification: Grease; aircraft and instruments (for low and high temperatures).
[2] MIL–L–3545 Military Specification: Lubricating grease; high temperature.
[3] MIL–G–7421 Military Specification: Grease; extreme low temperature.
[4] H. S. White, J. F. Swindells, and H. V. Belcher, Oil-soaked felt-pad lubrication of ball bearings at high speed and high temperature, Lubrication Eng. **11,** 182 (1955).
[5] MIL–L–7808 Military Specification: Lubricating, gas turbine, aircraft.
[6] 14L3c Navy Specification: Grease, ball and roller bearing (superseded by MIL–G–18709).
[7] MIL–G–25013 Military Specification: Grease, ball, and roller bearing, extreme high temperature.
[8] H. S. White, Small oil-free bearings, J. Research NBS **57,** 185 (1956) RP2709.
[9] E. A. Baniak and R. S. Barnett, (Beacon Laboratories, The Texas Company), Low-temperature operation of aircraft accessories, presented at ASLE meeting, April 1955.

Washington, D.C. (Paper 63C1–2)

Journal of Research of the National Bureau of Standards—C. Engineering and Instrumentation
Vol. 63C, No. 1, July–September 1959

Effect of Light and Water on the Degradation of Asphalt

L. R. Kleinschmidt* and H. R. Snoke

(April 14, 1959)

Coatings prepared from two blown petroleum asphalts in a thickness range of 0.002 to 0.04 inches were exposed to accelerated test conditions and outdoors. When exposed to light only, a surface film, insoluble in common asphalt solvents, was formed. The formation of this surface film was accompanied by a gain in weight of the coatings, apparently due to an oxygen pickup. This surface film retarded further degradation of the maltenes during the exposures made to light only. When the coatings were immersed in water after exposure, or sprayed with water during exposure, or exposed outdoors, they lost weight. These decreases in weight were found to be in part due to the extraction of water-soluble, light-degraded material. Their magnitudes were dependent upon the asphalt exposed, the thickness of the exposed coatings, and the exposure conditions. The relationship between the losses in weight and water-soluble material, when considered in conjunction with the oxygen content of the asphalts and the water-soluble materials, indicated that volatile degradation products were also formed.

When the surface skin formed by the action of light was partially removed by washing with water, percentage decreases were noted in the water-white oils, dark oils, and asphaltic resins. Since these decreases were unequal in magnitude and since the losses in weight were dependent on the thickness of the coating, it was concluded that light-degradable components of the asphalt had migrated to the surface to replace degraded material that had been washed away.

1. Introduction

The National Bureau of Standards, in conjunction with the Asphalt Roofing Industry Bureau, [1] is engaged in a study of the constitution and degradation of asphalt. Papers published recently in connection with this work describe methods for the preparation of test specimens [1,2], [2] the behavior of asphalt coatings when exposed to various accelerated test conditions [3,4], a chromatographic method for separating asphalt into groups of distinctive components [5], a study of the water-soluble degradation products of asphalt [6], the effect of mineral additives on the durability of coating-grade asphalts [7], and changes in the components of asphalt during the blowing operation [8]. This paper deals with a photochemical reaction occurring at the surface of asphalt on exposure to light and a combination of light and water.

2. Materials

From the three basic asphalts described by Greenfeld [7], asphalts Nos. I and III were selected for this study because previous work had indicated that asphalts II and III behaved similarly and were more resistant to weathering than asphalt I.

Products [3] 1 of asphalts I and III, with softening points [4] of 189° and 190° F, and penetrations [5] of 28 and 22, respectively, were used for the outdoor exposures and are identified hereafter as asphalts I–1 and III–1. Products 4 and 5 of these asphalts, respectively, with softening points of 223° and 232° F, and penetrations of 17 and 16, respectively, were used for the accelerated weathering exposures and are referred to hereafter as asphalts I–4 and III–5.

3. Exposure Methods

Exposure specimens were prepared by the hydraulic press or spinning methods described in references [1] and [2]. The hydraulic press method was used to prepare the 0.025-in. coatings for studies of changes in components. All other specimens were prepared by the spinning method.

The physical characteristics of the accelerated weathering machines and the spectral distribution range of the light [6] from the arc lamp are described in *Tentative Recommended Practice for Accelerated Weathering Test of Bituminous Materials*, A.S.T.M. Designation D529–39T. The drums holding the specimens revolved at the rate of 1 rpm. The spray units consisted of 4 mist-type spray jets, equally spaced on a vertical feeder. The spray units delivered approximately 20 gal/hr of demineralized water at a temperature of 77° ±3° F.

The exposure conditions, cycles 1 to 4, are outlined in table 1. The outdoor exposures were made on the roof of the Industrial Building, National Bureau of Standards, Washington, D.C. The specimens were exposed on racks at an inclination of 45 deg, facing south.

---

* Deceased.

[1] An association of manufacturers of roofing materials that has supported research at NBS under the Research Associate Plan for more than 30 years.

[2] Figures in brackets indicate the literature references at the end of this paper.

[3] An asphalt product is defined [7] as an asphalt blown to a desired softening point.

[4] Softening Point, Ring and Ball, A.S.T.M. Method D36–26.

[5] Penetration of Bituminous Materials, A.S.T.M. Method D5–52.

[6] Light as used in this paper refers to the radiant energy from a low-intensity, enclosed carbon arc light.

TABLE 1. *Accelerated exposure cycles*

Cycle	Light only [1]	Light and water spray [2]	Water spray [2] only	Water immersion [3]	No treatment [4]
	hr	*hr*	*hr*	*hr*	*hr*
1	20				4
2		21 [5]			3
3	22			1	1
4	20		1		3

[1] Temperature of specimens, 140°±3° F.

[2] The spray unit consisted of four mist-type spray jets, equally spaced on a vertical feeder. The spray jets delivered approximately 20 gal of water at a temperature of 77°±3° F each hour. Each specimen was directly under the spray jets for about 2 sec each minute of the spray periods.

[3] One gallon of distilled water used as the immersion bath for each set of eight test specimens for each 240-hr exposure period.

[4] Ambient conditions, approximately 80° F.

[5] The specimens were exposed for 51 min to light only, followed by a 9-min exposure to light and water each hour.

4. Procedures and Results

4.1. Accelerated Exposures

a. Light, Cycle 1

During the first 20 hr of exposure to light only, there were formed on the exposed surfaces of the coatings thin, continuous films of material insoluble in carbon tetrachloride, chloroform, and benzene, in which the unexposed asphalts were soluble.

Figure 1 illustrates the appearance of a specimen prepared from asphalt I–4, in a coating thickness of 0.012 in., which had been exposed to 120 hr of cycle 1. A metal shield held ¼ in. from the coating protected the lower half of the specimen from light during its exposure.

Four specimens prepared from asphalt I–4 in a coating thickness of 0.012 in. were exposed for 24, 48, 96, and 140 hr. After exposure the coatings were removed from the aluminum panels by digesting the specimens in *n*-pentane. The *n*-pentane-insoluble material from the coatings was recovered by filtration, using a porcelain bitumen crucible with an asbestos mat. This *n*-pentane-insoluble material when washed with chloroform yielded small amounts of insoluble material. This insoluble material was yellowish-brown in color, sheetlike in form, and weighed 3.0, 2.7, 2.8, and 2.6 gr/ft [2], respectively. It contained 22 percent oxygen.[7]

FIGURE 1. *Coating of asphalt I–4, 0.012-in. thick.*
Light area exposed to 120 hr of cycle 1 (light only). Dark area masked.

Fifteen specimens prepared from asphalt I–4 in a coating thickness of 0.025 in. were exposed to cycle 1. Three specimens were removed and examined for changes in weight and distribution of components [5] after 240, 480, 720, 1,080, and 1,440 hr of exposure. These data, based on the weights of the unexposed coatings, are reported in table 2.

The refractive indices of the water-white and dark oils separated at the five intervals of exposure, reported in table 3, were determined with an Abbe-type refractometer for the wavelength of the sodium-D line.

TABLE 2. *Changes in weight and distribution of components of specimens exposed to cycles 1 and 3*

	Cycle 1								
Exposure, hr	0	240	480	720	1,080	1,440			
Gain in weight, % [1]		0.2	0.1	0.1	0.1	0.0			
n-pentane-insoluble material, %	41.8	45.9	46.8	46.4	47.1	47.8			
Water-white oils, %	27.4	24.1	23.8	23.8	23.8	24.1			
Dark oils, %	18.2	14.2	13.4	13.9	13.4	13.7			
Asphaltic resins, %	10.3	11.7	11.9	11.6	11.1	11.2			
Total recovery, %	97.7	95.9	95.9	95.7	95.4	96.8			
	Cycle 3								
Exposure, hr	0	216	432	648	984	1,296	1,874	2,736	3,816
Loss in weight, % [2]	0	1.1	3.1	5.9	9.7	12.9	17.5	20.7	24.4
n-pentane-insoluble material, %	41.8	46.9	48.5	48.7	48.7	48.9	48.7	47.6	47.0
Water-white oils, %	27.4	24.5	22.9	21.6	20.3	18.5	17.9	17.8	15.7
Dark oils, %	18.2	13.6	11.3	10.0	8.9	8.1	7.0	6.9	6.2
Asphaltic resins, %	10.3	11.4	11.4	10.6	9.6	9.1	8.0	6.2	6.2
Total recovery, %	97.7	97.5	97.2	96.8	97.2	97.5	99.1	99.2	98.5

[1] The gain in weight for the 240-hr exposure period was the average gain of 15 specimens. For each successive inspection period the gain in weight was the average gain of three fewer specimens than the previous period. The distribution of components reported for each exposure period was the average for three specimens.

[2] The loss in weight for the 216-hr exposure period was the average loss of 24 specimens. For each successive period the loss in weight was the average loss of three fewer specimens than for the previous period. The distribution of components reported for each exposure period was the average for three specimens.

TABLE 3. *Refractive indices of water-white and dark oils recovered from specimens exposed to cycles 1 and 3* [1]

Cycle 1			Cycle 3		
Exposure	Water-white oils	Dark oils	Exposure	Water-white oils	Dark oils
hr	*at 77° F*	*at 122° F*	*hr.*	*at 77° F*	*at 122° F*
0	1.4982	1.534	0	1.4982	1.554
240	1.4954	1.542	216	1.4969	1.554
480	1.4956	1.543	432	1.4952	1.548
720	1.4952	1.542	648	1.4940	1.537
1,080	1.4952	1.544	984	1.4932	1.535
1,440	1.4952	1.543	1,296	1.4924	1.533
2,040			1,874	1.4912	1.527
3,000			2,736	1.4892	1.522
4,200			3,816	1.4888	1.516

[1] Determined with an Abbe-type refractometer for the wavelength of the sodium-D line.

[7] Determined by Shigeru Ishihara, Research Associate, Asphalt Roofing Industry Bureau.

b. Light and Water Spray, Cycle 2

Figure 2 illustrates the appearance of a specimen which has been exposed to 120 hr of cycle 2. It had been prepared from the same asphalt and in the same coating thickness as that used in preparing the specimen which had been exposed to light only (fig. 1). The shield which protected the lower half of the specimen from light was mounted approximately ¼ in. from the coating, which permitted water to flow over the entire coating during the spray periods. Only the light activated portion of the coating was matted. No cracking or grooving occurred.

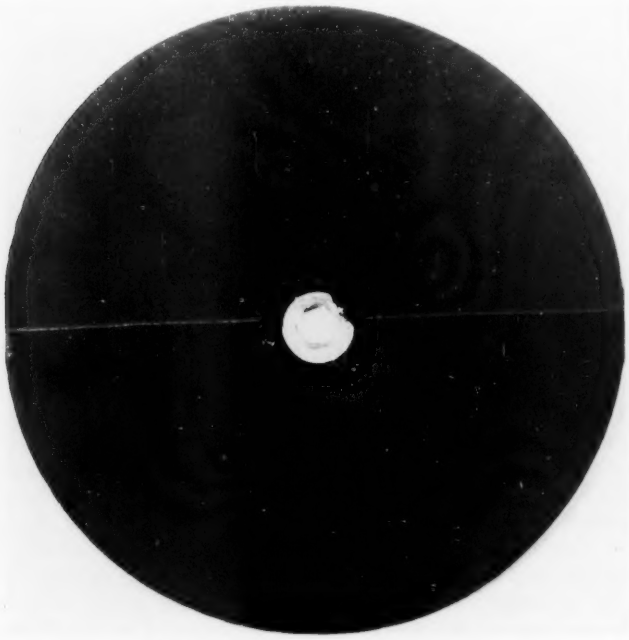

FIGURE 2. *Coating of asphalt I–4, 0.012-in. thick.*

Light area exposed to 120 hr of cycle 2 (light and water spray). Dark area masked from light, but exposed to water spray.

Figure 3 illustrates the losses in weight of 15 coatings of asphalt I–4 and 9 coatings of asphalt III–5, varying in thickness from 0.005 to 0.04 in., at selected intervals up to 1,440 hr of cycle 2.

c. Light and Water Immersion, Cycle 3

In table 4 are reported the losses in weight and the amounts of water-soluble degradation products recovered after 216, 432, 648, 984, and 1,296 hr of exposure to cycle 3, of eight specimens prepared from each of the Nos. I–4 and III–5 asphalts. The coatings ranged from 0.012 to 0.017 in. in thickness. One gallon of distilled water was used as the immersion bath for each set of eight test specimens for each 216-hr exposure period. The water-soluble materials leached from the coatings gave the immersion liquids a deep amber color, with only traces of suspended material. The *p*H of the immersion liquids at the end of the 984 to 1,296 hr exposure period was 3.18 for both asphalts I–4 and III–5.

TABLE 4. *Loss in weight and weights of recovered water-extracted degradation products formed on the exposure of asphalts I–4 and III–5 to cycle 3* [1]

Length of exposure	I–4		III–5	
	Loss in weight	Water extracted [2] material recovered	Loss in weight	Water extracted [2] material recovered
hr	*Grains/ft²*	*Grains/ft²*	*Grains/ft²*	*Grains/ft²*
216	7	10	12	14
432	32	31	28	27
648	54	54	41	41
984	76	71	61	----------
1,296	90	85	72	----------

[1] The loss in weight of the coatings and weights of the water-extracted material recovered were the averages of 8 specimens whose coating thickness ranged from 0.012 to 0.017 in.

[2] Oven-dried for 1 hr at 212° F before weighing.

The immersion liquids were filtered before being evaporated to dryness. The residues from these immersion liquids were oven-dried for 1 hr at 212° F before being weighed. After oven-drying, the residues were no longer completely soluble in water; they were, however, soluble in dilute alkali solutions. Direct oxygen determinations were made [7] on the water-soluble material formed during the 984- to 1,296-hr exposure period.

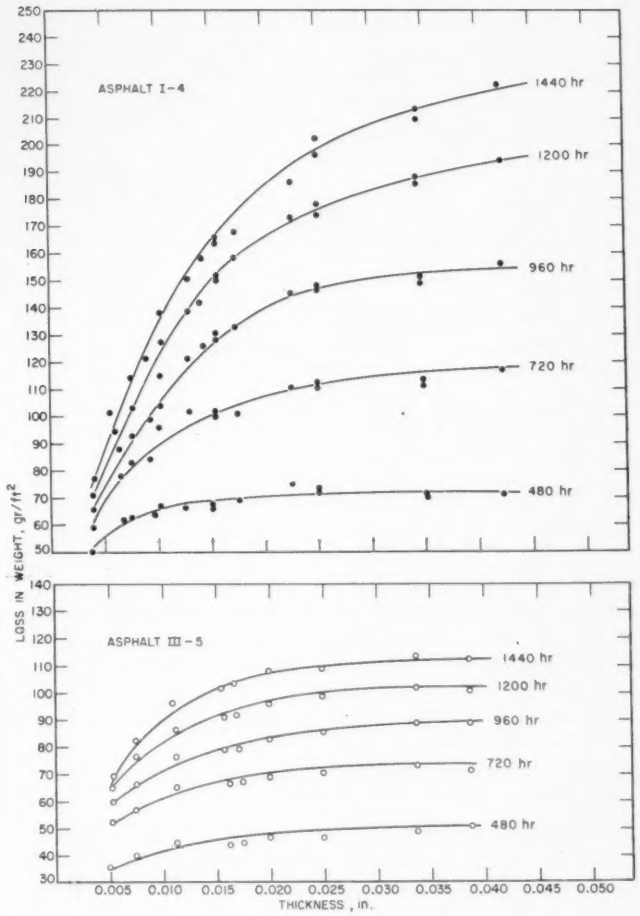

FIGURE 3. *Loss in weight of coatings prepared from asphalts I–4 and III–5 at 240-hr intervals of exposure to cycle 2.*

Twenty-four specimens prepared from asphalt I–4 in a coating thickness of 0.025 in. were exposed to cycle 3. Three specimens were removed and examined for changes in weight and distribution of components [5] after 216, 432, 648, 984, 1,296, 1,874, 2,736, and 3,816 hr of exposure. These data, based on the weights of the unexposed coatings, are reported in table 2. The refractive indices of the water-white and dark oils separated at the 8 intervals of exposure were determined with an Abbe-type refractometer for the wavelength of the sodium-D line and are reported in table 3.

d. Light, Followed by Water Spray, Cycle 4

In figure 4 are illustrated the losses in weight of four coatings each of asphalts I–4 and III–5, varying in thickness from 0.003 to 0.009 in., at selected intervals up to 1,920 hr of exposure to cycle 4.

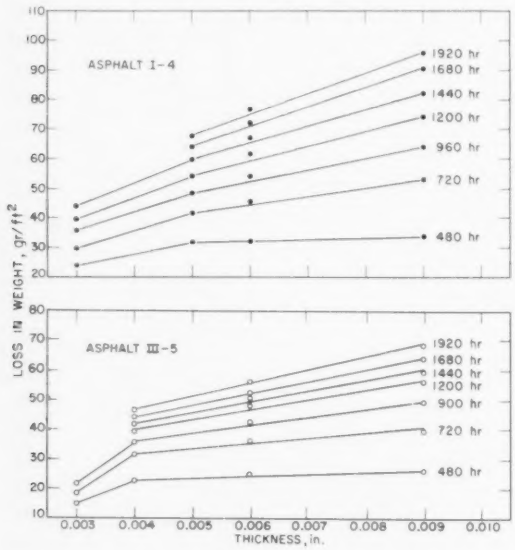

FIGURE 4. *Loss in weight of coatings prepared from asphalts I–4 and III–5 at 240-hr intervals to cycle 4.*

4.2. Outdoor Exposures

Figure 5 illustrates the losses in weight of 15 coatings of asphalt I–1 and 11 coatings of asphalt III–1, varying in thickness from 0.003 to 0.040 in., after 30 months of exposure outdoors in Washington, D.C.

5. Discussion of Results

5.1. Effect of Light Alone

It has been known for some time that asphalt exposed to light, in an oxidizing atmosphere, develops a thin surface film which is insoluble in common asphalt solvents such as chloroform, carbon tetrachloride, and benzene. Joseph N. Niepce [9] in 1816 reported that some natural asphalts became insoluble

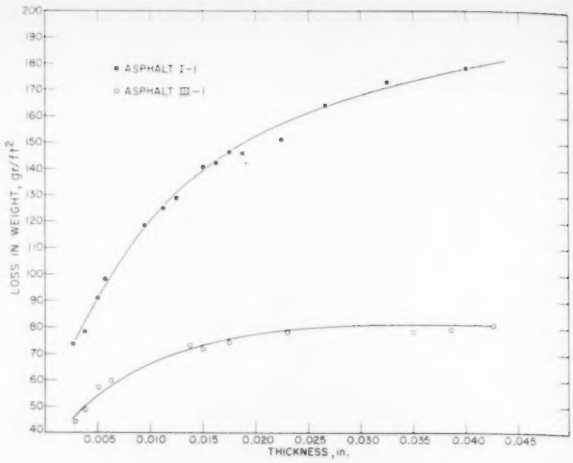

FIGURE 5. *Loss in weight of asphalt coatings prepared from asphalts I–1 and III–1 after 30 months of exposure outdoors.*

in certain asphalt solvents such as chloroform and carbon disulphide on exposure to light. This phenomenon has been used to a limited extent in photoengraving.

This surface film has been likened in its physical behavior to the film of tissue formed on the skin surface of a person who sunburns readily.

The surface film is apparently less ductile than the underlying asphalt and is therefore unable to follow the volume changes in the asphalt with changes in temperature. Consequently, after two or three cycles of 20 hr of light at a temperature of 140° F and 4 hr without light at approximately 80° F, the film cracked. During subsequent cycles the cracks widen and grooving occurs in the coating, giving it the appearance of the exposed coating in figure 1. A surface that is grooved deeply is described as "alligatored". With long-continued exposure this grooving will extend through the entire coating.

The gain in weight exhibited by the specimens exposed to light alone was mainly due to oxygen pick-up in the formation of light-degraded, water-soluble materials.

5.2. Effect of Light and Water

In 1936, Strieter and Snoke [10] demonstrated, by their exposures of asphalts in sealed tubes, that both oxygen and light were necessary for that part of the degradation process which resulted in the formation of water-soluble materials. They reported that the water-soluble materials were in part ketonic acids and that they reduced Fehling's solution. Evidence of the formation of water-soluble degradation products in outdoor exposures is found in the discoloration of standing water on roofs surfaced with asphalt, and its acidic nature is shown by the etching of metal flashings and gutters used with such roofs.

A part of the surface film insoluble in common asphalt solvents formed by the action of light on asphalt surfaces is soluble in water. Consequently, when this material is removed, either by spraying

with water or by immersing the specimen in water, no grooving of the coating occurs. Instead, the surface assumes the matte appearance shown by the light-exposed section of the specimen shown in figure 2.

a. Relation Between Loss in Weight and Water-Soluble Material Recovered

The data in table 4 show that the amount of water-soluble material recovered from asphalt coatings of approximately the same thickness, after exposure to cycle 3, is roughly equivalent to the loss in weight of the specimens. The oxygen content of the unexposed asphalt was approximately 2 percent; that of the oven-dried, water-soluble residue was approximately 35 percent. This difference in oxygen content, considered in conjunction with the relatively close agreement between the weight loss and water-soluble material recovered, indicates that other degradation products, probably volatile in nature, accompanied the formation of the water-soluble degradation products. This is in keeping with the findings of Thurston and Knowles [11], who reported that carbon dioxide and water were liberated and oxygen was absorbed when asphalt components in an oxygen atmosphere, in sealed tubes, were exposed to sunlamps.

b. Relation Between Loss in Weight and Thickness of Coatings

All of the data collected on exposures of asphalt coatings to cycles 2 and 4 and outdoors (figs. 3, 4, and 5) show that, for equal periods of exposure, the loss in weight per unit area exposed increased as the thickness of the coatings increased, and varied with different asphalts. If weathering were a simple process of erosion, the loss in weight should be independent of the coating thickness, though differences among asphalts could be expected.

The greater loss in weight by the thicker coatings could be explained by light and oxygen penetration into the coatings if these penetrated readily. However, Pfeiffer [12] reported that the light intensity was reduced to about one percent at a depth of 50μ in a layer of bitumen and that oxygen diffuses into it at a very low rate.

It seems reasonable to assume that the conversion of light-susceptible material on the surface to water-soluble material, and the loss of this material by washing, would tend to unbalance the distribution of components in the system. Migration of components in an attempt to restore equilibrium would follow. Since the thicker coatings contained more of the light-susceptible components, they would produce the greater losses in weight on long exposure.

Migration of components within an asphalt has been recognized previously. Federal Specification SS–A–666, *Asphalt for Built-up Roofing, Waterproofing and Damp-proofing*, issued in 1933, contains a requirement that when freshly melted asphalt is stored for one week in a closed container "its surface shall not become dull or show any separation of oil, grease, paraffin scale, or similar material". The American Society for Testing Materials has published "*Tentative Method of Test for Staining Properties of Asphalts*" (*Modified Pressure Method D1328*), to determine the tendency of oils to exude from asphalts. Oliensis [13] in his book, *Exudation and Allied Reactions Between Bitumens* discusses the movement of the maltenes within and between asphalts.

c. Effects of Exposure to Light and Light and Water on the Distribution of Components

Specimens prepared from asphalt I–4 in a coating thickness of 0.025 in. behaved similarly to the thinner coatings as regards gains in weight and the formation of the surface skin when exposed to light only.

Significant gains in weight and changes in percentage distribution of components were found only during the first 240 hr of exposure to light. Similarly, it was only during that period that decreases were found in the refractive indices of the water-white and dark oils. Specimens examined after 480, 720, 1,080, and 1,440 hr of exposure showed no appreciable changes in the percentage distribution of components, gains in weight, or changes in the refractive index of water-white and dark oils over those noted for the 240-hr exposure period. The surface skin formed during the initial period of exposure apparently served as a shield to prevent further degradation of the coating by light.

Losses instead of gains in weight were found during the first 216 hr of exposure to light and water. During this period the changes in the percentage distribution of components were essentially the same as those noted during the initial period of exposure to light only. However, after this period, the effects of water in conjunction with light became more and more apparent.

Specimens exposed to cycle 3 showed progressive increases in loss in weight and decreases in the percentage of water-white and dark oils at the 432-, 648-, 984-, 1,296-, 1,874-, 2,736-, and 3,816-hr exposure intervals. Progressive decreases occurred in the percentages of asphaltic resins after the 432-hr exposure period. Refractive indices of the water-white and dark oils also showed progressive decreases during the long exposure. After the 216-hr exposure, the percentage of matter insoluble in *n*-pentane remained essentially constant.

The lack of change in the percentage of matter insoluble in *n*-pentane and the progressive loss in weight of the other components can be taken as further proof of the migration hypothesis described under 5.2.b. Relation Between Loss in Weight and Thickness of Film.

Assuming a gel or sol structure for the asphalt, either structure would permit free movement of the maltenes. Degradation of the maltenes at the surface and removal of the light-degraded material by washing would unbalance the system. In an attempt to restore equilibrium, light-susceptible materials would move to the surface to replace those degraded and removed.

The unequal percentage decreases of the water-white and dark oils and asphaltic resins indicated a selective rather than an overall degradation of these components. A selective degradation of water-

white and dark oils is indicated also by the progressive decrease of the refractive index of the oils recovered from coatings exposed to cycle 3. Oils recovered from coatings exposed to cycle 1, light only, showed no appreciable change in refractive index after exposure for 240 hr.

6. Conclusions

Asphalt coatings exposed to radiant energy from the enclosed, low-intensity carbon arc lamp gained weight during the early periods of exposure. The gain in weight was accompanied by the formation of a thin surface film insoluble in solvents that are normally used to dissolve asphalts. This surface film, isolated with *n*-pentane and chloroform, was sheetlike and yellowish-brown in color and contained approximately 22 percent oxygen.

Water-soluble material was recovered from coatings on which the surface film had formed. The water-soluble material contained 35 percent of oxygen; the original asphalts approximately 2 percent, indicating that the film formation was a light-induced oxidation reaction, which would account for the gain in weight of the coatings exposed to light only. The close agreement between the amounts of water-soluble materials recovered and the loss in weight of the coatings, when considered in relation to the oxygen content of the asphalts and the water-soluble degradation products, indicated that volatile degradation products were also formed.

The loss in weight resulting from the exposures to combinations of light and water, either by accelerated or outdoor exposure, was dependent upon the asphalt exposed, the exposure conditions and the thickness of the exposed coatings. The actual loss in weight of the coatings increased as the coating thickness increased.

The percentages of *n*-pentane-insoluble material determined during the exposures of the specimens to light and water in cycle 3, when considered in conjunction with the weight losses, indicated a gel or sol structure of the coatings through which the maltenes could migrate. When light-susceptible components at the surfaces of the coatings were degraded by light and oxygen and removed as water-soluble material, the structure of the coatings became unbalanced. To restore an equilibrium in the coatings, certain components of the maltenes migrated toward the surfaces of the coatings. The differences in the percentage decreases in the water-white oils, dark oils and asphaltic resins indicated a different rate of migration of these components rather than an overall degradation. The refractive indices determined on the water-white and dark oils recovered from the specimens which had been exposed to cycle 3 showed progressive decreases which indicated also a selective degradation within these two groups of components.

The authors are indebted to S. H. Greenfeld, J. P. Falzone, and S. Ishihara, research associates for the Asphalt Roofing Industry Bureau, for the preparation and exposure of the 0.025-in. thick coatings used in the component studies and the stimulating discussions that helped to develop many of the concepts proposed in this paper.

7. References

[1] S. H. Greenfeld, A method of preparing uniform films of bituminous materials, Am. Soc. Testing Materials Bull. **194,** 50 (1953).
[2] L. R. Kleinschmidt, Preparation of bituminous films by spinning, Am. Soc. Testing Materials Bull. **193,** 53 (1953).
[3] S. H. Greenfeld, Effects of thermal shock on the durability of asphalt coatings under accelerated test, Am. Soc. Testing Materials Bull. **193,** 46 (1953).
[4] L. R. Kleinschmidt and S. H. Greenfeld, Influence of exposure conditions on the accelerated durability testing of asphalt, Am. Soc. Testing Materials Bull. **213,** 69 (1956).
[5] L. R. Kleinschmidt, Chromatographic method for the fractionation of asphalt into distinctive groups of components, J. Research NBS **54,** 163 (1955) RP2577.
[6] Alan Schriesheim and S. H. Greenfeld, Water-soluble degradation products of asphalt, Am. Soc. Testing Materials Bull. **220,** 43 (1957).
[7] S. H. Greenfeld, Effect of mineral additives on the durability of coating-grade roofing asphalts, NBS Building Materials and Structures Report 147 (1956).
[8] L. R. Kleinschmidt and H. R. Snoke, Changes in the components of asphalt during the blowing operation, J. Research NBS **60,** 169 (1958) RP2835.
[9] F. Elder, Geschichte der Photographie (1905).
[10] O. G. Strieter and H. R. Snoke, A modified accelerated weathering test for asphalts and other materials, J. Research NBS **16,** 481 (1936) RP886.
[11] R. R. Thurston and E. C. Knowles, Asphalt and its constituents, oxidation at surface temperatures, Ind. Eng. Chem. **33,** 320 (1941).
[12] J. P. H. Pfeiffer, The properties of asphaltic bitumens, 1st ed. Elsevier Publishing Co., Inc., New York, N.Y. (1950).
[13] G. L. Oliensis, Exudation and allied reactions between bitumens (Forest Publishing Co., Forest Park, Ill., 1947).

WASHINGTON, D.C. (Paper 63C1-3)

Journal of Research of the National Bureau of Standards—C. Engineering and Instrumentation
Vol. 63C, No. 1, July–September 1959

Current and Potential Relations for the Cathodic Protection of Steel in a High Resistivity Environment

W. J. Schwerdtfeger

(March 23, 1959)

In order to evaluate potential and current criteria for the cathodic protection of bare low-carbon steel in a high-resistivity environment, specimens were exposed in the laboratory for a period of two months to a soil having a resistivity of about 20,000 ohm-centimeter.

Previous work in low-resistivity environments by the author and by other investigators has shown that corrosion can be reduced to a negligible degree by polarizing a steel structure to −0.85 volt (protective potential) with reference to a copper-copper sulfate electrode. In such studies by the author, cathodic polarization curves have also been shown to be useful in indicating the current density required for cathodic protection.

In the present study the above criteria were again evaluated. In addition to protecting the steel at the protective potential (free of IR drop), the effect on protection of including IR drop caused by the protective current was also noted. Also, cathodic polarization curves were obtained on a recorder in conjunction with a bridge circuit to eliminate the IR drop.

The results show that the best degree of protection was achieved on the specimen controlled at −0.77 volt (without IR) with reference to a saturated calomel half-cell. This is approximately equivalent to the protective potential −0.85 volt with reference to the copper-copper sulfate electrode. Applied current indicated by the break (change-in-slope) in the cathodic polarization curve agreed reasonably well with the actual current necessary to maintain polarization at −0.77 volt (free of IR).

The current required for protection was about three times the magnitude of the corrosion current; therefore, the corrosion reaction was either under anodic control (unlike previous studies) or an equivalent type of control which was caused by high resistance at anodic areas.

1. Introduction

Studies of cathodic protection previously carried out in the laboratory at the National Bureau of Standards were all conducted with soils and waters having resistivities less than 1,000 ohm-cm. The experiments showed that the protective potential −0.77 v with reference to the saturated calomel half-cell (equivalent to −0.85 v with reference to the copper–copper sulfate electrode), when free of IR drop caused by the protective current, was effective in preventing appreciable loss of metal on steel specimens [1,2].[1] Corrosion processes were found to be controlled chiefly by cathodic reactions, and cathodic polarization curves were shown to be very useful in indicating the currents necessary to produce adequate polarization and virtually complete protection.

It was suggested by Sudrabin and Ringer, [3] as a result of some of their recent work, that useful information would be obtained if studies were continued in high-resistivity environments where corrosion rates are controlled largely by electrolytic resistance, rather than by polarization alone. Further research was suggested by the National Association of Corrosion Engineers Unit Committee (T–2C) [4] on "Criteria for Cathodic Protection" under which some task groups have been assigned to: (a) Examine basic criteria that can be used for determining the adequacy of cathodic protection, or (b) promote research and technical papers on criteria for cathodic protection.

In high-resistivity environments in the field, measured potentials often include considerable IR drop as well as polarization voltage resulting from the protective current. As the IR drop caused by the applied current within the cathodic branch of a corrosion cell assists in reducing the corrosion cell current, the question arises as to what extent IR drop can be tolerated under practical circumstances, for example, in potential measurements made on pipelines.

Cathodic polarization curves are generally recognized as being useful in estimating the current density required for cathodic protection when corrosion reactions are controlled by cathodic polarization(cathodic control). However, there is a question regarding their usefulness when the corrosion current is determined mainly by anodic polarization (anodic control), or when the resistance of the electrolyte (high resistivity) is a limiting factor along with polarization.

The study to be described was conducted by exposing low-carbon steel specimens to a soil (sandy loam) having a resistivity of about 20,000 ohm-cm. In such a high-resistivity environment, it was presumed that the IR drop between the reference electrode and the specimen would probably be greater than the polarization voltage and thereby present the opportunity of evaluating the effect of each factor. Preliminary laboratory experiments revealed that cathodic polarization did not take place as readily as in low-resistivity environments and that the currents required for protection were larger than anticipated. This suggested a divergence from the usual cathodic type of control.

[1] Figures in brackets indicate the literature references at the end of this paper.

2. Experimental Procedure

2.1. General Procedures

All specimens were cut from one piece of cold-drawn steel tubing (1 in. o.d. by 0.125 in. wall thickness) to lengths of 8 in. The tubes were degreased with carbon tetrachloride and the ends rounded so as to be without burrs. The inner and outer surfaces of the tubes were wire-brushed, smoothed with 1G emery paper, washed in hot water, and then weighed to the nearest milligram. A rubber-covered stranded copper wire was soldered to one end of each specimen for the electrical connection. A coating of oil was flowed over the inside surface of each tube and both ends plugged with rubber stoppers. A heavy coating of bitumastic was applied over the edges of the tube, covering the wire and soldered connection, insuring a moisture seal around the stopper and leaving 24 in.^{2} of cylindrical surface for exposure to the soil.

The soil, a sandy loam from Lanham, Md., after being removed from the field, was air dried and sifted using a No. 10 sieve. Preliminary measurements of soil resistivity versus moisture content were made in order to determine a moisture range which provided a fairly stable soil resistivity without saturating the soil. A satisfactory amount of water was found to be about 15 percent by weight of the dry soil. By adding distilled water to the soil this moisture content resulted in a soil resistivity of about 20,000 ohm-cm at 80° F.

Five specimens were used in the experiment, two of which were without cathodic protection, serving as controls, while the other three had currents applied. Exposure to the soil was for a period of 61 days. Four Pyrex jars were used to hold the soil, the two controls being placed in one jar. The soil was moistened in four batches of equal weight, one batch for each jar. The wetting procedure was carried out by slowly adding water to the soil, mixing, adding more water, mixing again, et cetera.

A high-purity zinc rod (0.0375 in. diam by 10 in. long) was permanently exposed to the soil of each jar for use as a reference electrode. Continual or even intermittent ordinary use of an agar-salt bridge to a saturated calomel half-cell would have greatly lowered the soil resistivity. Thus, contact of the soil with an agar-salt bridge was limited to about 10 sec each day in order to measure the potential of the zinc electrode so that the specimen potentials, either measured or controlled, with reference to the zinc could be converted to the saturated calomel scale.

After 61 days of exposure to the soil the specimens were removed for cleaning and measurement of metal loss. The corrosion products, which were very adherent, were loosened by cathodic cleaning for 2 hr at a current density of 1 amp/ft^2 in a 10-percent solution of ammonium citrate neutralized with ammonium hydroxide. This was followed by scrubbing with a brass bristle brush under hot water. The oil preserved the inner surfaces of the tubes from corrosion. The soldered wire connection was removed by applying heat from a soldering iron and the last bits of solder were removed by scraping with a soft metal tool. Finally all specimens were again rinsed in hot water, blown dry with compressed air, and weighed.

2.2. Arrangement for Exposure

Cross-sectional views of the setup for exposure are shown in figure 1. Two cylindrical Pyrex jars were used, the inner one (8.75 in. o.d. by 10 in. high) containing the soil, steel specimen and auxiliary electrodes, and an outer jar (12 in. o.d. by 12 in. high) containing the smaller jar resting in distilled water about 1 in. deep. The outer jar was covered with a loose-fitting inverted pan which helped to control the moisture content of the soil and yet permitted entrance of air. Wires (not shown) from the specimen, zinc reference rod, and steel anodes were brought outside over the edge of the jar slightly tilting the cover as shown. These wires were fastened to the outer wall of the jar.

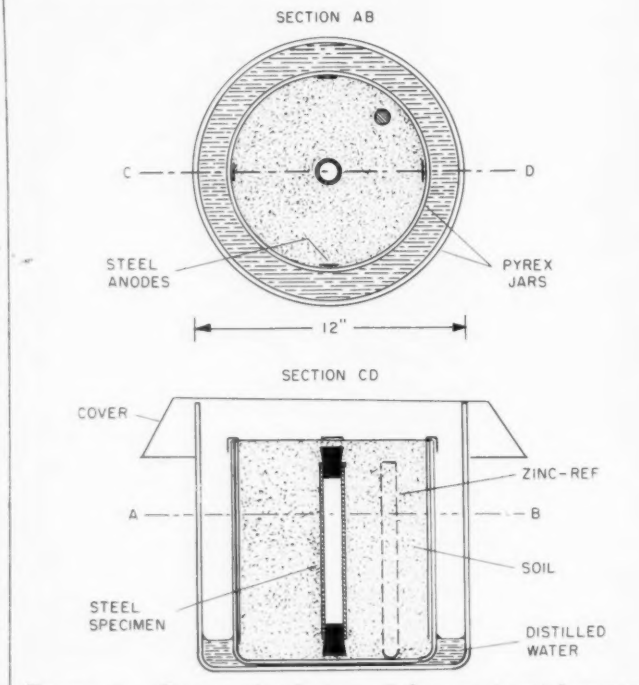

FIGURE 1. *Cross-sectional views of the experimental arrangement for exposing specimens to the soil.*

The specimen and the zinc rod were separated by about 2¾ in. of soil, with ½ in. of soil between the zinc and jar wall. Four anodes, consisting of strips of sheet steel (1.5 in. wide) running from top to bottom, were interconnected by soldered wires. The surfaces of the anodes adjacent to the glass were covered with insulating tape. Wet soil, prepared as previously described, was packed uniformly around the electrodes. As previously mentioned, the control specimens were both in the same jar. One was centrally located as shown in figure 1 and the other was in line with the center specimen and the zinc rod and on the side opposite the zinc rod. One

inch of soil separated the off-center specimen from the jar wall, the axes of the specimens being parallel to each other.

2.3. Instrumentation

Currents were applied to three of the specimens for the entire exposure period. The criterion of cathodic protection for the first specimen was the current adjusted in accordance with values from cathodic polarization curves obtained on the controls. The criterion of protection for the second specimen was the potential −0.77 v (reference saturated calomel electrode) free of *IR* drop. Protection of the third specimen was also based on the potential −0.77 v, except that the potential included the *IR* drop between the specimen and the reference electrode caused by the externally applied current.

The circuit used for obtaining polarization curves and for measuring potentials free of *IR* drops is shown in figure 2, the bridge being basically that described by Holler [5]. Resistors Q and D were each 100,000 ohms and the variable resistor, X, was used for balancing out the *IR* drop between the specimen and the reference electrode (zinc). When the bridge was balanced, the actual potential of the specimen was equal to twice the indicated or recorded value. A balanced bridge was indicated by no movement of the recorder pen when the current applied to a specimen was momentarily interrupted. Too small or too large a value of resistance X would cause the pen to suddenly shift in one direction or the other when the applied current was interrupted, but movement of the pen due to changes in polarization emf were relatively minor.

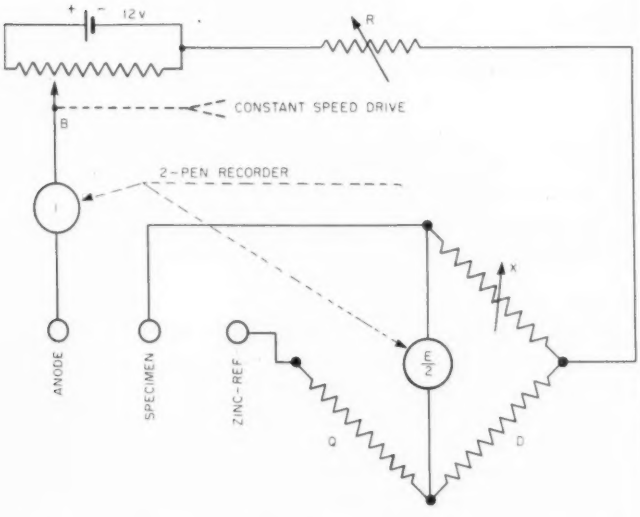

FIGURE 2. *Circuit for obtaining polarization curves automatically and for measuring potentials of specimens free of IR drops.*

One recorder pen indicated current and the other potential.

The procedure followed for measuring potentials (without *IR*) of the three specimens under protection was to first measure the current to a specimen and then, without interrupting the current, to transfer the specimen to the voltage supply associated with the bridge circuit, which was preadjusted to furnish the same current. Before reading the potential, the setting of resistor X was checked for bridge balance as described in the previous paragraph or by simply varying resistor X by fixed amounts, above and below the set value, until equal left and right deflections of the potential pen were in evidence.

Cathodic polarization curves were recorded automatically for all specimens on the second and final days of exposure. Both cathodic and anodic polarization curves were recorded on the controls at about weekly intervals throughout the exposure period. The polarizing current was varied from zero to a suitable value by linear increments of voltage from a 10-turn voltage divider, shunted across a 12-v storage battery (fig. 2) and driven by a synchronous motor. The rate of polarization could be adjusted by the resistor R, the total polarizing time usually being about 20 min.

The specimen under current control was protected with current from a 22.5-v heavy duty dry battery in order that any change in potential of the specimen would make no appreciable change in the current. A series resistance was used for adjusting the current.

The circuit used for controlling the specimen potential at −0.77 v (free of *IR*) is shown in figure 3. It utilizes the bridge circuit just described in conjunction with an electronic balancing unit used previously [2]. The control voltage, A, was adjusted to a value equal to one-half the difference between the potential of the zinc reference electrode and the protective potential for steel. Although the balancing unit was very sensitive to a potential difference across its terminals PS, the accuracy with which the potential of the specimen was actually maintained was obviously also dependent upon two other factors, namely: the stability of the potential of the zinc rod and the actual electrolytic resistance between the specimen and the zinc rod which was presumably balanced out by the variable resistance X. These two factors did change, but the changes were gradual and were not difficult to cope with. Nevertheless, they did limit the accuracy of the potential measurements to perhaps ±20 mv. The applied current was continuously recorded by R (fig. 3).

Figure 4 shows the circuit used for controlling potential at −0.77 v (including *IR*). It is the same as figure 3, except for the elimination of the bridge circuit. Control voltage A was adjusted to a value equal to the difference in potential between the zinc electrode and the protective potential for steel. Control accuracy here depended chiefly on the stability of the zinc potential and was about ±10 mv.

Currents and potentials were measured daily or less frequently. First, in addition to continuously recording the applied current to the specimen held

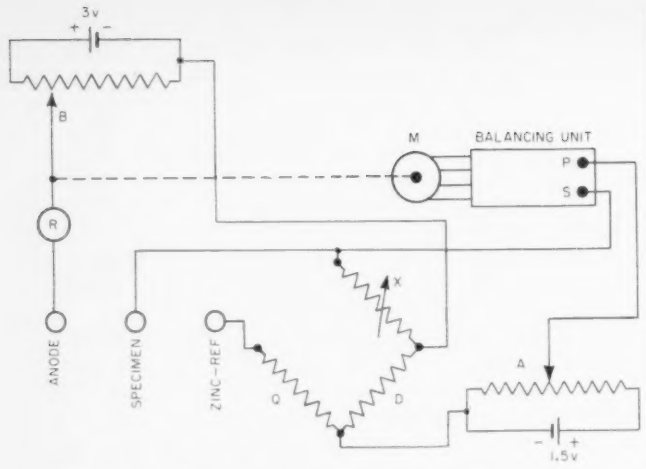

FIGURE 3. *Potential control circuit and bridge circuit for balancing out the IR drop between the specimen and the associated zinc reference electrode.*

The control voltage, A, was based on the protective potential of the specimen and on the potential of the zinc referred to saturated calomel.

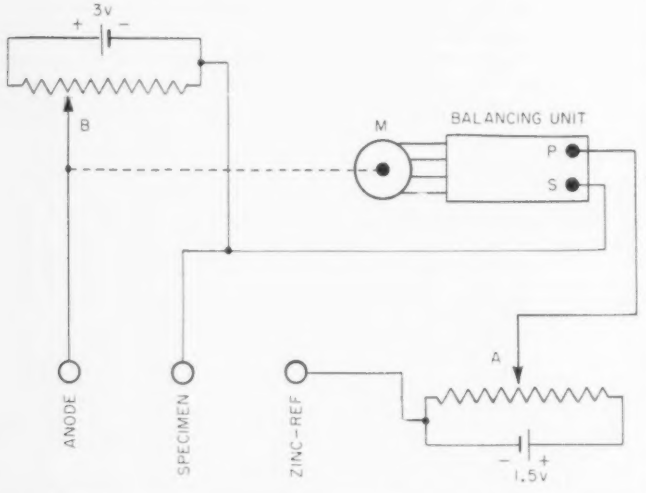

FIGURE 4. *Potential control circuit used on the specimen where the IR drop between it and the zinc reference electrode was included.*

The control voltage, A, was based on the protective potential of the specimen and on the potential of the associated zinc referred to saturated calomel.

at −0.77 v (free of *IR*), currents were measured with an indicating milliameter inserted without interrupting the circuits. Next, potentials between the specimens and the zinc electrodes were measured with an indicating potentiometer, *IR* drops caused by applied currents being included. This was followed by measuring the same potentials (without *IR*) by use of the bridge circuit as previously described. Finally, the potentials of the zinc rods were measured with reference to a saturated calomel half-cell. The potentials of the specimens were then converted to the saturated calomel scale and adjustments were made on the control potentiometers, if necessary.

3. Data and Discussion

For the first two days of exposure all specimens were allowed to corrode freely. On the second day, cathodic polarization curves were obtained on one of the controls and on the three specimens subsequently to be placed under cathodic protection. At this time, an anodic polarization curve was also obtained on the same control, with substantially no polarization in evidence. The cathodic curves are shown in figure 5, plotted on semilogarithmic coordinate paper in order to aid in estimating the change-in-slope point (hereafter designated as I_p) indicated by the intersecting straight lines. Similarly, figure 6 shows the cathodic polarization curves obtained on control specimen No. 1 at intervals throughout the exposure period. Those for control specimen No. 2 were similar. Hereafter, the currents from these curves and all other measured currents are expressed as current densities in milliameters per square feet.

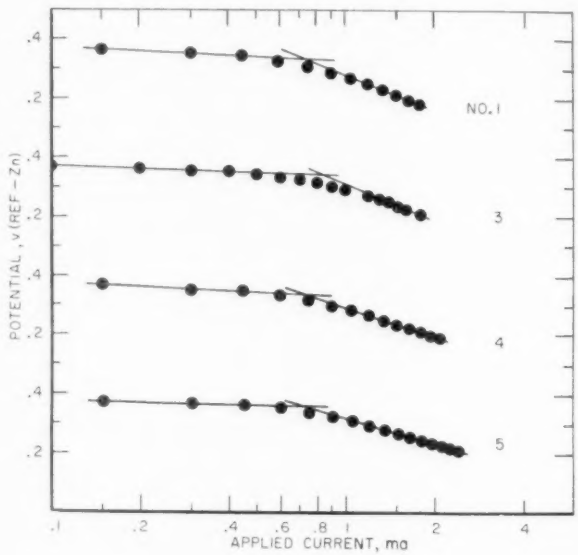

FIGURE 5. *Cathodic polarization data for steel specimens, obtained on the second day of exposure, transferred from recorded charts to semilogarithmic coordinate paper.*

One milliampere is equivalent to 6 ma/ft.^{2} After the second day, specimen No. 1 was allowed to corrode freely, except when obtaining polarization data, and protective currents were applied to specimens Nos. 3, 4, and 5.

Currents and potentials measured on the specimens throughout the 61-day exposure period are shown in figure 7. Figure 8 is similar except that potentials include the *IR* drops, and the potentials of the control specimens are omitted. Specimen No. 3 is the one where current alone was regarded as the protective criterion. The initial current applied to specimen No. 3 was the value shown by the polarization curve (fig. 5), and subsequent adjustments of current were based on the average of currents, I_p, observed on the control specimens Nos. 1 and 2.

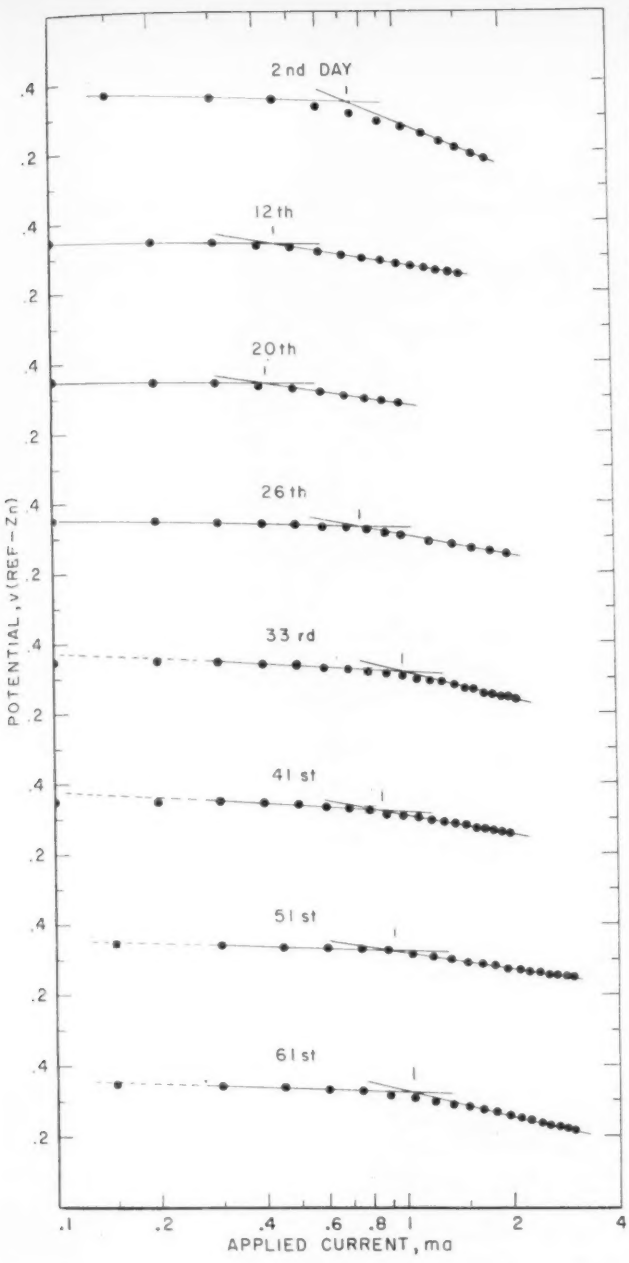

FIGURE 6. *Cathodic polarization curves of control specimen No. 1 at intervals during the exposure period.*

One milliampere is equivalent to 6 ma/ft.²

From the 4th day onward, specimen No. 4 was controlled at −0.77 v (free of *IR*) and at the same time specimen No. 5 was placed under control at −0.77 v (including *IR*). Currents applied between the 2d and 4th days were estimated to produce the desired effects without control.

In figures 7 and 8, two values of current or potential for any one specimen on the same day means that adjustments were made. For example, in the case of specimen No. 3, except after the 49th day, the applied current was changed to conform with the polarizing currents, I_p, measured on the controls. However, the resultant changes in potential on that specimen were not measured until the following day or later. When adjusting the potential of specimen No. 4, the control was usually set at −0.78 v, thus allowing a 10-mv margin of safety. In fact, some control difficulties were experienced around the 27th day when for a period of about 7 days the control was even set at a somewhat more negative potential. The changes in applied current resulting from such changes in the potential adjustment were measured the same day as shown in figures 7 and 8. A mechanical failure in the control equipment caused specimen No. 4 to be without applied current from the 44th to 46th day. When the trouble was discovered on the 46th day, the potential measured −0.62 v. Before putting the controller back into operation, a cathodic polarization curve was obtained on specimen No. 4 which curve revealed that 4.2 ma/ft² was required for protection. This agreed reasonably well with the values of applied current required for the following 6 days, except for a short time immediately after making adjustments in potential.

After the 22d day of exposure, the polarization on specimen No. 3 began to decrease and the current applied to specimen No. 4 started to increase. It may also be observed (fig. 7) that a few days later, the current to specimen No. 5 began to increase, yet polarization on No. 5 gradually kept falling. On the 26th day, cathodic polarization curves of the controls showed that more current, I_p, was necessary for protection and consequently the current to specimen No. 3 was increased accordingly. Subsequent values of current, I_p, were even larger, yet the potential of specimen No. 3 continued to become less negative until, on the 49th day of exposure, it was decided to arbitrarily increase the current as shown. Even at this high current density (9.5 ma/ft²), maintained for the remainder of exposure, only once did the potential approach −0.77 v.

The foregoing trend of increasing current requirements is not consistent with the results of previous studies [1,2] wherein the current required for cathodic protection usually diminished and leveled off as time of exposure increased. In the previous studies in low-resistivity environments, the corrosion reactions usually closely approached cathodic control. The protective currents ordinarily were equal to or slightly larger (not over 20% larger) than the corrosion currents. The results obtained in the present investigation (table 1) provide an explanation for this divergence. The corrosion current, calculated from the weight losses, is equivalent to a current density of 1.5 ma/ft². A mean-current density of 4.2 ma/ft² was required to protect specimen No. 4 at −0.77 v. This protective current is in fair agreement with the mean currents, I_p, from the cathodic polarization curves of the controls. As the current necessary for protection is about three-times the magnitude of the corrosion current, the corrosion reaction was either under anodic control [6] or a type of control equivalent to anodic control caused by high resistance at the anodic areas. That

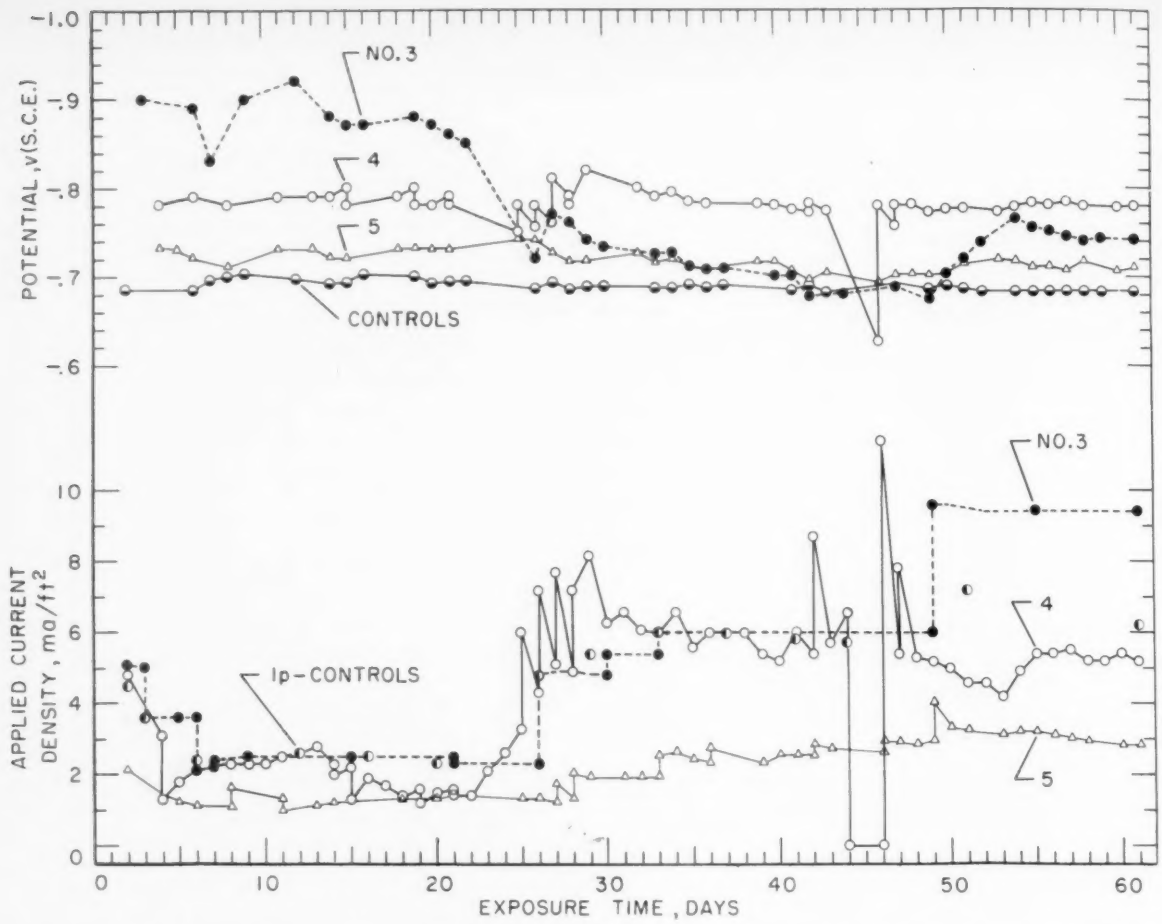

FIGURE 7. *Relationship between potential (no IR) and applied current density for different degrees of cathodic protection on specimens Nos. 3, 4, and 5. S.C.E.=saturated calomel electrode.*

Ip is the protective current requirement averaged for control specimens Nos. 1 and 2 based on cathodic polarization curves; No. 3 specimen, except after 49th day, constant current conforms with Ip; No. 4 specimen, variable current based on controlled potential −0.77 v (no *IR*); No. 5 specimen, variable current based on controlled potential −0.77 v (including *IR*).

one condition or the other probably prevailed is supported by the anodic polarization curves (not shown) on the controls which were obtained the same days following cathodic polarization. The anodic curves in the beginning of the exposure period were indicative of cathodic control in that there was very little or no polarization. Later, polarization occurred and the break (change-in-slope) appeared in the anodic curves at currents of about the same magnitude as the cathodic currents, I_p. Finally, during the latter half of the exposure period the anodic curves revealed breaks at currents smaller than I_p. Thus, while the current necessary for cathodic protection increased as the exposure time lengthened, the anodic currents, presumably required to stop local action, became smaller.

The weight losses of specimens Nos. 3, 4, and 5 shown in the table have been adjusted for the time the applied currents were off, namely: 2 days for each of specimens Nos. 3 and 5, and 4 days for specimen No. 4. The adjustments were made on a proportionate basis of the control weight losses. One might conclude that the degree of protection achieved on specimen No. 4 was less than would have been expected, as this specimen was protected at a potential equivalent to −0.85 v free of *IR* with reference to the more familiar Cu–$CuSO_4$ electrode. However, the measured potentials at best were only average values and in the 20,000 ohm-cm soil, because of current distribution difficulties, the potentials on some areas of the exposed surface might not have been at the protective level. Also, the adjustments made in weight losses are actually rather conservative. In the case of specimen No. 4, had the adjustment for the current off periods been based on weight losses calculated from the polarization curves, the degree of protection would have been about 76 percent.

Under the environmental conditions, a comparison of the data pertaining to specimens Nos. 3 and 4 shows the importance of maintaining polarization at the protective potential level if the goal is complete protection. Figure 7 shows that, during more than half of the exposure period, the potential of specimen No. 3 was less negative than −0.77 v even though the mean current (table 1) applied to specimen No.

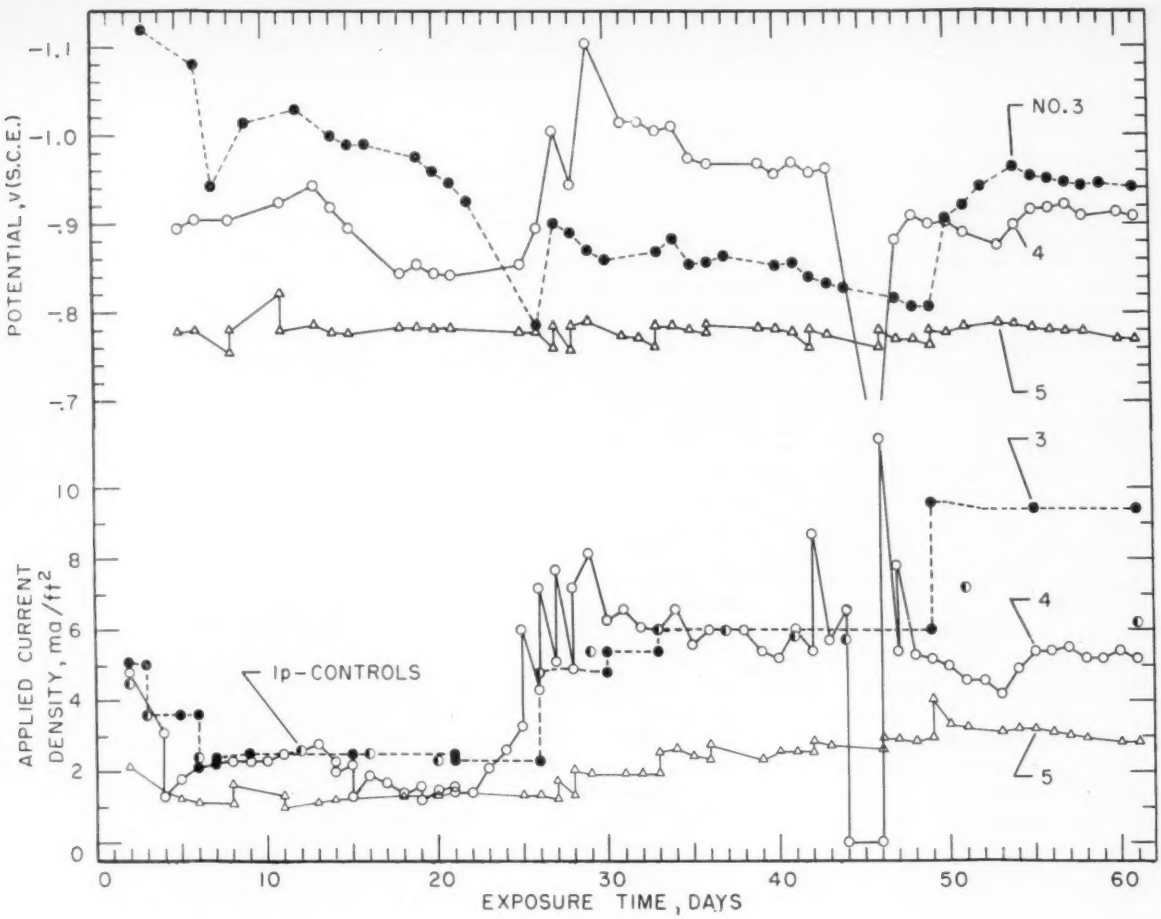

FIGURE 8. *Same as figure 7, except that all potentials include IR drop, and the potentials of the controls are omitted.*

TABLE 1. *Steel specimens exposed for two months to a high resistivity* (ρ=20,000 ohm-cm) soil

Specimen No.	Protective criterion	Cathodic polarization curve									Potential of specimen						Corrosion[a] current I	Weight[b] loss of specimen 61 days	Effectiveness[c] of protection
		Current at break, Ip			Potential at break, E_a[d]			Protective current to specimen			No *IR*			Including *IR*					
		Range		Mean	Range		Mean	Range		Mean	Range		Mean	Range		Mean			
		Min	Max		Min	Max		Min	Max		Min	Max		Min	Max				
		ma/ft²	*ma/ft²*	*ma/ft²*	*v*	*v*	*v*	*ma/ft²*	*ma/ft²*	*ma/ft²*	*v*	*v*	*v*	*v*	*v*	*v*	*ma/ft²*	*mg*	%
1	Control	2.1	6.6	4.6	−0.695	−0.730	−0.710				−0.683	−0.702	−0.689				1.5	375	
2	Control	2.3	8.7	5.0	−.710	−.740	−.721				−.683	−.705	−.689				1.5	375	
3	Current							2.1	9.6	5.2	−.675	−.920	−.777	−0.785	−1.12	−0.920		161	57
4	Potential (no *IR*).							[e]1.2	11.4	4.2	[e]−.750	−.820	−.778	[e]−.842	−1.10	−.914		107	71
5	Potential (with *IR*).							1.0	4.0	2.1	−.693	−.740	−.717	−.755	−.823	−.780		182	51

[a] Based on Faraday's law, $I=W/kt$, where K=2.8938X10⁻⁴ g/coulomb; W=wt loss of controls (average grams); and t=exposure time (seconds).
[b] Corrections made on specimens Nos. 3, 4, and 5 for initial freely corroding period and also for two intermediate days on specimen No. 4 when it was without protective current.
[c] Effectiveness of protection=100 (Wc–Wp)/Wc, where Wc=avg wt loss of controls; and Wp=wt loss of the protected specimens.
[d] E_a=open-circuit potential of the anode (average).
[e] Specimen No. 4 was without protective current from the 44th to the 46th day when the potential (min) was actually −0.627 v on the 4 th day.

NOTE: Each specimen had an exposed area of 24 in.². Potentials are referred to the saturated calomel electrode.
Specimens Nos. 1 and 2 were without cathodic protection.
Specimen No. 3 had current applied based on values of the current, I_p, averaged from polarization curves of specimens Nos. 1 and 2.
Specimen No. 4 was controlled at −0.77 v (no *IR*).
Specimen No. 5 was controlled at −0.77 v (including *IR*).

3 was equal to or greater than that applied to No. 4. Thus, current density alone cannot be relied upon as a satisfactory criterion for cathodic protection.

Assuming that the inherent rates of corrosion on specimens Nos. 3 and 5 were about the same (cathodic polarization curves indicated that they were), it might be concluded that, based on the comparative applied current densities, the corrosion on specimen No. 5 was more economically controlled than that on specimen No. 3. Although more than twice as much current was applied to specimen No. 3, only a slightly better degree of protection resulted. On the other hand, the data also bring out the fact that any benefits of *IR* drop while cathodically protecting a bare surface must be examined with caution. The degree of protection on specimen No. 5 was considerably less than that obtained on specimen No. 4, which received only a fair degree of protection, even though the *IR* drop was not included in the controlled protective potential. Potential values which include *IR* drops can be very misleading, as shown by figure 8 and the data in the table. In the case of specimen No. 5 (table 1), based on the mean control potential (−0.689 v), the mean potential change (91 mv), caused by the protective current, to the potential −0.78 v (including *IR*) was comprised of only 28 mv attributable to polarization.

The data pertaining to specimen No. 5 also lead to questions concerning the proper positioning of the reference electrode. It is recognized that, in a theoretical consideration of the potential criterion for cathodic protection, the *IR* drop in the cathodic area of a corrosion cell reduces the cathodic polarization required to fulfill the protective criterion, i.e., polarization to the open-circuit potential of the anode. The benefits of *IR* drop (with reference to current flow to bare surfaces) resulting from applied currents to cathodic areas have been very ably demonstrated by Miller [7], Sudrabin [8], and others. Miller made measurements in a wet clay of about 1,000 ohm-cm resistivity. He showed that the cathode (a rusty iron pipe) of a galvanic cell need not be polarized to the open-circuit potential of the anode (a bright iron pipe) in order to reduce the galvanic current to zero. The additive effect of the *IR* drop within the cathodic branch was made very apparent. Miller showed that the open-circuit anode potential criterion was fulfilled when the reference electrode was placed directly over the anode or when placed in a remote position so as to include all of the cathodic *IR* drop. However, Miller also recognized the possibility that his tests did not necessarily duplicate all actual conditions existing on a pipeline which presumably contains innumerable corrosion cells on its surface. Using a 22,000 ohm-cm resistivity water environment, Sudrabin demonstrated that the open-circuit anode potential (peculiar to the conditions) while the protective current was flowing, was indicative of complete protection if the reference electrode was placed directly over the anode or away from the cathode sufficiently far to include *IR* drop within the boundary of the corrosion cell. He also showed that placing the reference electrode inside of the cell boundary resulted in excessive protective current but positioning it outside of the cell boundary resulted in insufficient protection. Sudrabin found that spacial factors, relative to the anodes and cathodes of a corrosion cell, control the correct location for the reference electrode and that these factors become more significant as the resistivity of the electrolyte is increased.

Measurements made in the laboratory at the National Bureau of Standards have shown that geometric factors should be given consideration when placing the reference electrode for potential measurements while cathodically protecting bare structures [9].

In the laboratory experiments described in this paper, it appeared as though the corrosion cells on the surface of the steel tubes had small dimensions and consequently any beneficial cathodic *IR* drops must have been close to the metal surface. Were this not so, all the specimens would have received a better degree of protection. If most corrosion underground can be attributed to local action, and there is evidence that it can [10, 11], the inclusion of any *IR* drop must be evaluated with understanding. It might be well to interject the thought brought out by Sudrabin [8] that the location of the reference electrode is not so critical when a highly resistive coating separates the bare metal surface from the corrosive environment.

4. Summary

The external surfaces of low-carbon steel specimens, in the form of tubes, were exposed for a period of 2 months in the laboratory to a soil having a resistivity of about 20,000 ohm-cm.

There were five specimens, two of which were used as freely corroding controls and also for obtaining polarization data at approximately weekly intervals throughout the exposure period while the other three specimens had protective currents applied continuously. Periodically adjusted current was applied to one of the three on the basis of average values of current from the cathodic polarization curves obtained on the controls. Variable current was applied to each of the other two specimens based on the controlled potential −0.77 v referred to the saturated calomel half-cell. The control of the two specimens held at −0.77 v differed in that for one specimen the protective potential included the *IR* drop caused by the protective current between the specimen and a reference electrode (a zinc rod) while the other specimen was controlled without including this *IR* drop.

During the 2-month period of exposure a change occurred from a cathodic type of corrosion control to an anodic type or a type equivalent to anodic, seemingly caused by high resistance of the anodic areas on the specimens. This was evidenced by the characteristics of the cathodic and the anodic polarization curves of the controls, by increasing currents required for protection at the controlled potentials,

and finally by the ratio of the value of protective current to the corrosion current.

The best degree of protection was achieved on the specimen controlled at −0.77 v (free of *IR* drop). The other two specimens were protected to a lesser degree because of insufficient polarization. As in previous laboratory studies at the Bureau, the data show that cathodic polarization curves are a means for measuring the current required for cathodic protection but that the degree of protection being achieved is indicated best by changes in potential resulting from polarization.

The data show that *IR* drop included in a potential reading (indicative of protection) can be very misleading, especially when bare iron or steel is exposed to a high-resistivity environment.

The author thanks Mr. E. A. Anderson, New Jersey Zinc Company, for furnishing the high-purity zinc rods used in the experiments.

5. References

[1] W. J. Schwerdtfeger and O. N. McDorman, Potential and current requirements for the cathodic protection of steel in soils, J. Research NBS **47,** 104 (1951) RP2233; Corrosion **8,** 391 (1952).

[2] W. J. Schwerdtfeger, Current and potential relations for the cathodic protection of steel in salt water, J. Research NBS **60,** 153 (1958) RP2833; Corrosion **14,** 446t (Oct. 1958).

[3] L. P. Sudrabin and F. W. Ringer, Reply to discussion, Some observations on cathodic protection criteria, Corrosion **13,** 836t (Dec. 1957).

[4] NACE Unit Comm. T–2C, Corrosion **13,** 105 (Nov. 1957).

[5] H. D. Holler, Studies on galvanic couples 1. Measurement of electromotive force and internal resistance of cells during current flow, J. Electrochem. Soc. **97,** 271 (Sept. 1950); Corrosion **7,** 52 (Feb. 1951).

[6] W. J. Schwerdtfeger and O. N. McDorman, Measurement of the corrosion rate of a metal from its polarizing characteristics, J. Electrochem. Soc., **99,** 407 (1952).

[7] M. C. Miller, Galvanic couples and cathodic protection, Petrol. Eng. (May 1946).

[8] L. P. Sudrabin, Some observations of cathodic protection potential criteria in localized pitting (A report of T–2C on minimum current requirements for cathodic protection NACE Pub. 54–2) Corrosion **10,** 232 (Aug. 1954).

[9] W. J. Schwerdtfeger and Irving A. Denison, Geometric factors in electrical measurements relating to corrosion and its prevention, J. Research NBS **54,** 61 (1955) RP2566; Corrosion **11,** 25 (Oct. 1955).

[10] Gordon N. Scott, An aspect of the pipe-to-soil potential and related measurements, NBS Soil Corrosion Conference 1943 (unpublished). Excerpts of this paper appeared in Gas (Feb. 1944).

[11] K. H. Logan, S. P. Ewing, and I. A. Denison, Soil corrosion testing, Symposium on Corrosion Testing Proc., ASTM (1937).

WASHINGTON, D.C. (Paper 63C1–4)

Journal of Research of the National Bureau of Standards—C. Engineering and Instrumentation
Vol. 63C, No. 1, July–September 1959

A Tilting Air-Lubricated Piston Gage for Pressures Below One-Half Inch of Mercury [1]

U. O. Hutton

(May 8, 1959)

A description is given of a tilting dead-weight piston gage constructed at the National Bureau of Standards for ranges of differential pressure up to about 0.5 inch of mercury. A resolution of better than 1 part in a hundred thousand of full scale has been obtained by use of the toolmaker's sine bar method of angle measurement. The scale is a linear function of the sine. The instrument can be calibrated from basic measurements of length and weight, is rugged, and may be constructed in almost any laboratory mechanical shop. Sources of possible errors in reading are discussed in detail. Comparative tests with certain other gages or manometers are cited wherein linearity was found to be within 1 part in 10,000 and agreement within 2.5 parts in 10,000. The uses of the gage are briefly discussed.

1. Introduction

A need exists for pressure-measuring or controlling devices for ranges of low pressure, particularly the pressure range corresponding to atmospheric pressure at high altitudes. The need is more acute where measurement and control are both required. For the study of the pressure-deflection characteristics of diaphragms of high sensitivity, no device discussed in available literature [1] seemed conveniently applicable to the problem where constancy of pressure difference from a datum was desired for various lengths of time up to 24 hr. Conventional air-lubricated piston gages are nicely applicable to this problem approaching within about 0.4 in. of mercury of the datum pressure with a resolution of at least 1 part in 10,000. This report describes a piston gage to cover from about 0.5 in. of mercury to the datum pressure with a resolution of 1 part in 100,000 and means of pressure adjustment without resort to weight changing.

In exploring the characteristics of gages suitable for the contemplated tests, several air-lubricated piston gages were made from medical hypodermic syringes of 25- and 100-cm^3 capacity. These syringes had hollow pistons and could be employed to as low a pressure as 0.4 in. of mercury. Schemes for employing such gages with opposed pistons were abandoned because of the loss of resolution as the pressure difference set up by the pistons becomes small. In handling a well-lapped syringe it was observed that air lubrication for a low-density piston was surprisingly adequate even if the piston was not vertical. Brubach's experiments [2] encouraged an attempt to devise a piston gage, the incremental loading of which would be adjusted by changing the angle of tilt instead of the weights as on the conventional dead-weight testers. Distinct advantages of this design are that it reaches high resolution without resort to delicate structures and requires neither optical nor electrical amplification. The extended scale available is gained through the use of a micrometer and end gage block.

2. Description of Piston Gages

In development, two models were constructed that will be referred to as Models I and II. Model II incorporates all the features of Model I so that a discussion of Model I is possibly not of great value; however, its simplicity of construction and the high sensitivity and resolution attained may make it applicable in some cases where the additional complexity of Model II is not warranted. The first model is of such simplicity that it may be constructed and a basic calibration made in a short time in almost any laboratory. The principles of the gage are so elementary that adherence to the details being described is not suggested as being necessary. Dimensions and other specific details as used are included for guidance in understanding the structures on which performance data is presented.

2.1. Description of Gage, Model I

For the piston-cylinder combination, four 100-cm^3 syringes were obtained. Two of these were found to be sufficiently tight for adaptation. They were put through a hand-lapping operation where lapping powder, Linde A ($\frac{1}{2}$ μ), was used in a creamy water suspension. From $\frac{1}{2}$ to 2 hr lapping was employed using a combination of rotary and longitudinal motion with the addition of water or lapping compound as required. The lapping operation was considered complete when a piston, washed and dried, would just fall of its own weight in its cylinder oriented in a vertical position with the piston at any radial angle. It does not seem possible to overlap such a combination with this size of lapping particle using water as a lubricant because of the hydrodynamic lubrication furnished by the lapping motion; however, it was always possible to remove the high areas on the

[1] The major part of this work was sponsored by the Flight Control Laboratory, Wright Air Development Center, Wright-Patterson Air Force Base, Ohio.

piston and cylinder so that the freedom-of-fall condition described was obtained. The tighter areas may be recognized while lapping by the degree of dispersion of the lapping compound and after drying by the higher grade finish on the closer surfaces. Extra attention may be given the high areas by localized finger pressure on the cylinder and by choice of the piston orbit to bring them into frequent play. In some of the better lapped areas, white light interference fringes have been visible but this is not necessary for proper performance.

After lapping, the cylinder and piston were cut with a diamond saw as shown in figure 1, then mounted on a sine bar, shown in figure 2 to form a piston gage. The piston is weighted as desired and floats without rotation in the cylinder on an air film as a bob. The cylinder is supported on another portion of the original hypodermic piston employed as an air-lubricated pinion bearing. The micrometer anvil and sine pivot are at such a relative height that the piston is horizontal when the micrometer is fully retracted.

The cylinder must be rotated to keep the piston free. It was originally rotated by an air jet directed against the teeth of a 4-in. diam spur gear concentrically mounted on the cylinder, but later by a 25-w, 2,700-rpm shaded-pole induction motor operated at ⅓ voltage with a rubber band (No. 32) as a belt over the motor shaft and around the cylinder. A slight finger spin is sometimes required for starting, and under the light load conditions prevailing, the rubber band, as a belt, lasts several weeks and vibration or temperature transmissions from motor to cylinder are negligible.

The piston is eccentrically loaded to prevent its rotation as shown in figure 2. One inch of vertical travel of the micrometer corresponds to 40 revolutions of the micrometer screw. The length of the scale on the barrel of the micrometer is 1.5 in., which gives a total scale length for 40 revolutions of 60 in., with a readability of 0.005-in., corresponding to 1 in 10,000.

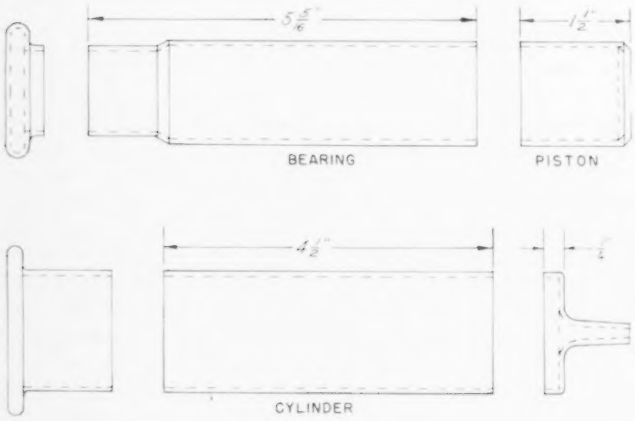

FIGURE 1. *Sawing of hypodermic syringe to obtain parts for piston gage.*

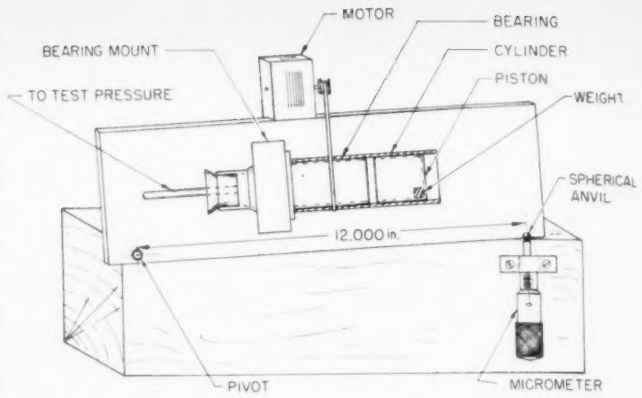

FIGURE 2. *Tilting piston gage, Model I.*

2.2. Description of Gage, Model II

As a result of the experience with Model I, a second gage, Model II, was built. The design was changed so that the tilt can be measured over a 90-deg angle from the horizontal by means of gage end-blocks and 1-in. micrometer caliper. The cylinder on this model was made from 1.250-in. diam precision-bore glass tube. The piston and bearing were prepared, by lapping, from ordinary Pyrex tubing in an attempt to avoid the slight taper that is present in a hypodermic syringe. See figures 3, 4, 5. Instead of the wood base of the original model, a 2×6×12-in. surface plate was used as a base. This provides a satisfactory surface on which to wring the gage blocks used to establish the altitude of the triangle (this being the measure of the tilt). The pivots for the piston support bar and for the micrometer mount are hardened steel cones and spaced 10.000 ±0.002 in. apart.

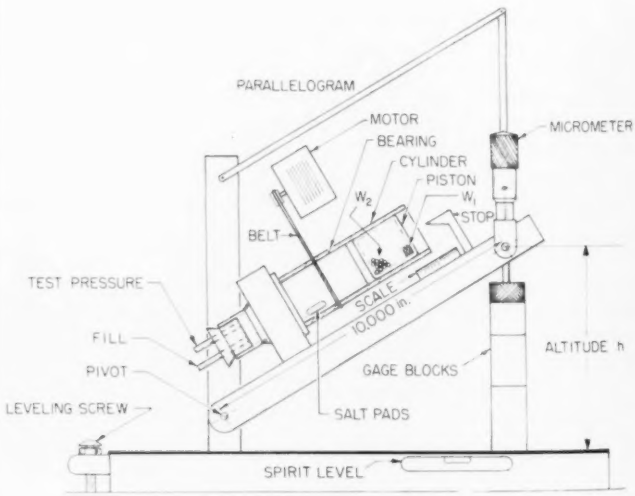

FIGURE 3. *Tilting piston gage, Model II.*

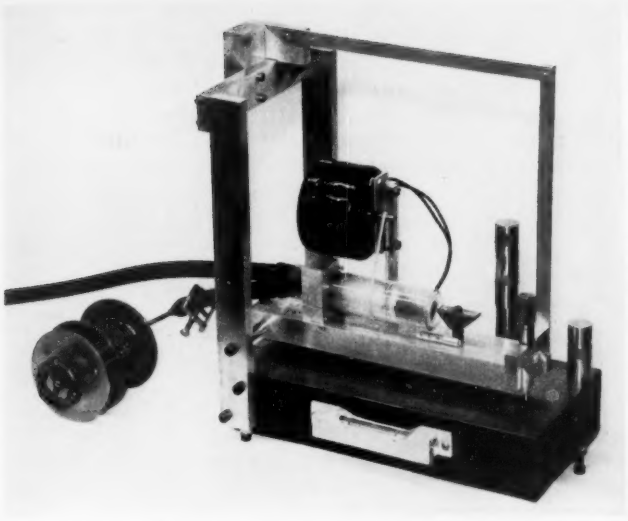

FIGURE 4. *Tilting piston gage, Model II, in zero position.*

The micrometer support mount is positioned by a parallelogram structure so that the micrometer axis is maintained perpendicular to the surface of the base plate. The pressure connection is made through the pivot bearing as shown. A stop is provided to prevent the piston being blown out, and for convenience in observing that the level of the base plate is unaltered, a sensitive spirit level is provided. A small fan motor with a rubber belt provides the rotational movement of the cylinder. The piston is closed with an inside fitted cap and a fixed cast lead weight, W_1, is used and is advantageously located at the upper end of the piston so that its vertical component will be as nearly as possible through the center of the piston supporting area with a tilt of 3–4 in. In addition to the main weight, W_1, the piston is loaded with an auxiliary weight, W_2, composed of lead shot or other such movable weights, the purpose of which will be discussed in section 5.5.

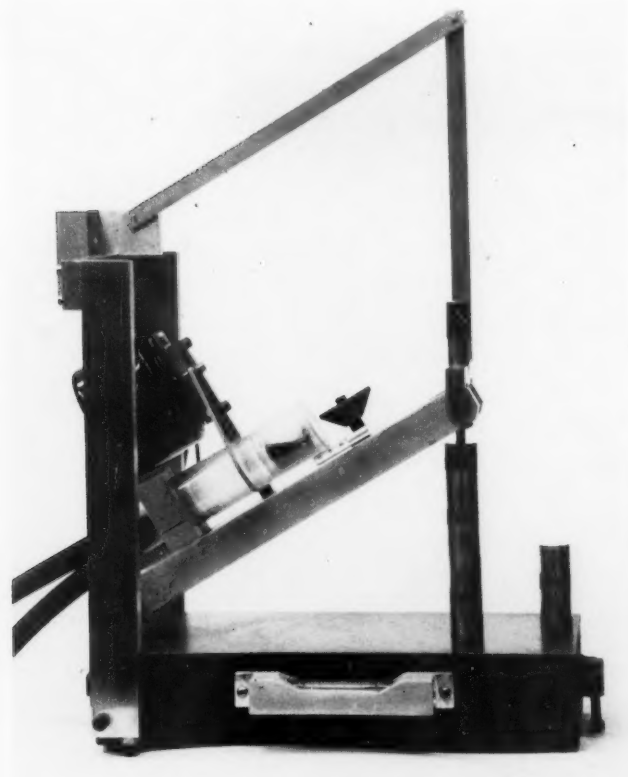

FIGURE 5. *Tilting piston gage, Model II, in tilted position.*

A change in altitude, h of 1 in. is provided by each 1-in. end-block placed under the micrometer and each 1-in. block is equivalent to 10 percent of the piston weight which is carried by the air pocketed under the piston. The pressure developed by the piston in this pocket is in direct proportion to altitude, h. Altitudes up to 8 in. have been employed. For altitudes from 8 to 10 in. the eccentric position of the weights will not always overcome the cylinder drag and prevent rotation.

The scale length of this model using the combination of the micrometer and end blocks is effectively eight times the scale length of Model I, and thus is readable to 1 part in 80,000. Some experiments have been made with a 6-in. diam reading dial such as used on the more precise micrometers. This provides a scale length of 6,000 in. readable to 1/32 of an inch and a zero stability of the same order as the resolution.

Two pressure connections to the lower surface of the piston are provided, one for connection to the chamber or space in which the pressure is to be measured and the other, marked "Fill" in figure 3, to replenish air lost by leakage. A controllable volume shown in figure 4 is connected to the "Fill" opening. The function of the salt pad is discussed in section 5.4.

3. Calibration

The pressure difference p between the two end surfaces of the piston is determined by the relation

$$p=\frac{mg}{a}\sin A=\frac{mgh}{ad}$$

where m is the mass of the weight; g, the acceleration of gravity; h, the altitude of the triangle (fig. 3); a, the effective cross-sectional error of the piston; d, the distance between the pivots of the sine bar and calipers (fig. 3); A, the angle of elevation of the sine bar.

It is seen that mg/ad is a constant for any one design, weight of piston and at any one location. When these constants are known, it is only neccssary to measure h to determine the pressure. If the weight mg is in grams and the other quantities in centimeters, p is in units of grams per square centimeter; similarly if mg is in pounds and the other quantities in inches, p is in units of pounds per square inch.

The piston weight is readily determined, if desired, to 1 part in 100,000.

In the investigation, relative readings of high precision and reproducibility were desired, but the basic calibration was of lesser concern. Consequently, the precise determination of effective area was not attempted. The effective area has been assumed to be the mean of the cylinder and the piston areas. The diameter of the piston was measured to approximately 1 part in 10,000 by means of a micrometer caliper. The cylinder diameter which is difficult to measure accurately with mechanics' micrometers had an accuracy of about 1 part in 4,000. Thus the effective area was probably known to an accuracy of about 1 part in 2,000. Higher precision in this determination would require not only more precise measurement but a combination of piston and cylinder without measurable taper or dimensional irregularities. Meyers and Jessup [4] (as well as later workers) suggest effective diameter determination by manometric methods, and with a suitable manometer available this method would be perferred to clearance measurements. Where a basic gage calibration is required, effective area determination to 1 part in 25,000 for a 1-inch piston should not be too difficult.

There is also some change in area possible, due to internal pressure in the cylinder. Correction for this error may be made from empirical data. And, finally, the effective area may be slightly influenced by the change in the eccentricity of the piston for different angles of tilt. No error from this source has been separated, but some allowance for such an error is indicated in the later tabulation. No dimensional changes have as yet (after 1 year) been recognizable due to either wear or secular changes.

The vertical component of the piston weight is proportional to the sine of the angle of tilt which requires a knowledge of both the altitude and hypotenuse of the triangle (see fig. 3). The leg or altitude of the triangle, measured by the micrometer and gage blocks, can be measured to an accuracy of 0.00005 in. For equal absolute accuracy in the value of the sine of the angle, the hypotenuse must be known to the same accuracy as the altitude.

4. Performance

The base of the instrument must be maintained level. Since the resolution is equivalent to the sine of an angle of 2 sec of arc, the axis of the base should be maintained to within at least 1 sec of the horizontal. For highest accuracy, the gage needs to be leveled on a rigid table in a room free from excessive drafts and where the temperature uniformity is such that a thermal expansion error of significance will not exist in either the altitude or area measurements.

The first step is to zero the gage. This is the condition where the pressure connection is open to the room, and the piston in the rotating cylinder is at an equilibrium position touching neither end-stop. Under this condition the axis of the piston is, of course, horizontal. The gage is then connected, to the test pressure, using an independent connection to some type of reservoir to introduce or release air for the repositioning of the piston when desired. When it is desired to provide a definite pressure to a gage to be calibrated, set the altitude h with the micrometer or with micrometer and end-gage blocks to give the pressure desired. This pressure will be maintained at the test connection so long as the piston floats without touching either end-stop. If an unknown pressure is to be determined, connect the apparatus in the same manner but set h, step by step, until all axial motion of the piston is canceled. This can ordinarily be accomplished in less than a minute.

Tests of various sorts have been improvised to determine the performance of this type of piston gage. Certain tests were performed on Model I and not repeated on Model II. Also, some tests were devised after Model II was in operation and were not performed on the earlier model. Test results are included irrespective of their being obtained on the earlier or on the more advanced model where they seemed to provide pertinent information on the gage performance.

The readings of the piston gages were compared with those of several sensitive pressure-measuring instruments in order to obtain information on its performance characteristics. These were: (a) An Ascot-Casella micromanometer [3]; (b) a vertical air-lubricated piston gage adapted from a 100-cm^3 hypodermic syringe; and (c) a sensitive 2-in. mercury manometer having a null indicator based upon a capacitance bridge [5]. The Ascot-Casella instrument has a torsion balance to measure the difference in the product of the pressure and area of two bells floating on kerosene.

4.1. Zero Stability

Particular attention was given to a study of the repeatability of the gage zero since full advantage of the gage resolution is available here, whereas under the loaded condition stability can be determined only to the degree that the load may be held constant. The zero, as referred to, is determined under the condition of both ends of the piston exposed to atmospheric pressure. The altitude h is adjusted by means of the micrometer until the piston floats without axial drift. The repeatability of the zero, determined after altering the former setting by varied amounts, with either intermittent or continuous rotation, has been found to be in the same order as the resolution of the micrometer reading. Six consecutive hourly readings showed variations of $+0.0002$ to -0.0001 in. in altitude. Daily readings with no rotation of the cylinder during the night have repeated within the same limits for at least 5 days. The influence of other factors on the zero were studied and the results of the tests may be summarized as follows:

(a) There was no visible change in zero with an ambient temperature change of 5° C.

(b) A change in the axial position of the piston of ⅛ in. each side of the initial balance point caused a total zero variation of 0.0002 in.

(c) A doubling of the cylinder rotational speed was observed to affect the zero by 0.0002 in.

(d) The piston weight was increased 5-fold without observable change in the zero.

(e) A piston with an end load of 500 g was reversed so that the load was positioned first in an outboard position, then inboard position. The average readings, in each position, were identical with a variation in individual readings of only 0.0002 in.

Some later tests were made with a 6-in. dial on the micrometer. Altitude resolution with this micrometer was 0.00005 in. and zero repeatability in tests over several days was to the same limit. With a 30-g piston weight this corresponds approximately to a pressure of 4×10^{-7} in. of mercury.

4.2. Comparison Tests, Pressure Controlled by Tilting Piston Gage

The first experiments to determine the stability of the reading when the pressure was controlled by maintaining a constant tilt of the piston gage were made with the Ascot-Casella micromanometer as a reference standard. Readings were made on the micromanometer for a period of 20 min while a constant altitude, or tilt, was maintained on the piston gage during which the axial position of the piston varied ¼ in. The micromanometer indications varied approximately 0.2 scale divisions with a full-scale reading of 250 scale divisions. This indicated a repeatability of about one part in 1,000 at a pressure corresponding to about 1 percent of full scale on the piston gage.

Additional comparisons were made in the above pressure range using a hook gage with a resolution of about 0.001 in. of water as the reference standard. The repeatability in readings of the piston gage was about the same as with the Ascot-Casella micromanometer. The stability and reproducibility of the zero position of the tilt gage was considerably better than the readings as obtained with either the Ascot-Casella or hook gage. For this reason it was believed a more reliable reference should be used and subsequent comparison tests were made with the 2-in. mercury manometer or the vertical air-lubricated gage.

Comparison tests were made at three pressure ranges obtained by varying the weight of the piston. For each piston weight the tilt, or altitude, of the piston gage was varied. In all of these tests the tilting piston gage is acting as a pressure regulator. The pressure readings were made on the reference instrument, in this case the 2-in. mercury manometer.

The results of the low-pressure range comparison are given in table 1. The check readings were made 5 min after the first reading. The resolution of the 2-in. manometer is about 0.00005 in. of mercury. It will be seen that the increments for successive increases of 0.2 in. in altitude decrease somewhat as the altitude increases; this increase in sensitivity is not considered significant since the total variation is within the resolution of the 2-in. manometer.

The results of the comparison at an intermediate pressure range are shown in table 2. The test was again made on Model I piston gage but with a greater load on the piston. The pressure given in column 2 of table 2 was calculated from the constants of the piston gage and the altitude following the procedure outlined in section 3. The difference in the pressures calculated for the piston gage and determined from readings on the 2-in. manometer are given in column 4. The difference amounts to about 1 part in 2,000 of the pressure and is compatible with the resolution of the 2-in. manometer and the uncertainty in the determination of the effective area of the piston.

TABLE 1. *Low-pressure range comparison [a] tilting piston gage Model I and 2-in. manometer*

Tilting gage	2-in. manometer		Increments
Altitude in.	*Reading in. Hg*	*Average*	*For 0.2 in.*
0.2000	0.00160		
.2000	.00161	0.00160	0.00160
.4000	.00320		
.4000	.00320	.00320	.00160
.6000	.00479		
.6000	.00476	.00478	.00158
.8000	.00633		
.8000	.00635	.00634	.00156

[a] The reference pressure is 1 atm.

TABLE 2. *Intermediate pressure range comparison [a] tilting piston gage Model I and 2-in. manometer*

Tilting gage		2-in. manometer	Difference
Altitude in.	*Pressure in. Hg calc.*	*Pressure in. Hg*	*Inches Hg*
1.0000	0.03741	0.03745	0.00004
3.0000	.11223	.11227	.00004
5.0000	.18705	.18709	.00004
7.0000	.26187	.26197	.00010
9.0000	.33669	.33684	.00015

[a] The reference pressure is 1 atm.

The results of the comparison at the highest pressures thus far employed are shown in table 3. The test was made on Model II piston gage. Again the pressures calculated from the piston gage altitude and constants are compared with the pressures derived from readings made on the 2-in. manometer. Here the pressures agree within about 3 parts in 10,000, an amount far less than the expected uncertainty in determining the effective area of the piston. The linearity, which is independent of the piston area, is within about 1 part in 10,000.

TABLE 3. *High pressure range comparison [a] tilting gage Model II and 2-in. manometer*

Tilting gage		2-in. manometer	Difference
Altitude in.	*Reading in Hg calc.*	*In. Hg*	*In. Hg*
0	0	0	0
4.0000	.28700	.28706	.00006
7.0000	.50225	.50242	.00017

[a] The reference pressure is 1 atm.

4.3. Comparison Tests, Pressure Controlled by an Auxiliary Instrument

The experimental model of a vertical piston gage was employed at the lowest pressure of its range in a test where the pressure in the system was set and controlled by the vertical piston gage. The altitude of the tilting piston gage, adjusted to bring both pistons to an approximately steady axial position was read at intervals of time. The same point was observed over several hours and repeated the following morning. The results are shown in table 4.

TABLE 4. *Comparison of tilting air-lubricated [a] piston gauge with a vertical air-lubricated piston gauge*

Elapsed time	Tilting gage		Vertical piston gage
hr	*Altitude in.*	*Pressure in. Hg calc.*	*Pressure in. Hg*
0	8.6535		0.32321
½	8.6535		.32321
4	8.6545		.32321
24	8.6537		.32321
Average	8.6538	0.32313	0.32321

[a] The reference pressure is 1 atm.

The maximum departure in the altitude reading of the tilting piston gage from the average was 0.0007 in. or less than 1 part in 10,000. The difference between calculated pressures as determined by the two gages is on the average 0.00008 in. of mercury or 3 parts in 10,000. Again this is less than the expected error in the determinations of the effective areas of the pistons.

This test demonstrated also the ease of balancing the pressures in the two gages by the adjustment of the tilt altitude with the micrometer. The initial balance would be obtained within 4 min and, after an altitude change of smaller magnitude, balance could be restored in less than one minute. With careful attention and with optical magnification of piston drift a balance can often be effected in one quarter of this time.

None of these comparative tests provided data that shows reproducibility of the reading deflection to the precision anticipated from the performance of the instrument at zero. Although the 24-hr test interval in table 4 showed only a change of two parts in 80,000, one intermediate reading in the series showed a departure of five times this. An imperfect regulation of the test pressure could be the cause for such variations. In another test Model I tilting gage set at two arbitrary heights, was used as a pressure regulator and Model II was repeatedly adjusted to this pressure. The data are given in table 5. Here the reproducibility of the setting is 1 part in 25,000.

4.4. Off-Center Loading of the Piston

The effect on the pressure generated by the tilting piston by off-center piston loading was investigated. The center of gravity of the piston for small angles of tilt may be readily positioned over the approximate center of the load supporting area. However, wide variations are desired in tilt, say up to 75° or 80° from the horizontal, in which case the center of gravity of the piston may not even lie directly above any portion of the bearing support area. To test for this effect the piston was end loaded with lead weights and the tilting piston gage connected to the 2-in. mercury manometer. The altitude of the tilting piston gage was set to 7 in., producing a pressure of approximately 0.225 in. of Hg. The difference in height of the two mercury columns of the manometer was observed, first with the piston inserted into the tilting gage with the piston weight at the elevated end, and then with the piston reversed end-for-end. This procedure was repeated several times.

TABLE 5. *Repeatability test on Model II, Model I performing as a regulator* [a]

Elapsed time	Model I	Model II
Minutes	*Altitude in.*	*Altitude in.*
0	0.900	0.6038
40	.900	.6038
125	.900	.6038
0	4.0	2.5587
5	4.0	2.5588
10	4.0	2.5587
15	4.0	2.5587
30	4.0	2.5588
55	4.0	2.5588

[a] The reference pressure is 1 atm.

The difference in the readings of the mercury manometer, for the orientations of the weighted piston in the tilting piston gage, corresponded to 0.000125 in. in altitude in the 7-in. deflection. This is less than 1 part in 50,000 and is about equivalent to the least reading of the null indicator of the mercury column.

5. Other Factors Affecting the Performance

A number of factors are considered which may affect the satisfactory operation of the piston gage and in some measure may contribute to errors in pressure readings.

5.1. Maintenance

The maintenance to keep this gage in excellent calibration and operating condition has been of very minor character. The maintenance so far required has been an occasional cleaning of the piston and cylinder. Cleaning has usually been at intervals of at least 1 month. As there is no wear on the gage itself in use, the precision parts should be expected to have a long life.

5.2. Temperature

The most significant error believed present is that due to the change in effective area of the piston through the thermal expansion of the materials of

which they are made. For Pyrex glass the thermal expansion affects the area less than one part in 100,000/°C, for which an approximate correction is readily applied if necessary. If wide temperature variations are anticipated and the highest accuracy is required, the material in the sine bar configuration should, of course, have the same temperature coefficient as the gage blocks.

5.3. Low-Pressure Limits of Operation

Only exploratory tests have been conducted at reduced absolute pressures. In these tests the entire piston gage was placed in a pressure chamber and usually the piston gage has been at its zero position.

While the results of these tests indicate the possibility of operation of the piston gage at lower absolute pressures than anticipated, greater difficulty has been experienced in the dissipation of electrical charges on the piston. The use of the salt pad to control the humidity was ineffective. A conductive piston and cylinder might be a solution to this problem but fabrication of these elements was not undertaken. In lieu of conducting materials several "antistatic" agents have been employed. For example a very thin film of sulfuric acid on the glass surface has given completely satisfactory operation to a pressure of a few mm of mercury for at least an hour. Also, but with an accumulating electrical charge, the piston gage has operated at zero position for several hours at an absolute pressure of below 0.01 mm of Hg and at 0.0025 mm of Hg for more than an hour. Remarkably there was no indication or suggestion of "lubrication" failure.

The axial motion of the piston at very low pressure becomes very sluggish. The rotational drag on the piston produced by the rotating cylinder first decreases as the pressure is lowered, reaching a minimum at about 2 mm of Hg, then as the pressure is lowered further there is a rapid increase in the drag which remains about constant to the lowest pressures reached. A "coefficient of friction" calculated for this lowest pressure was 0.4 as compared to a value of only 0.025 at the 2 mm abs pressure and 0.1 at atmospheric pressure.

At low pressures the static and kinetic friction appear to be about equal, differing from the case at atmospheric pressure where it is sometimes necessary to start the motor repeatedly to secure cylinder rotation without spinning the piston.

The piston had been in use for many hours, thus wearing off the high spots, before the low-pressure tests were made, and the continued smooth operation at low pressure was only obtained when the film of sulfuric acid was present. Without the acid film it was not ordinarily possible to keep the piston in a floating condition at pressures below 1 mm of Hg. This beneficial behavior of the acid film may be due to its action as a lubricant or to its power to reduce formation of electrical charges or both. The effect of electrical charges on the axial control of the clean piston was estimated to be as much as 20,000 times greater than the effect when the glass surfaces were acid treated.

The air lubrication of the close-fitting bearings of the piston gage particularly at low pressures, warrants further discussion. The horizontal air piston may be regarded as a journal bearing to which the classical hydrodynamical theory of lubrication applies. Computations based on Sommerfeld equations as given by Hersey [6] indicate the load bearing capacity to be at least 10 g/cm^2, more than adequate and the calculated coefficient of friction is a few percent, which is in reasonable agreement with experience.

However, a number of the factors involved in the operation of this instrument are not so easily treated by theory. The Sommerfeld equations assume that the bearing fluid is incompressible and Newtonian, with a definite viscosity. At atmospheric pressure, with a bearing load of the order of 5 g/cm^2 the assumptions of incompressibility would be expected to apply fairly well. At reduced pressures, however, the compressibility of the gas becomes important. To support the bearing load the pressure below the piston must exceed that above the piston by some 3 to 5 mm of Hg. At 1 mm of Hg ambient pressure the gas must, in the crevice below the piston, be compressed by several times and the Sommerfeld theory would be expected to break down. Also when the mean-free path of the gas becomes comparable to the clearance the phenomenon of slip would become important. This will also occur at ambient pressures of the order of a millimeter of Hg. Down to these pressures there is only a slight variation of viscosity with pressure and so there should be very little difference in the coefficient of friction from this source.

At the very low ambient pressures of a few microns of Hg the ratio of load pressure to ambient pressure and also the ratio of mean free path to clearance are of the order of 100 or a thousand to 1 and the classical lubrication theory would not be expected to apply. An attempt was made to setup the theory of lubrication for the case in which the mean-free path was very large in comparison with the clearance. This bogged down because of the geometrical complexity but it was possible to see resemblances to the classical theory.

The direction of eccentricity makes an angle with the direction of the load which is on the order of 90 deg. The rotation of the cylinder sets up a drift which forces gas into the converging wedge, building up a pressure which will support the load. In the classical theory the gas escapes from the wedge by the viscous flow, in the molecular case the escape is by diffusion. Qualitatively the two cases are similar, but with a different dependance on the local clearance. It appears that at least part of the load can be supported by hydrodynamic lubrication even in the range of molecular flow.

Another mechanism might be expected at the lowest pressures. The treatment with sulphuric acid probably leaves the glass with a large content of water which might out-gas for a long time when

first evacuated. Also the surface of the glass may be somewhat more slippery than when it is quite clean.

The preliminary considerations of theory are quite obviously raising more questions than can now be answered and it is clear that there is room for more study.

5.4. Force From Static Charges

In the earlier use of the gage a sluggishness in the response of the piston was occasionally observed. This was connected with the phenomenon reported by Brubach [2] who states "Some of the syringes had a tendency to center themselves, that is, when the plunger was stabilized at a given point and then pushed in or out of the barrel, the plunger would return approximately to the original point of stabilization." It was suggested in his paper that this action is a function of the asymmetry of the cylinder or piston. However, this phenomenon was believed due to the accumulation of static charges on the piston and was soon connected with changes in the room humidity. The sluggishness was usually present when the relative humidity was lower than 50 to 55 percent and always absent at higher humidities. A simple method of elimination of this trouble was through humidity control. This was readily accomplished by inserting in the hollow bearing of the tilting gage a small blotting paper disk soaked in saturated sodium chloride. This maintained the required humidity for several weeks without rewetting. Since the remedy for this trouble was so simple an exhaustive study of the phenomenon was not made.

The entire force from the electrical charges on the piston when at rest axially, seemed radial and no error in the controlled pressure was observed. When piston motion is required to counterbalance any volume change, the restraining force may, for a few seconds, be a substantial proportion of the piston weight but entirely disappears in 20 to 30 sec if a new position is established. In effect it is as though a considerable amount has been added to the inertia of the piston but nothing to its weight. The piston behaves as though it had a frictionless spring control on its axis with the spring support attached to a frictionless dashpot.

5.5. Piston Oscillations

Usually the piston operates with a slight rotational oscillation of several degrees; sometimes the oscillation is entirely absent, but at other times, with some condition critical, such as tilt, piston weight, or rotational speed, the oscillation of the piston increases in amplitude until the piston weight carries over the top. When this occurs the piston continues to rotate at the speed of the cylinder and the gage is inoperable. In the search for some history of this phenomenon a letter of Professor Ott, Ohio State University [7], relative to the failure of the Hackensack bascule bridge which he likened to "a pendulum suspended from a rotating shaft" was unearthed as describing a similar situation. In his discussions, Professor Ott states "for low speeds the friction decreases rapidly with speed, and the relative motion being greater during the back than during the forward stroke, the angular momentum imparted during the forward stroke would be more than that taken away during the back stroke" and consequently the amplitude of the oscillation increases. This analysis was applied to an oil-lubricated bearing in the reference but would appear to similarly explain the encountered oscillation on this air-lubricated device.

It was found that internal damping in the piston could be used to control the oscillation over a wide range, so instead of using only the eccentrically positioned cast lead weight, loose lead "bird shot" were added to approximately 25 percent of the total piston weight. The movement of the shot on small oscillations is sufficient to damp out any progressive increase in their amplitude.

These oscillations limit the highest pressure that can be reached with the tilting gage. With Model II about 0.5 in. of Hg can be developed at a tilt angle of about 60° at 400 rpm of the cylinder with maintenance of good piston stability. Higher pressures should be possible with closer fitting and greater precision in the cylinder surfaces. A recent loading with tungsten carbide granules instead of lead has allowed an angle of tilt of 80° because of higher damping and a lower center of gravity due to the higher density of the material.

5.6. Centrifugal Force

As the cylinder rotates some rotational spin is imparted to the air in the cylinder. This spinning force increases with increase in the rotational speed of the cylinder or with increase, longitudinally, in the distance between the piston and the bearing which would expose more of the cylinder area to the enclosed air. The effect of this centrifugal force was investigated by increasing the space between the piston and the bearing from $\frac{1}{16}$ in. to $\frac{5}{16}$ in., reading any change in altitude with the micrometer. The altitude change was +0.0001 in., which is the least reading of the micrometer. As an additional check the rotational speed of the cylinder was advanced from 200 rpm to 600 rpm. The reading of altitude at the higher speed was within 0.0001 in. of the lower. It was concluded from these tests that any pressure developed by this centrifugal force under normal conditions of operation was without significant effect.

5.7. Pressure Variations Due to Dynamic Sources

The piston gage itself is not sensitive to high-frequency fluctuations in pressure but under certain circumstances the fluctuations created by the piston gage may objectionably affect the connected apparatus. These fluctuations can arise from three sources; first, seismic motions, horizontal or vertical; second, any axial component of symmetrical character imparted by the cylinder rotation; and third, from the mechanism used to make up losses in the

enclosed volume. Such an effect in the order of 2×10^{-5} in. of Hg has been found when following the deflections of a sensitive diaphragm with light fringes. Effects exceeding one light fringe have been observed. These fluctuations have been satisfactorily controlled by connecting the gage to the diaphragm with some damping interposed such as small bore tubing.

5.8. Leakage

Leakage from the enclosed volume back of the piston may take place past the piston and the bearing since both are air-lubricated. The test made on Model I with a very low rotational speed while in a vertical position showed a leakage of air of 0.5 cm^3/min at a differential pressure of 0.3 in. of Hg. The leak decreases to zero, of course, when the piston gage axis is horizontal. This leakage is usually obscured by the pumping which occurs.

5.9. Pumping

The volume enclosed by the piston is subject to change due to pumping through the air bearings while the cylinder is rotating and may be either into or from the atmosphere. Usually the rate of volume change exceeds the rate of leakage. In the applications for which this gage is being developed the actual loss or gain of volume by leakage and pumping is not significant. When the piston gage is used either as a manometer or as a pressure regulator, the reading has been proven independent of the piston position over a range of $\frac{5}{16}$ in., also little manual manipulation is required to maintain the piston position constant to within even $\frac{1}{16}$ in. by venting or admitting air in some manner, such as by the adjustment of the screw compressed bellows illustrated in figure 4. It has been found practical to control an admitting valve by a photocell sensing the piston position. Such a controller may readily be added so the chief concern has been to determine whether any error is introduced in the gage readings by any axial forces acting on the piston produced by the pumping or variation in the pumping.

Various influences on the pumping rate were investigated. The pumping action was generally assayed by closing off the line into the gage, observing the axial motion of the piston over a suitable time, usually 5 min, and converting the linear motion of the piston into an equivalent gain or loss in gas volume in the closed space. The results of some of the tests are given below:

(a) With a 90-g piston at zero altitude the pumping rate was, for instance, 0.4 cm^3/min loss in volume. With other conditions of piston loading, belt tension, or altitude, the rate might be up to 1 cm^3/min and as frequently a gain in volume as a loss.

(b) The speed of rotation of the cylinder had but slight effect on the pumping rate within the limits tested. Practically identical rates were obtained with a four to one range in the speed of cylinder rotation. Even reversing the direction of rotation by running with a crossed belt, in various trials, gave the same rate of pumping, and in the same direction, as before. This seems to reduce the possibility of the pumping being due here to any screw conveyor action from surface marks or scratches on the cylindrical surfaces.

(c) The weight on the piston had a large influence on the pumping rate. At normal speed and with a piston weight of 30 g a gain of 0.2 cm^3/min was noted; and under the same conditions but with a piston weight of 150 g the rate of gain was 2.0 cm^3/min.

(d) A test was made in which the belt tension was progressively increased. Since the belt pull was upwards on the cylinder and positioned near the outboard end of the bearing, tightening the belt would decrease the bearing load and would at a certain point approximate an equally distributed loading. Under the conditions where light belt tension gave a pumping rate of 1.0 cm^3 loss per minute the gradual increase in tension passed through a condition where there was no pumping and on to where the rate was an 0.4 cm^3 gain per minute. The increase in belt tension did not result in an observable tilt of the piston axis.

(e) The piston was allowed to rotate with the cylinder by sealing it to the cylinder with a drop of machine oil. The rate of volume gain was found unchanged, indicating no pumping through the piston-cylinder clearance.

(f) The load in the piston was now arranged as unsymmetrically as possible. A 116-g end load was used, arranged so that the center of gravity was slightly off any portion of the piston area. On making tests with this weight in both the outboard and inboard positions the same rate of pumping was obtained in each case, 0.04 cm^3/min loss. Also as noted previously under zero stability the identical zero was obtained with both configurations. The effect of the unbalanced loading of the piston on the readings, as previously noted, was negligible.

(g) With a piston load of 116 g and the pumping in a direction to increase the air volume in the cylinder, the tilt of the gage was increased until the leakage rate and pumping rate were identical. Under this condition the pressure in the gage corresponded to 0.1 in. of mercury.

This series of tests seemed to prove that the pumping is chiefly through the cylinder-bearing clearance. Even if some pumping does occur through the piston-cylinder clearance, the magnitude of this effect is less than the resolution of the gage.

A more refined study may be attempted when opportunity is presented in order to determine if, under any conditions not yet covered, there is a measurable axial component reacting on the piston.

Hints as to the mechanism of the pumping are presented in some references on oil lubrication. McKee and McKee [8] studied the distribution of oil pressure in journal bearings and in their eccentric loading test show that the maximum pressure line in the bearing is askew with respect to the axis of the bearing. Also, considerably later, F. W. Ocvirk [9] reported on axial and twisted misalinement as affecting oil-pressure distribution in a similar bearing and clearly illustrated with three-dimensional graphs the askew maximum pressure area under these load conditions.

Neither author discusses transfer of oil through the bearing, but it does seem obvious that if the maximum pressure line (due to dynamic lubrication forces) is askew to the axis of the cylinder the minimum clearance line is also askew, although possibly not in the identical position, and the combination of an askew pressure line followed by a parallel minimum clearance line creates the condition for an axial flow of the lubricant. It is likely that some bell-mouthing also exists to accentuate the off-axis conditions. The conditions causing this askew pressure line, that is, eccentric loading, axial and twisted misalinement, and bell-mouthing (the latter occurring because of the former three) are all present to a much greater degree in the bearing than on the piston. This seemingly bears out the empirical evidence associating the pumping with the bearing. This analysis also suggests methods for reducing the pumping. One method would be to concentrically load the bearing, possibly by the addition of a second bearing or by arranging the bearing to lie outside of the cylinder. A second method would be to lessen twisting misalinement forces by having the rotational drive placed advantageously. Reduction of these latter forces will decrease the likelihood of bell-mouthing in use.

This pumping action is of limited importance in the piston gage. The considerable discussion presented here arises because of the difficulty encountered in the attempt to discover if any errors in pressure measurement arise from this action. The primary cause of the difficulty is the fact that the gage has a resolution some 10-fold greater than any conveniently available instrument on which an error from this source could be evaluated by comparative testing.

5.10. Gage Volume

In apparatus where a small constant volume system is required or desired the volume of this gage may be excessive, particularly when combined with the gage leaking and pumping that have just been discussed.

The motion of the piston can be observed, if desired, by low-power optical magnifying means and the position change corresponding to the gain or loss of 0.05 cm^3 is reasonably visible, but the volume change of the gage is always significant when there is a movement of the piston. At differential pressures less than 0.1 in. of Hg, the increased volume may be contaminated by "in" pumping from the atmosphere in which the gage is operated.

5.11. Centrifugal Force on the Piston

An axial force on the piston will exist if the cylinder rotates with any eccentricity. If eccentric motion is imparted to the piston, an axial component may result, affecting the apparent mass of the piston. The construction employed, where the same straight bore of the cylinder is used both to position the cylinder on its bearing and to support the piston, is believed to reduce the eccentricity error to a very low value. No error from this source on either of the models has been detected by change in zero with change in cylinder rotational speed.

5.12. Summary of Accuracy Limitations

The limitations upon the accuracy introduced by all factors are collected and summarized in table 6. Where dependent upon deflection, the values listed may be assumed for a tilting gage set at an altitude h of 5 in. and having a medium-weight piston. Many of these listed values are not known to sufficient precision to establish their variation with gage deflection. Values have been assigned in various cases to represent what is, at present, believed to be the maximum error that would be contributed by the listed factor. In many cases the value of 0.0001-in. is assigned because this represents the resolution of the gage reading at the time of the error investigation. Some of these errors may not even be of this significance. A few of the values entered are lower than this since they were studied when higher resolution was available for the reading.

Table 6

Factor	Accuracy limit in inches of altitude	
	Basic	Relative
1. Level	0.0001	0.00005
2. Temperature	.0001	.0001
3. Area	.0005*	.0002
4. Sine	.0001	.00005
5. Static charges	.0001	.0001
6. Piston oscillation	.0001	.0001
7. Centrifugal pressure	.0001	.0001
8. Dynamic pressure	.0001	.0001
9. Leakage	.0001	.0001
10. Pumping	.0001	.0001
11. Gage volume	.0001	.0001
12. Centrifugal force on weight	.0001	.0001
13. Weight determination	.0001*	.00005
14. Zero reproducibility	.00005	.00005
15. Reading reproducibility	.0001	.0001

In the error columns the values under "Basic" are assigned to cover the error of the instrument as a primary standard. In the column under "Relative" the values are based on the ability of the gage to repeat a reading either as a gage or as a pressure regulator. The errors without asterisks are subject to variations dependent on random influences. The errors marked with the asterisk are unidirectional. The 5-in. altitude with the medium-weight piston corresponds to a pressure reading of about 0.4 in. of Hg. The maximum predicted error in the basic measurement is 8×10^{-5} in. of Hg and in the relative measurement is less than 4×10^{-5} in. of Hg.

6. Design Modifications

Although because of its simplicity, an air-lubricated bearing has been employed for the cylinder, this is by no means essential and does have the inconvenience of considerably increasing the exchange between the atmosphere within and without the gage. Oil-lubricated journals or ball bearings

could be employed and the pressure chamber sealed with O-rings.

Where it is desired to work from a pressure datum other than that of the room, this may be accomplished by several means. For instance, identical air-lubricated bearings for the cylinder may be employed at both ends of the piston. This has been done at times, but a very nice mechanical assembly is required to allow disassembly for cleaning or adjusting the piston weight. If self-alinement ball bearings were employed this need not be a difficult reassembly.

Alternately, a particularly compact structure could be made by making the outer surface of the cylinder the bearing face, concentric with and outside the piston support area and fitted with two end pressure taps, as shown in figure 6. Alternatively the whole device may be enclosed by a belljar or to insure ease of access to the micrometer for adjustment, the cylinder section only might be enclosed and driven through a magnetic coupling.

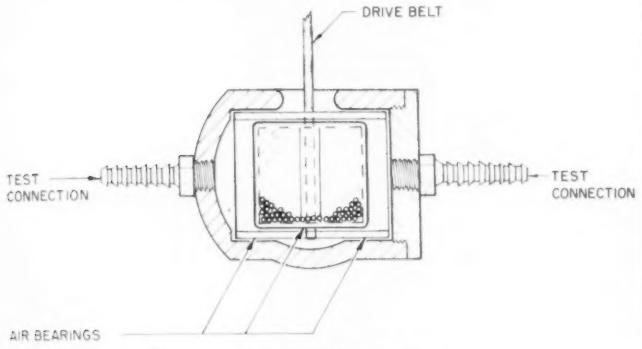

FIGURE 6. *Modified piston gage.*

Symmetrical pressure connections are provided to control the reference pressure also. The bearings are outside of the cylinder.

If the reference pressure is to be a high vacuum, the highest precision would be necessary in the cylinder fitting. Even with the smallest working clearance between the piston and cylinder the approach to the reference pressure would presumably be limited by the leakage past the piston, and the operation would be limited to an average pressure that would allow an air film for lubrication of the piston.

For a reference standard, it is believed that the most desirable piston and cylinder combination would be of fused quartz because of the stability of this material and also because of its nice working qualities. The fitting of the piston to the cylinder and area measurements might be performed to a much higher order of accuracy than with glass. Transparency of the cylinder seems desirable for observation of the piston although for a structure such as figure 6 an end window would suffice, in which case the cylinder and piston could both be metallic. It is desirable for the piston and cylinder to be of identical materials to avoid temperature effects in the close fits required.

To reach the lowest pressures the piston weight should be the least possible. No attempt has been made to determine the optimum diameter of the piston. A diameter on the order of 1 in. is convenient to work with, but smaller diameters might be employed with equal satisfaction if the volume or leakage of the gage is particularly significant. The eccentric weight for the piston may be, on various arrangements, suspended outside of the cylinder in order to provide greater leverage if needed.

The micrometer or height setting means might be driven by a servomotor to maintain a null piston position. Increased resolution is available if the micrometer were provided with a 6-in. reading circle or a digital readout, and provided that the screw has commensurate accuracy.

7. Field of Application

Because of its sensitivity and inherent accuracy it is believed that this gage has application as a calibrating standard in the range of differential pressure up to at least ½-in. of mercury and possibly can be extended to twice this. Its aperiodic motion and low-temperature coefficient (particularly if of quartz) reduces the time for a calibration.

Tests at zero differential pressure but at low absolute pressure indicate that measurements can be made at absolute pressures down to a few millimeters of Hg. With further development, it appears possible to extend the lower pressure limit down below a 0.1 of a millimeter of Hg.

As a manometer to read an unknown pressure in the above range, it has considerable versatility and with its dead-beat characteristics allows readings to be obtained rapidly. As a pressure regulator to reproduce precise settings, it has the unique advantage of the commonly used dead weight tester.

8. References

[1] W. G. Brombacher and T. W. Lashof, Bibliography and index on dynamic pressure measurement, NBS Circ. 558 (1953).

[2] H. F. Brubach, Some laboratory applications of the low friction properties of the dry hypodermic syringe, Rev. Sci. Inst. **18,** 363 (May 1947).

[3] H. R. Hindley, A differential manometer, J. Sci. Inst. **24,** 295 (1947).

[4] C. H. Meyers and R. S. Jessup, A multiple manometer and piston gage for precision measurements, BS J. Research **6,** 1061 (1931) RP 324.

[5] Manometer for calibrating high-altitude pressure devices, NBS Tech. News Bull. **43,** 71 (1959).

[6] M. D. Hersey, A short account of the theory of lubrication, J. Frankl. Inst. **220,** 93 (1935).

[7] P. W. Ott, Letter to Eng. News Rec. **103,** 785 (1929).

[8] S. A. McKee and T. R. McKee, Pressure distribution in oil films of journal bearings, Trans. Am. Soc. Mech. Eng. **APM–51–15,** 161 (Nov. 1931).

[9] F. W. Ocvirk, Measured oil film pressure distribution in misaligned plain bearings, Lub. Eng. **10,** 262 (Oct. 1954).

WASHINGTON, D.C. (Paper 63C1–5)

Journal of Research of the National Bureau of Standards—C. Engineering and Instrumentation
Vol. 63C, No. 1, July–September 1959

Compact Multi-Anvil Wedge-Type High Pressure Apparatus

E. C. Lloyd, U. O. Hutton, and D. P. Johnson

(May 8, 1959)

Apparatus for generating high pressures by application of force by an anvil against each face of a solid polyhedron is described. The equipment constructed utilizes a tetrahedron of pyrophyllite and four tungsten carbide anvils as described earlier by H. T. Hall. External force is applied to only one of the anvils, and wedge reaction forces act on the other anvils, permitting the equipment to be used in a conventional hydraulic press. Examples of results of use of the equipment are given. Success of the design has been shown by the repeated generation of pressures in excess of 100,000 atmospheres indicating that large existing presses might be used to generate pressures of this order in volumes of several cubic inches. For higher pressures a two-stage multi-anvil apparatus is proposed in which the second-stage anvils are embedded in a large pyrophyllite tetrahedron to obtain necessary supporting forces.

1. Introduction

A multiple-anvil apparatus for generating high pressures by application of force by an anvil against each face of a solid polyhedron is described. Such an arrangement was described by Hall [1] for pressures up to 100,000 atmospheres using four independent hydraulic rams to apply force to the faces of a tetrahedron of pyrophyllite. The present equipment employs an assembly in which external force is applied only to one of the four anvils, and wedge reaction forces act on the remaining three anvils. This results in a compact equipment that can be used in a press of conventional design, with the further advantages of easy manipulation and rapid assembly and disassembly. Although apparatus of the type described here lends itself, in special applications, for use with solids having a larger number of faces, the regular tetrahedron appears to be the most generally desirable shape, and is the ouly one used with the apparatus so far.

This configuration has the attractive possibility of permitting the use of existing presses of very large capacity to obtain high pressures in volumes of several cubic inches. The availability of high pressure in volumes of this size would present the possibility of practical two-stage devices to obtain still higher pressures.

2. Constructional Features and Operation

Figure 1 shows the wedge-type tetrahedral assembly in place in a small hand-operated press used for applying ram forces up to 50 tons. Figures 2 and 3 illustrate the general construction, and the drawings of figures 4 and 5 show some of the details of the equipment. The initial apparatus, illustrated here, utilizes anvils having triangular faces ½-inch on an edge (face area about ⅛ in.^{2}) to accommodate tetrahedrons of pressure-transmitting material of 9/16-inch edge-length. The half-angle of the inner surface of the conical ring is 18½ degrees.

In operation, the clamping force of a hydraulic press applied to the upper anvil and the bottom of the containing ring causes the three lower anvils to slide downward along the inner conical surface of the containing ring, and the resulting wedging forces result in substantially equal motion of all four anvils toward the center of the pyrophyllite tetrahedron.

FIGURE 1. *Wedge-type tetrahedral apparatus in place in a 50-ton hand-operated press for use in pressure range up to 60,000 atmospheres.*

[1] H. Tracy Hall, Rev. Sci. Inst. **29**, No. 4, 267 (1958).

Measurements made during initial tests of the equipment at 100 tons load (calculated pressure near 125,000 atm) showed deformation of the conical ring into a three-lobed shape that fitted inside a circle about 0.001-inch larger in diameter than the unloaded ring. Based on this deformation, stresses in the ring appear to be consistent with design stresses, which were selected to be conservative with respect to the strength of the SAE 4340 steel. No evidence of permanent deformation of the ring or anvils has been found after more than 10 cycles to a ram load of 100 tons.

The machining of the butt-faces of the three lower anvil assemblies (to conform to the shape of the ring in the final position of the anvils) was done with the use of the guide block shown (fig. 3). This block was originally also used during application of load to guide the anvils. This was found to be unnecessary, however, because of the self-locating effect of the faces of the wedges and their low frictional reaction in the cone, and the use of the guide block for this purpose was discontinued in order to simplify electrical insulation of the anvils.

FIGURE 2. *View of wedge-type apparatus with upper bolster removed showing arrangement of anvils in conical ring.*

The butt-ends of the three lower anvils are shaped so that in their lowest position they exactly fit the ring.

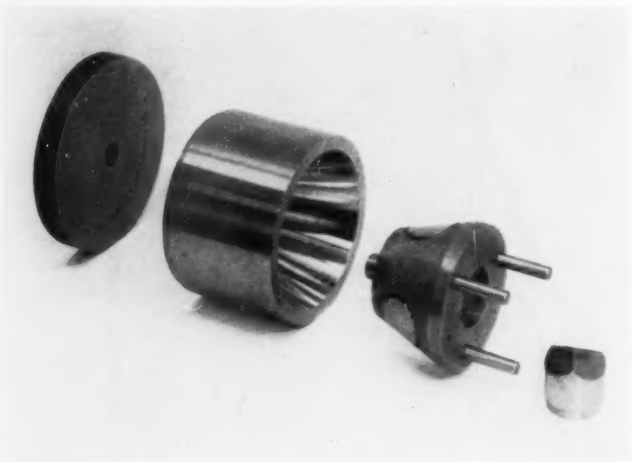

FIGURE 3. *Disassembled view of apparatus, with lower anvils installed in conically shaped guide block used for machining the butt-faces.*

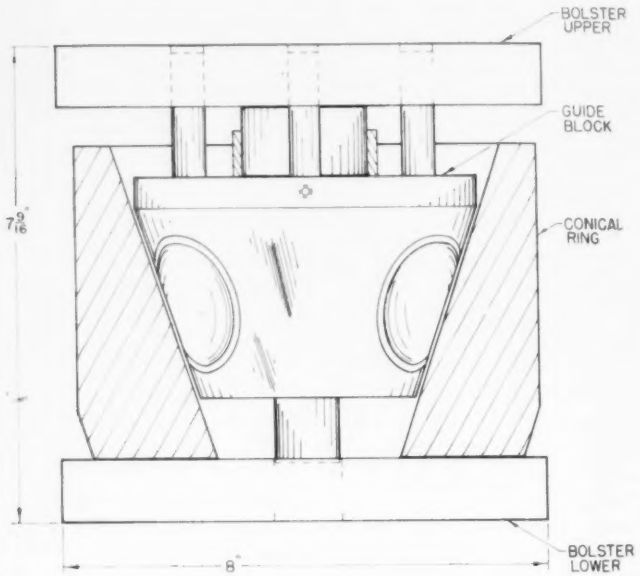

FIGURE 4. *Sectional drawing of wedge-type apparatus showing guide block inside conical ring.*

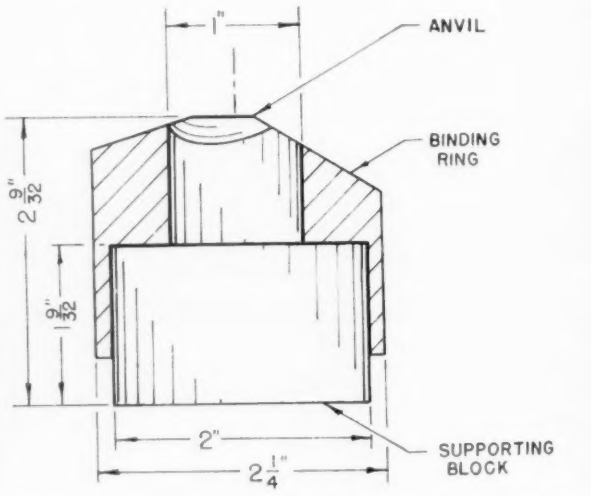

FIGURE 5. *One of the four three-piece anvil assemblies, showing the tungsten carbide anvil supported by a steel binding ring and supporting block.*

The material used for the anvil assemblies and conical ring was SAE 4340 steel heat treated to Rockwell 40/41C, except the anvils which were of Allegheny Ludlum grade CA–4 tungsten carbide. The upper and lower bolster plates and the guide block were cold rolled steel.

The pressure-transmitting material used has been pyrophyllite (hydrous aluminum silicate, $4\ SiO_2 \cdot 3Al_2O_3 \cdot H_2O$) and, as in Hall's equipment, this pressure medium extrudes between rouged surfaces of the anvils to form a compressible gasket. The specimen to be studied is contained in a cavity inside the tetrahedron, frequently a hole drilled between centers of opposite edges. The specimen size has been varied from 5 to 50 percent of the tetrahedral volume, but if the specimen has been more than 10 percent of this volume difficulty in preventing extrusion of the specimen through the gasket has frequently been encountered. This difficulty is decreased by more precise fitting of the tetrahedron.

With pyrophyllite tetrahedrons of $\frac{9}{16}$-inch initial edge-length, measurements made in initial trials of the equipment showed the total vertical motion of the upper anvil to be about 0.030-inch as the load was increased from 5 tons to 100 tons. The stroke for the initial 5-ton load varied depending on the amount of "slack" in the system. The time required to reach a load of 100 tons could be selected over a wide range, and any intermediate load could be held for periods up to several hours without difficulty.

Using $\frac{9}{16}$-inch tetrahedrons the extrusion of pyrophyllite forms a gasket between the parallel anvil surfaces having a width of about $\frac{3}{32}$-inch, and a thickness of about 0.006-inch, as shown in figure 6. In order to obtain an equal gasket thickness in all gasket areas the three lower anvils are initially spaced with plastic buttons near the tetrahedral die area, of thickness to provide symmetrical positioning of the four anvils around the over-sized tetrahedron inserted in the cavity. Spacers of indium, block tin, or Teflon (when a nonconductor is desired), have been used with equal success, and the gasket is ordinarily extruded in quite a symmetrical configuration on all edges.

One of the difficulties to be expected in designing this equipment lies, of course, in overcoming the effects of excessive friction between the sliding anvils and the conical ring. A number of materials have a low coefficient of friction under heavy loading and appeared to be suitable for use as lubricants between these surfaces. Sheet Teflon 0.003-inch thick was first tried, and found to be so satisfactory that no other material has been used. In addition to serving as a lubricant the Teflon provides electrical insulation between the anvils and the ring. Tests on 0.003-inch sheet Teflon using the method [2] of measuring the torque required to turn a smooth right circular cylinder loaded longitudinally with the sample to be tested as a lubricating film at each end of the cylinder gave the values of friction listed in table 1.

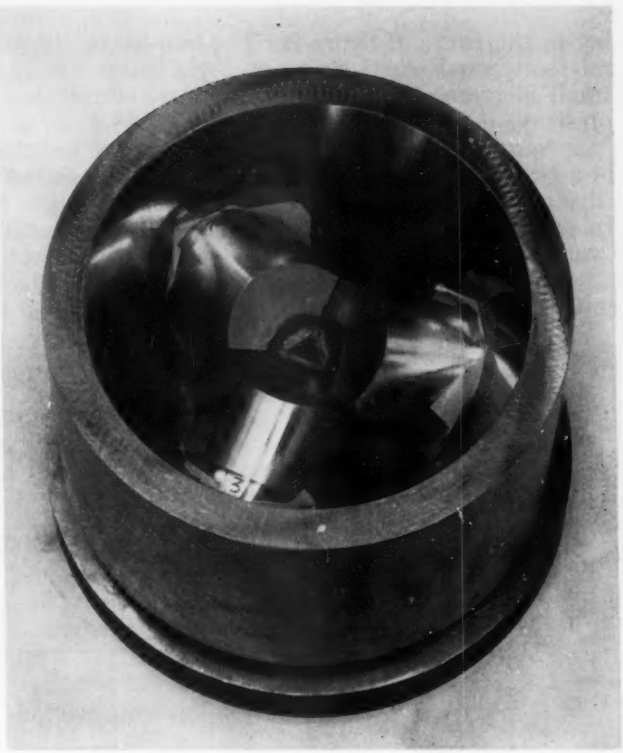

FIGURE 6. *Wedge-type apparatus with top anvil removed, after application of pressure, showing pyrophyllite tetrahedron in place.*

The gasket is the light area adjacent to tetrahedron, and the surrounding darker area is rouge coating. Sheets of Teflon to act as lubricant are in place between the bases of the anvil assemblies and the conical ring.

TABLE 1. *Coefficient of dry friction between sheet Teflon and smooth steel*

Average pressure	Starting friction	Sliding friction
psi		
33,000	0.011	0.007
66,000	.012	.008
83,000	.014	.010

These values of coefficient of friction correspond to a sliding angle of about ½ to 1 degree; accordingly, the half angle of the conical surface of the ring was made 18.5 degrees, or one degree smaller than the angle complementary to the angle between faces of the tetrahedron (70.528 degrees). This results in the forces exerted on the lower three anvils being within ½-degree of the axes of the anvils.

The adequacy of the Teflon lubricant has been well demonstrated in more than 30 force applications, of which about 10 were in the neighborhood of 100 tons, without any evidence of metal-to-metal contact. In one test the same Teflon pieces were used in three successive force applications at 100 tons without failure.

Measurements of the dimensions and density of pyrophyllite tetrahedrons after being subjected to various pressures showed that this material increases

[2] P. W. Bridgman, Phys. Review **48,** 825 (1935).

nearly irreversibly in density with pressure, according to the curve of figure 7. The material exhibited relatively small elasticity in compression, so that only small increases in volume occurred after release of pressure.

Specimens to be subjected to pressure are inserted in a hole (up to ⅛ in. diameter) drilled from edge to edge of the tetrahedron, as may be seen in figure 8. In order to study the extent to which the pressure over such a specimen departs from true hydrostatic pressure, cylinders of indium were used, and the resulting deformations noted. Such a specimen is shown in figure 8. In specimens which were not extruded through the gasket there is a characteristic flattening of the ends parallel to the adjacent edges of the tetrahedron. The shear yield strength of indium under high pressures, comparable to those encountered here, is reported by Bridgman to be about the same as at ambient pressure, about 1,000 psi. This suggests that the departure from uniform pressure over the surface of the indium specimen is only of the order of a few hundred atmospheres at most. A specimen material which is embedded, or sheathed, in an indium cylinder would thus be subjected to uniform pressure within pressure variations of this magnitude. Tests with still softer materials are planned to determine whether they can be contained by the pyrophyllite, and thus obtain a still better approximation to true hydrostatic pressure.

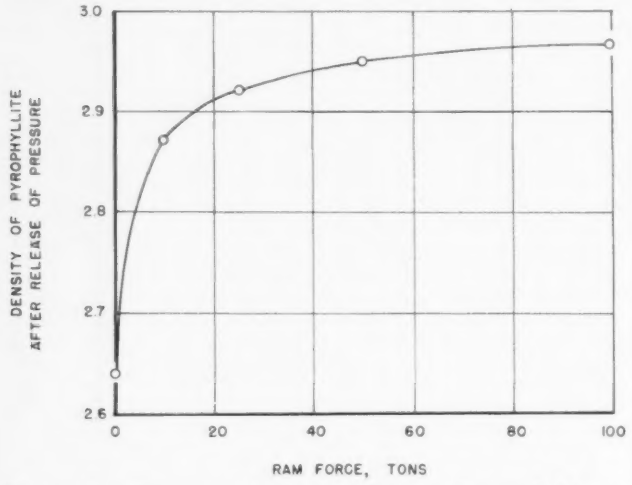

FIGURE 7. *Permanent increase in density of pyrophyllite due to application of pressure.*

Figures 9 and 10 are examples of pressure-resistance relationships obtained on specimens of bismuth and antimony, respectively. In each case the volume of the specimen was approximately 4 percent of the volume of the tetrahedron. In the measurements of resistance of these specimens under pressure a four-lead circuit was used, in which two of the anvils served as current leads and the other two as potential leads. Connection to the specimen was by use of silver foil strips as described by Hall, and as illustrated by one of the tetrahedrons of figure 8. In investigations requiring heating of the specimen this arrangement of electrical connections is available, of course, for conducting heating current and for tem-

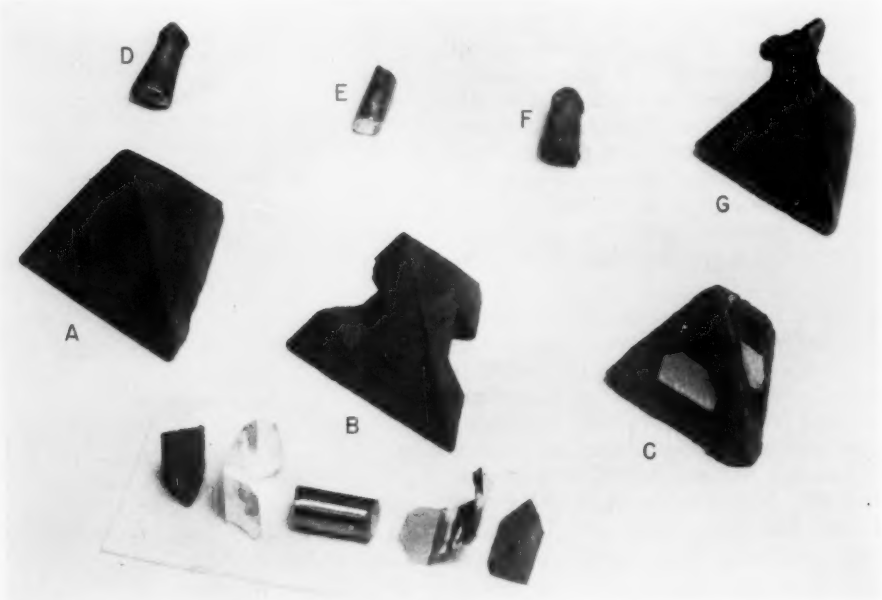

FIGURE 8. A. *Pyrophyllite tetrahedron as cut.* B. *Pyrophyllite tetrahedron with drilled hole to receive specimen shown, with silver foil contacts and prisms of phrophyllite to fill notches at ends of hole.* C. *Pyrophyllite tetrahedron, assembled as in B, after removal from high pressure equipment.* D, E, F. *Specimens of indium, bismuth, and antimony, respectively, after release of pressure. Specimens were originally of cylindrical shape.* G. *Pyrophyllite tetrahedron after removal from high pressure equipment, showing example of extrusion of specimen of bismuth.*

perature measurements, and additional electrical connections would be available in a configuration using other shapes having a larger number of faces and anvils.

In figure 9 pressure is shown in terms of ram force for increasing and decreasing pressure. Superimposed is the pressure-resistance curve by Bridgman in which the pressure scale (abscissa) is linear; the first transition points on increasing pressure have been made to coincide. The abrupt fall in resistance of bismuth reported by Bridgman [2] to occur at 25,000 atm is evident in figure 9. Bridgman's second transition at 27,000 atm (increasing resistance) is not sharply defined as to point of onset, but the maximum in resistance is definite. The displacement of the ascending and descending force versus resistance curves

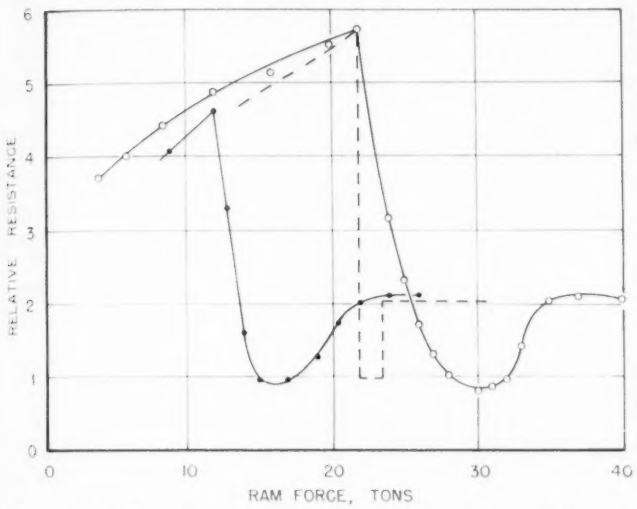

FIGURE 9. *Ram force versus resistance of specimen of bismuth, 99.99 percent pure.*

○, Increasing force; ●, decreasing force. Bridgman's results, plotted to a linear pressure scale, are shown by the dashed line for comparison.

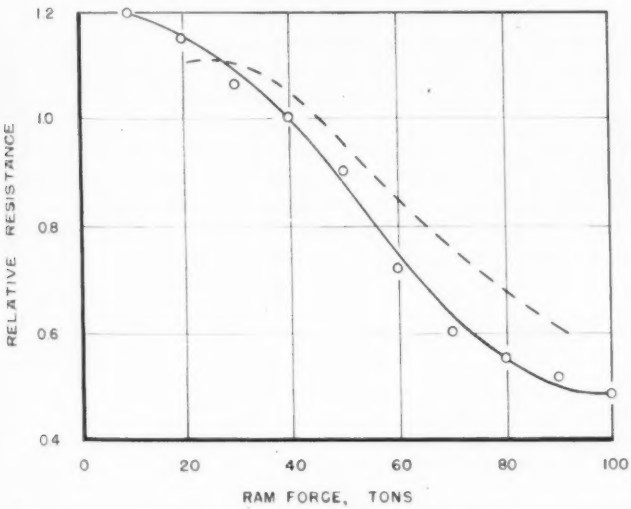

FIGURE 10. *Ram force versus resistance of antimony, 99.99 percent pure, on increasing force.*

Bridgman's results, plotted to a linear pressure scale, are shown by the dashed line for comparison.

gives an indication of the hysteresis of this particular configuration of pyrophyllite and bismuth. The appreciable slope of our curve and the relatively wide force range over which the resistance transitions occur is probably due principally to two factors: the departure from uniform pressure over the surface of the bismuth due to internal friction in the pyrophyllite, and a departure from proportionality between ram load and specimen pressure during the constant-pressure reductions in volume of bismuth at its two transition points (which amounts to 4½ percent and 3 percent for the first and second points, respectively.) This departure from proportionality evidently results from the additional gasket compression required to effect the reduction in bismuth volume at constant pressure. On decreasing pressure it will be noted that both transitions are displaced to ram forces corresponding to pressures considerably lower than Bridgman's values. This hysteresis is attributable partly to pressure "held" by the hysteresis effect of the pyrophyllite, which appears to increase significantly with the irreversible increase in density on application of pressure, and partly to friction between the anvils and the gasket.

Figure 10 shows results for antimony, in which the relative resistance changes continuously up to the highest pressure reached, probably over 100,000 atm. Although a volume discontinuity is reported by Bridgman [2] at 85,000 atm, he found no corresponding specific resistance change at this pressure. The antimony used in the present case was probably of substantially higher purity than Bridgman's sample. Bridgman's result is plotted for comparison, on a linear pressure scale derived from the lower curve of figure 11.

Estimates of the pressures obtained have initially been by measurement of the ram force and the areas of pyrophyllite under pressure. Two principal uncertainties are involved in this method: the reduction in effective ram force due to the force supported by the extruded gasket, and the effect of internal friction in the pyrophyllite. Measurements made on the gaskets formed by single applications of force from 25 tons to 100 tons to $\frac{5}{16}$-inch tetrahedrons gave a gasket lateral area, nearly independent of the force, of approximately 50 percent of the total area subjected to ram force. If the pressure in the gasket falls linearly from the edge of the tetrahedron to the free edge of the gasket, the net force acting on each face of the tetrahedron is approximately 75 percent of the total ram force.[3] However, the loss in pressure, on increasing force, due both to gasket forces and to internal friction of pyrophyllite appears to be only about 10 percent, as indicated by values of ram force required to reach the first resistance transitions of bismuth and barium. The lower line plotted in figure 11 was drawn from data obtained on transitions of bismuth and barium, and the upper line is the calculated average pressure on the faces of the tetrahedron without correction made for gasket force.

[2] P. W. Bridgman, Phys. Review **48,** 825 (1935).

[3] Actually, the variation in pressure in the gasket probably lies between a linear and an exponential function, and the force supported by the gasket is appreciably less than 25 percent.

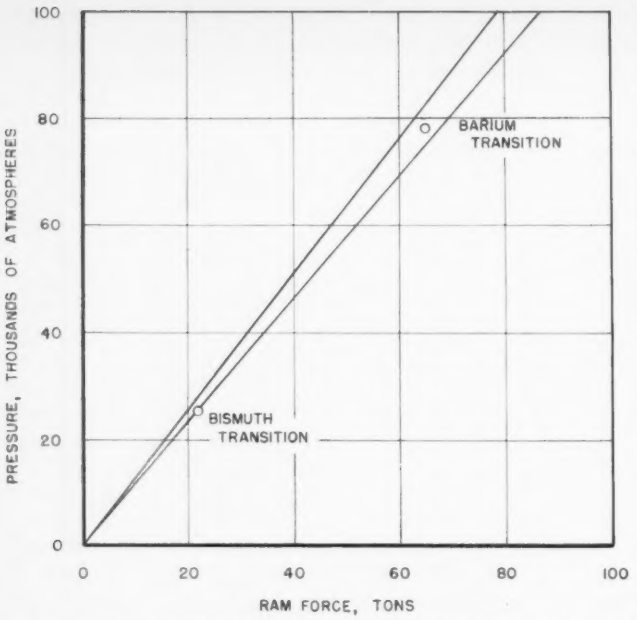

FIGURE 11. *Calculated average pressure on face of ½-inch tetrahedron (upper curve), and actual pressure on cylindrical specimen (lower curve) versus ram force.*

The lower curve is based on the bismuth transition of figure 9, with a point similarly obtained for barium shown for reference. The value of pressure for barium is due to Bridgman (78,000 atm).

The difference in ordinates of these two lines indicates the lag in pressure due to internal friction in the pyrophyllite and the loss of pressure due to force taken by the gasket.

3. Future Work

This high pressure equipment will be used, as well as stepped-piston equipment, to study properties of materials at high pressures, with the objective of establishing "fixed points" on the pressure scale, and of devising improved pressure measurement techniques.

Further investigations of pressure-transmitting media appear desirable to provide improved performance of the equipment in various pressure ranges. Combinations of tetrahedron material and specimen sheath material having more nearly optimum properties may substantially improve the uniformity of pressure applied to a specimen.

The use of a larger tetrahedron would improve the ratio of tetrahedron volume to specimen volume, should reduce the proportion of force taken by the gasket, and would evidently provide more uniform pressure in the central volume. New apparatus is under design to apply 600 tons to tetrahedrons of about 1-inch edge-length, to investigate the advantages of larger size.

The ultimate pressure attainable with the present equipment will be determined with the use of larger presses that will be available for further work. The absence of failure of any sort with repeated ram loads of 100 tons, the relatively low stresses in the conical ring, and the excellent performance of the teflon lubricant, give an indication that substantially higher ram loads may be used.

The adaptability of the equipment to conventional hydraulic presses makes feasible consideration of the use of very large ram forces, with a corresponding increase in size of the tetrahedron to perhaps 2½ or 3 inches. The availability of high-pressure volumes of this size may make a two-stage device practicable. Such a device is proposed, utilizing a large tetrahedron, in each face of which is embedded a second stage one-piece carbide anvil of such dimensions as to enclose a small tetrahedron at the center. The four second stage anvils would probably be tapered with the small ends faced to accommodate a tetrahedron and its gasket, as in the present equipment, and with the large ends in contact with the faces of the primary anvils. The secondary anvils would be subjected to the pressure of the large tetrahedron over their lateral surfaces to provide the necessary supporting forces. An alternative to the use of two sets of anvils is the machining of each anvil pair as one piece. It seems likely that adjustment of the parameters available, including relative dimensions of the large and small anvils, the elastic properties of the anvils and of the pressure transmitting media, and the relative volumes of large and small tetrahedrons, would provide a good chance of success of a two-stage device. Important in the proposed two-stage device is the availability of four electrical connections into the highest pressure volume via the four anvil pairs.

We are indebted to Dr. H. T. Hall of Brigham Young University for information on the construction of his tetrahedral anvil equipment. Mr. H. J. Zoranski of the Mechanical Instruments Section prepared shop drawings of the equipment and made suggestions that were valuable in selecting the design finally adopted. The excellent machine work of the NBS Shops Division was an important factor in successful performance of the equipment.

WASHINGTON, D.C. (Paper 63C1–6)

Journal of Research of the National Bureau of Standards—C. Engineering and Instrumentation
Vol. 63C, No. 1, July–September 1959

A Coulometric-Titration Coulometer

Stanley W. Smith[1] and John K. Taylor

(April 28, 1959)

A highly precise coulometer is described which permits time integration of currents totaling 100 coulombs or more with a precision of about 1 part in 100,000. The current to be integrated oxidizes hydroquinone in an electrolysis cell, producing quinone and acid. The quinone is then reduced by constant-current coulometric titration, the end point being indicated by hydrogen-ion concentration measurements.

1. Introduction

The increased interest in coulometric methods of chemical analysis has created a need for a current integrator of higher precision than the mechanical, electrical, or electrochemical devices now available. Such an integrator should be simple to operate and give precise results for small quantities of electricity.

Overall considerations indicated that it should be possible to integrate a total charge of 100 coulombs, corresponding to 1 milliequivalent of chemical reaction, with a precision of about 1 part in 100,000, using an electrochemical coulometer. The purpose of this investigation was to develop such a device.

The simplest arrangement which might be expected to fulfill the requirements is an acidimetric type of electrochemical cell in which the current to be integrated generates strong acid in a neutral electrolyte. The amount of acid so generated is then determined precisely by constant-current coulometric titration.[2] A titration coulometer of the acidimetric type has been reported in the literature,[3] but preliminary investigations showed that the electrode reactions involved were not efficient to the degree required for this application.

As a result of the experiments which showed the defects in this method, it was decided to use an oxidation-reduction type of reaction. Upon investigation of several possibilities, the hydroquinone coulometer was selected as best fitting the requirements placed on the method. The reaction involves the oxidation of hydroquinone to quinone by the current to be determined, and the subsequent reduction back to hydroquinone by constant-current coulometry. The reactions may be represented as follows:

$$\text{Hydroquinone} + \text{integrated current} \rightarrow \text{quinone} + H^+ \quad (1)$$

$$H^+ + \text{quinone} + \text{constant current} \rightarrow \text{hydroquinone} \quad (2)$$

Reaction (2) is the reverse of (1), so that the quantity of electricity required to return the cell to the starting point, reaction (2), is equivalent to that responsible for reaction (1).

[1] Present address, Delco-Remy Division, General Motors Corporation, Anderson, Ind.
[2] J. K. Taylor and S. W. Smith, J. Research NBS (in press).
[3] J. A. Page and J. J. Lingane, Anal. Chim. Acta **16** 175 (1957).

Since hydrogen ions are involved in the reaction, it is possible to use a hydrogen-ion concentration (pH) measurement as the means for detection of the end point, that is, when the reverse reaction is complete. This has the distinct advantage over other possible systems in that an indicating electrode system and related measuring equipment are readily available which are very stable and of a high degree of refinement, making additional investigation in this area unnecessary.

2. Reagents and Apparatus

The supporting electrolyte is made up from reagent-grade sodium chloride, precipitated from the saturated solution by hydrogen chloride gas, and recrystallized from water.

The hydroquinone is recrystallized once from air-free water and dried under reduced pressure. The product of the recrystallization consists of white needles appearing slightly violet in large quantities.

The electrical system used is shown in figure 1. The voltage is supplied by a 48-v lead storage battery isolated from ground. Variable resistor R_1, a voltage dropping resistor, supplies several ranges of current. Switch S_2 is a double-pole, double-throw knife switch of the Leeds and Northrup potentiometer type. When in position (1), the current is passed through a dummy resistor R_2 which is ad-

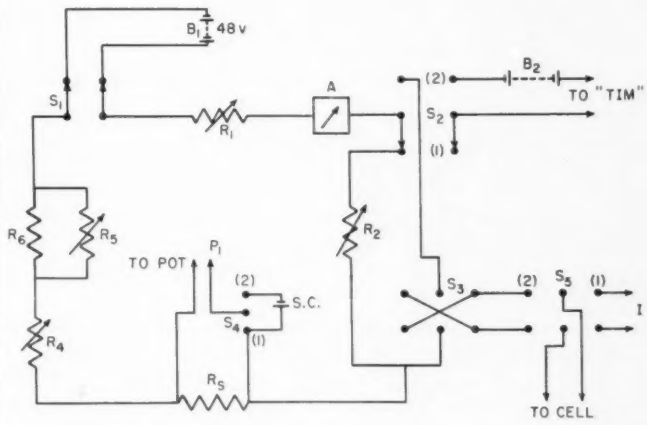

FIGURE 1. *Schematic diagram of electrical circuit.*

justed to have the same resistance as the cell. When switch S_2 is thrown in position (2), the current flows through the cell and simultaneously the quartz crystal controlled time-interval meter, TIM, Berkeley Model 7250 CD, is triggered by the pulse from battery B_2.

Switch S_3 is a reversing switch, allowing the current to flow through the cell in either direction. When switch S_4 is in position (1), the voltage drop across standard resistor R_3 is measured by the precision potentiometer P_1. When switch S_4 is in position (2), the voltage across R_3 opposes the standard cell, *S.C.*, and the difference is measured by P_1. The resistor network R_4, R_5, and R_6 is for adjustment of the current. The coarse adjustment, R_4, is composed of resistance decade boxes. Fine regulation is obtained by means of a fixed resistor and a carbon compression resistor, R_5. The resistance range of the network, R_5–R_6, is approximately 18 ohms, and the range of R_4 is 2,000 ohms in 0.1 ohm steps. The resistance is adjusted during a determination to maintain a null deflection of the galvanometer of potentiometer P_1.

Switch S_5, when in position (1), connects the cell to the source of current to be integrated according to reaction (1). Position (2) is used for the coulometric titration according to reaction (2).

The end point is determined by a commercial *p*H meter equipped with standard glass and reference electrodes. In addition, a precision potentiometer is connected across the recorder terminals of the *p*H meter, allowing a precision of 0.002 *p*H units in determining the end point.[2]

The stability of the *p*H meter is of prime importance, since the reproducibility of the end point is directly related to this factor. A commercial meter providing automatic zero standardization is very satisfactory in this respect.

The cell and associated equipment are shown in figure 2. Water-pumped nitrogen is passed successively over copper at 500° C to remove oxygen, through ascarite to remove carbon dioxide, through a 1-*N* sulfuric acid wash-solution to entrap any dust from the ascarite, and finally through two wash-solutions of distilled water to remove traces of acid and saturate the gas with water vapor. The function of the stopcock arrangement will be explained under experimental procedure.

The cell consists of two electrode compartments, 4.5 by 10 cm, connected by a bridge containing 3 sintered glass disks, of which (1) and (2) are of medium porosity and (3) is of fine porosity. An agar plug at the entrance port of compartment *C* effectively prevents transfer of solution to or from this compartment. The bridge is provided with tubes for blowing the solution from its compartments by means of nitrogen pressure.

The stopper assembly which closes working compartment *A* is filled with three glass tubes: one for bubbling nitrogen through the solution for the purpose of removing carbon dioxide and oxygen; one for flowing nitrogen over the solution during the determination; and one for exit of the nitrogen from

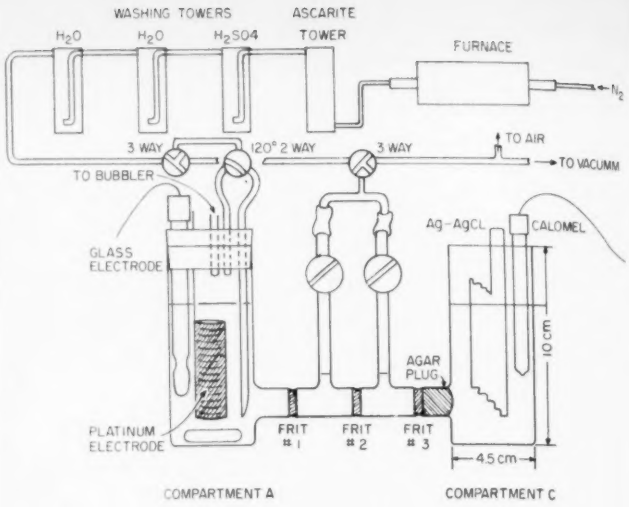

FIGURE 2. *Coulometric cell and associated apparatus.*

the cell through a water trap. A hole is provided for the introduction of the glass electrode. A cylindrical platinum gauze electrode, 5 by 1.5 cm in diam, completes the assembly.

Compartment *C* is separated from the rest of the cell by a 5-percent agar plug as described above. It contains the silver–silver chloride working electrode, constructed from a piece of fine silver 5 by 10 cm, and the calomel reference electrode.

To hasten the rate of attainment of equilibrium at the end point, it is desirable to immerse the cell in a water bath maintained at 45° C. A satisfactory arrangement is to place the cell in an aluminum pan sitting on a combination hotplate-magnetic stirrer to provide both stirring and temperature control.

3. Experimental Procedure

Before assembly, the cell is cleaned in hot sulfuric acid-chromic acid solution and rinsed by drawing large quantities of hot distilled water through the sintered glass disks to ensure removal of all traces of the cleaning solution.

The agar plug is formed in the side arm of the clean cell as follows. An agar solution, made by dissolving 5 g of agar-agar in 100 ml of a 2-*M* sodium chloride solution and heating to near boiling, is poured into the side arm. The gel sets on cooling and will not soften unless the temperature is raised above 60° C.

The supporting electrolyte is prepared by adding 10 g of sodium chloride to each compartment, plus sufficient distilled water (approximately 85 ml) to cover the platinum electrode when the bridge is filled. After the stirring bar is added, the stopper assembly is fitted to the cell and it is placed in position in the water bath. The nitrogen manifold connections are then made as shown in figure 2.

After the *p*H electrodes have been standardized in a buffer solution at the operating temperature,

45° C, the glass electrode is inserted in the stopper assembly. The reference electrode is placed in the isolated compartment with the silver–silver chloride electrode. Nitrogen is then bubbled through the cell and the bath temperature is raised to 45° C. After purging for 20 to 30 min, the stopcock is turned to allow the gas to flow over the surface of the solution. The bridge is then filled by applying suction to the center compartments.

The current is adjusted to 10 ma and passed through the cell until the *p*H reaches 7. At this point, the solution in both central compartments is pushed into compartment *A* by nitrogen pressure. After mixing, it is drawn back into the bridge. The *p*H is again brought to 7 by electrolysis and the process is repeated until there is no change in *p*H.

Hydroquinone (0.50 g) is now added to compartment *A* and allowed to dissolve. The equilibrium *p*H (approximately 5.6) is recorded and used as the end point.

For accurate results, the cell is preconditioned in the following manner. With the platinum electrode as anode, the current is adjusted to 100 ma and acid is generated for approximately 1,200 sec. The polarity is then reversed and base is generated for about 1,150 sec. The current is then changed to 10 ma and the generation of base is continued to the end point. The bridge is emptied, then refilled, and the solution is brought to the end point again. This rinsing process is continued until no change occurs. The cell is now ready to be used as a coulometer.

Performance testing is carried out in the following manner. The current is adjusted through the dummy resistor to 100 ma. With the platinum electrode as anode, acid is generated for about 1,000 sec, while the current is monitored continuously to maintain a constant and known value.

The acid so produced is then titrated by reversing the polarity, and passing a constant and accurately measured current of about 100 ma until approximately 95 percent of the acid is neutralized. The current is then reduced to 10 ma and the end point (original equilibrium *p*H) is reached by the same process as described for conditioning the cell.

The procedure is the same for integrating an unknown current. However, if the total quantity of charge is not known approximately, the *p*H must be observed occasionally to avoid generating past the end point. When the solution is back to the end point, the cell is ready for another determination.

4. Results

When following the procedure described in section 3, a precision of approximately 1 part in 100,000 may be obtained. The results of a number of determinations made over a period of 10 months are given in table 1. These data were all obtained with approximately 100 coulombs input and are given as percent recovery; namely, (coulombs, oxidation/coulombs, reduction)$\times$100.

TABLE 1. *Performance data*

1958	Recovery	1958	Recovery
	%		%
Jan. 14	100.000	Jan. 30	100.001
Jan. 15	100.001	Feb. 27	99.999
Jan. 16	100.002	Oct. 13	99.999
Jan. 16	99.999	Oct. 14	100.002
Jan. 29	100.000	Oct. 14	100.001

5. Discussion

The method does not involve any precision chemical operations which would require the services of a highly skilled chemist.

The precision and accuracy of this method depend on the control maintained over a number of factors, including: Accidental loss of electrolyte, diffusion and migration of ions, efficiency of electrode reactions, slope of the *p*H-time curve, stability and calibration of the circuitry, and freedom from ground loops.

Accidental loss of electrolyte could occur through the gas exit tube, around the stopper assembly, or through the bridge into the isolated compartment. If the nitrogen is flowed over the solution during the entire run and the stopper assembly is carefully made and fitted, there is no appreciable loss from this source. The possibility of loss through the bridge is negligible if the agar plug is firm and does not soften at the temperature of operation. It has been demonstrated experimentally that only a minute amount of acid reaches the second bridge compartment, mainly by convection through the frits (1 and 2). None is transferred through an agar plug in good condition.

The use of a rather concentrated salt solution to carry the current effectively minimizes electromigration of hydrogen ions across the bridge during reaction (1).

The reactions at the platinum electrode are 100 percent efficient as long as the silver–silver chloride electrode is maintained in a separate compartment. In experiments where this electrode was installed in the same compartment with the generating electrode, the efficiency of the reduction reaction (2) was found to be less than 100 percent due to the finite solubility of silver chloride in the electrolyte and the subsequent reduction (plating out) of silver on the cathode.

It is necessary, of course, to exclude all traces of foreign acid or alkali from the cell. For example, the leaching of 10^{-4} ml of cleaning solution from the walls of the cell would result in an error of about 3 parts in 10,000.

The precision of the detection of the end point depends on the reproducibility of the *p*H-meter readings and on the slope of the *p*H-time curve. Experience has shown that the experimental arrangement is of sufficient stability and sensitivity to make the *p*H measurements reliable to about $\pm$0.002 unit.

The slope depends on the concentration and volume of the electrolyte in the cell. Hydroquinone is a very weak acid, $K_1 = 1.1 \times 10^{-10}$, and exhibits slight

buffering action at the end point. Since the slope increases as the solution is diluted, it is desirable to use the most dilute solution practicable. At the same time, the volume of the working compartment of the cell must be kept small to insure significant changes in the *p*H for small amounts of reduction near the end point.

Theoretically, 55 mg of hydroquinone is oxidized by 100 coulombs of electricity. To minimize concentration-polarization effects, a larger amount must be used. For example, poor results were obtained with a two-fold excess of hydroquinone present, but a six-fold excess was found to be adequate for efficient operation of the cell. As a conservative measure, a nine-fold excess of hydroquinone was adopted, corresponding to 500 mg or to a concentration of 6 g/liter in the 85-ml cell.

The variation of the *p*H of the electrolyte with concentration of hydroquinone is shown in figure 3. The theoretical curve is shown for comparison. The *p*H value indicated at the operating concentration of 6 g/liter is 5.63 (average deviation $= \pm 0.10$) and is the average of the end-point values for 20 integrations.

Figure 4 shows the variation of the *p*H of the cell as the end point of reaction (2) is reached, for two different concentrations of hydroquinone. For the cell containing 50 mg of hydroquinone, approximately the theoretical amount for 100 coulombs, 0.0004 coulomb produces a change in *p*H of 0.002 unit. For the cell containing 500 mg of hydroquinone, the same change in *p*H requires 0.001 coulomb.

With reference to the data of table 1, the reproducibility found is what would be expected from the uncertainty of the end point.

If the components of the electrical circuitry are properly calibrated, any errors from this source will be at least an order of magnitude below the other errors in the method. However, it is necessary to control the temperature of the standard resistor and the standard cell for high accuracy. Also care must be exercised to prevent the formation of accidental ground loops (high resistance pathways to ground) in the system, particularly through the reference electrode of the *p*H meter, since the system as described is grounded only at this point. Errors from this source could be as much as several parts in one thousand.

The performance of the coulometer was studied extensively at the 100-coulomb level because this amount of charge corresponds to 1 milliequivalent, a convenient amount of chemical reaction. For small amounts of electricity, a somewhat lower precision of integration would be expected. Larger amounts of current should be integrable with precision comparable to that found here, provided appropriate modifications of the technique, including concentration of electrolyte and electrode dimensions, were made.

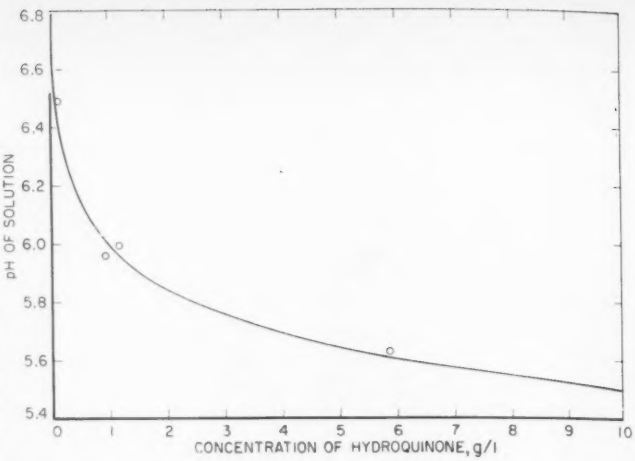

FIGURE 3. *The dependence of the pH value of the cell-electrolyte on the concentration of hydroquinone.*

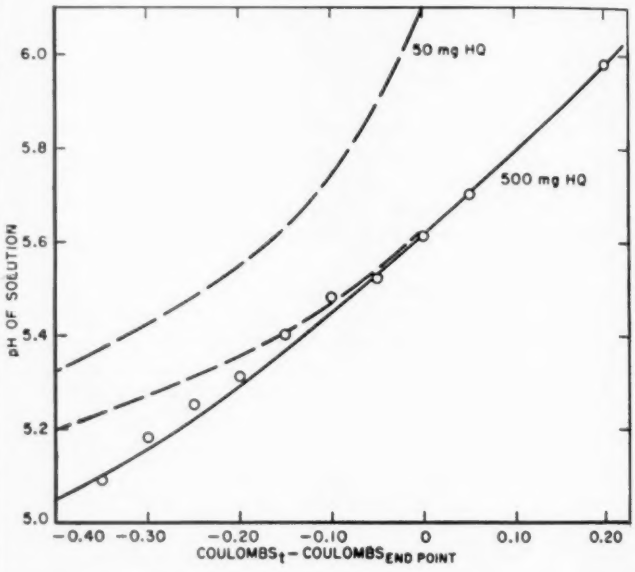

FIGURE 4. *Titration curves at the end point of reaction (2).*

Calculated and experimental values are represented by the broken curves and the solid curve, respectively. The current is 10 ma, corresponding to 0.05 coulomb for each 5-sec titration interval.

WASHINGTON, D.C. (Paper 63C1–7)

Journal of Research of the National Bureau of Standards—C. Engineering and Instrumentation
Vol. 63C, No. 1, July–September 1959

Electron Beam Magnetometer [1]

L. Marton, Lewis B. Leder, J. W. Coleman,[2] and D. C. Schubert

(April 28, 1959)

A theoretical investigation of the electron optics of an electron beam deflection method for detecting small magnetic fields is presented. It is shown that remarkably high sensitivity can be reached. A laboratory model of such a magnetometer was constructed, and it was demonstrated that the theoretical estimate of sensitivity, 3×10^{-5} ampere per oersted, could be attained in practice. A discussion of the possible improvements which could extend the sensitivity of the device is also given.

1. Introduction

The work to be described was performed in 1952, and at its conclusion a report for the sponsoring agency only was prepared [1].[3] Since at present there appears to be revived interest in electron beam magnetometers, it was felt that a published account of our results would serve a useful purpose.

The electron beam magnetometer is based on the fact that an electron beam will be deflected by a magnetic field. However, to obtain optimum performance the electron optics of such a system must be considered in detail. In 1955 Cragg [2] reported on an electronic magnetometer which consisted essentially of a miniature cathode-ray tube. The magnetic field was measured by compensating the beam deflection with a voltage applied to deflecting plates. With such a system he was able to measure a field of 10^{-4} oersted. It will be shown below that the electron beam magnetometer can theoretically measure changes of field as small as 3×10^{-8} oersted.

2. Theoretical Considerations

We will consider a system which consists of an electron gun, a long-focus lens and a detector, and will determine the minimum detectable field for a given geometry and operating conditions. If we assume that we have a line source of electrons of finite width and perpendicular to the axis, then the current distribution in the image at the detector after the electrons have passed through the lens would look as in figure 1 (dashed line). In the case of a point source of electrons, the figure represents a section along a diameter of the image. The ordinate is current density and the abscissa is distance across the image. When diffraction and lens aberration are present a decrease in current density from maximum to zero takes place at the edge of the image in a distance $2r$ (solid line fig. 1).

If the detector consisted of two slits each of width $2r$ and at a distance R-r from the center of the image, one could then measure a difference in current as

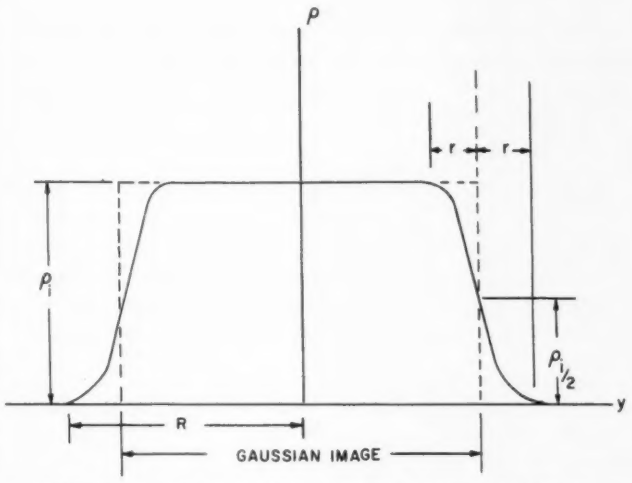

FIGURE 1. *Cross section of electron beam at detector.*

Dashed line is cross section without aberrations, and solid line with aberrations. $2r$ is the aberration region.

the electron beam moved across the slits. Because the current density is changing so rapidly in the aberration region, a small motion of the beam would give a relatively large signal change. The minimum (min) detectable deflection would be

$$y_{\min}=\frac{ri_{\min}}{i_0} \tag{1}$$

where i_0 is the maximum current difference when the image has moved so far that no current appears in one slit, and $i_{\min}$ is the minimum detectable current difference due to the movement $y_{\min}$ of the image.

The aberration region is due to three principal terms:

$$\text{spherical aberration, } r_s\cong\frac{5L^3\alpha^3}{(M+1)^2Gd^2} \tag{2}$$

$$\text{chromatic aberration, } r_c=\frac{2LT\alpha}{1.16\times10^4V} \tag{3}$$

$$\text{diffraction, } r_d=\frac{7.38\times10^{-8}M}{\alpha V^{1/2}} \tag{4}$$

where d is the effective lens thickness in centimeters,

[1] This work was in part supported by the U.S. Office of Naval Research and the Office of Basic Instrumentation of the National Bureau of Standards.
[2] Now at RCA Laboratories, Camden, N.J.
[3] Figures in brackets indicate the literature references at the end of this paper.

G is a lens figure of merit,[4] T is the absolute temperature of the emitter, L is the total length of the beam path in centimeters, and V is the energy of the electron beam in electron volts. In practice, the lower limit of the lens aperture will be set by the requirement that the maximum current density in the image must be

$$\rho_i = \frac{i_0}{2rl} \tag{5}$$

where l is the length of the detector slit. If we assume that a ratio of 50 for l/r is a practical limit, this gives

$$\rho_i = \frac{i_0}{100r^2}. \tag{6}$$

One can consider the crossover image formed by the electron gun as an effective object since the filament to crossover distance is, normally, small. This effective object then has a current density [3]

$$\rho_0 = \frac{eV\alpha^2}{300kT}\,\rho_f \tag{7}$$

in directions that will be intercepted by the long focus lens, where ρ_f is the current density at the filament, e is the charge of the electron, and k is Boltzmann's constant. Then at the final image

$$\rho_i = \frac{\rho_0}{M^2} = \frac{1.16\times10^4 V\alpha^2}{M^2T}\,\rho_f = \frac{i_0}{100r^2} \tag{8}$$

Thus when other parameters have been chosen, α must be made large enough so that

$$\alpha^2 \gg \frac{M^2Ti_0}{1.16\times10^6 Vr^2\rho_f} \tag{9}$$

Since r is the width of the aberration region, and in the worst case would be the sum of the absolute values of r_s, r_c, and r_d, one can substitute the sum of eq (3), (4) and (5) squared for r^2 in eq (9) and solve for α.

If we now select reasonable parameters as follows: $V=1{,}000$ v, $L=100$ cm, $M=1$, $T=3{,}000°$ K, $i_0=1\times10^{-9}$ amp, $i_{min}=4\times10^{-12}$ amp, $\rho_f=1$ amp/cm^2, $G=0.2$, and $d=0.5$ cm, then

$$\alpha = 3.06\times10^{-4} \text{ radians}$$
$$r_s = 1.43\times10^{-4} \text{ cm}$$
$$r_c = 0.159\times10^{-4} \text{ cm}$$
$$r_d = 0.036\times10^{-4} \text{ cm}$$

Therefore, r becomes approximately 1.67×10^{-4} cm (the sum of r_s, r_c, and r_d) so that from eq (1)

$$y_{min} = \frac{ri_{min}}{i_0} = 6.66\times10^{-7} \text{ cm}$$

[4] Upper limits for G are given; the optimum for a magnetic lens is $G=2.0$; for a unipotential electrostatic lens, $G=0.267$. Equation (3) is valid only when $d/L \ll 1$.

Now the deflection of an electron beam due to a magnetic field is given by

$$y = \frac{bHL^2}{2c}\sqrt{\frac{150\,e}{mV}} = \frac{0.15\,bHL^2}{V^{1/2}} \tag{10}$$

where H is the unknown magnetic field in oersted, e the electronic charge in esu, m the mass of the electron in grams, and c the velocity of light in centimeters per second. The constant b depends on the optics of the system as follows.

If the electron gun produces a beam which has no crossover or has a crossover in the strong field between cathode and anode, the beam will appear to diverge from a point behind the cathode. This is shown as the dashed trajectory on figure 2. Then it can be shown that

$$b = 1 - \frac{x_1^2(d+x_1+x_3)}{(x_1+x_3)^2(d+x_1)}. \tag{11a}$$

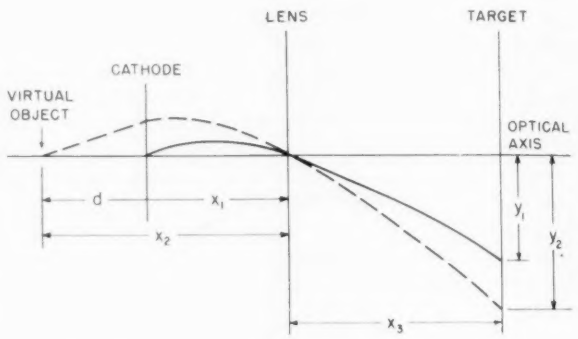

FIGURE 2. *Electron trajectories for electron source at cathode and virtual object position.*

If, however, the beam forms a crossover at the anode or a short distance in front of it, the beam can be considered as originating at the cathode since the cathode to anode distance is small compared to the total length of the electron beam path. In this case d in eq (11a) is equal to zero and the beam would then follow a path as shown by the solid line in figure 2. Then b simplifies to

$$b = 1 - \frac{x_1}{x_1+x_3}. \tag{11b}$$

Since x_3/x_1 is the magnification M, b in eq (12b) turns out to be equal to $M/M+1$.

L and V can be considered constants of the system and therefore the deflection of the beam is proportional to the field. From this we determine, using eq (10), that $H_{min}=2.8\times10^{-8}$ oersted. This is the minimum field which the device can detect when the selected parameters are used. In terms of current sensitivity this gives a value of 1.42×10^{-9} amp/γ (where γ equals 10^{-5} oersted).

Since the width of the aberration region r is approximately 1.67×10^{-4} cm, the proposed slit-system

detector of $2r$ by $50r$ would be 3.34×10^{-4} cm by 8.35×10^{-3} cm. Below, we consider a somewhat simpler system wherein the detector (fig. 3) consists of two plates overlapping in such a way that the image will, in balance, appear half on each plate.

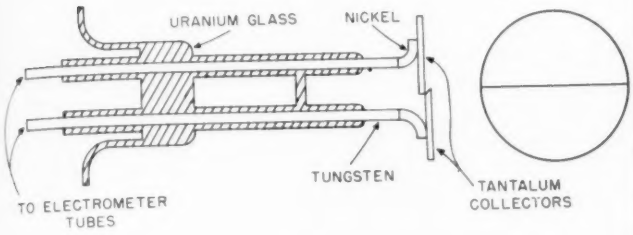

FIGURE 3. *Collector plate assembly.*

3. Alternate Detecting System

Whereas in the previous section the current density was considered in a region on the edge of the image, in this case we consider half the image as the sensing element, so that the current density will be

$$\rho_i=2i_1/\pi R^2 \tag{12}$$

where i_1 is the current due to half the image appearing on one collector plate and R is the radius of the image. Then

$$i_{\min}=4y_{\min}R\rho_i \tag{13}$$

where $y_{\min}\ll R$, or

$$i_{\min}=8i_1y_{\min}/\pi R. \tag{14}$$

For this system we now select parameters: $V=1{,}000$ v, $L=100$ cm, $M=1$, $T=3{,}000°$ K, $i_1=1\times10^{-8}$ amp, $R=0.01$ cm. We retain the minimum field $H=2.8\times10^{-8}$ oersted for a deflection $y=6.66\times10^{-7}$ cm and find the minimum current to be

$$i_{\min}=\frac{(8)(1\times10^{-8})(6.66\times10^{-7})}{(3.14)(0.01)}=1.7\times10^{-12}\text{ amp.}$$

For the same expected minimum field as in the first case we now have a sensitivity of 6×10^{-10} amp/γ. This is 0.42 times the signal in the first case, but, as will be pointed out later, reasonable changes can be made in i_1 and R to bring the minimum current output to a much larger value.

4. Sources of Noise

The above calculations are made on the assumption that no interference or noise exist. Since the smallest detectable signal is ultimately determined by the magnitude of interfering signals, it is necessary to form some idea of what such limitations may be.

1. External interference can be due either to (a) time fluctuations in the ambient field, or (b) geologic anomalies (i.e., nonuniformities in the earth's field caused by variations in the magnetic properties of the earth's crust). For the first fluctuation Fromm [4] has found that in the frequency range 0.1 to 2 cps the noise does not exceed 0.03 γ (3×10^{-7} oersted) for more than 50 percent of the time. It is believed that a gradient system of measurement, wherein this fluctuation is cancelled out, can be used successfully with a stationary magnetometer. This will be discussed later. Signal (b) occurs if the magnetometer is in motion so that for a fixed instrument, which we are considering, this can be ignored.

2. Internal or instrumental noise can be caused by several factors which will be investigated individually. While vibration can cause considerable noise, this is merely a question of rigidity of construction and mounting which can be overcome successfully.

The other sources of noise occur in the electron gun and in the input stage of the measuring circuit. They are (a) resistor (thermal) noise in the input resistor, (b) flicker noise in the detector tube, (c) grid current of the detector tube, and (d) shot noise in the magnetometer tube.

(a) Resistor noise is given by [5]

$$\overline{E_R^2}=4kTRB$$

where R is the resistance in ohms and B is the bandwidth in cycles per second, k is Boltzmann's constant and T the absolute temperature. With $R=10^9$ ohms, $B=1$ cps and $T=300°$ K, the rms value of $E_R=3.98$ μv.

(b) Flicker noise in the detector tube is given by O'Meara [6] for electrometer tubes as being between 400 μv and 900 μv for randomly selected tubes, and 200 μv for compensated circuits. With careful selection of tubes the electrometer may be operated down to the limit of sensitivity set by the thermal grid noise.

(c) Tubes are available and can be selected whose thermal grid noise (grid current) is 10^{-14} amp or less.

(d) Shot noise in the magnetometer arises in the electron gun. According to Haine and Mulway [7] the type of gun used can be considered as a temperature limited diode, so that the noise current would be given by [5]

$$i_s=\sqrt{2ei_1B}\text{ amps} \tag{16}$$

where i_1 is the emission current, B was defined previously, and e is the charge of the electron. Then for the alternate detection system

$$i_s=\sqrt{(2)(1.6\times10^{-19})(4\times10^{-8})(1)}=1.13\times10^{-13}\text{ amps}$$

The first three types of noise, (a), (b), and (c), will not present any serious problem, since with the minimum signal current of 1.7×10^{-12} amps imposed on a 10^9-ohm resistor we will have a signal of 1,700 μv. For the worst case of flicker noise this should

506301—59——6

still give a signal-to-noise ratio of 2 and in the best case approximately 8.5. With the parameters previously chosen, the shot noise turns out to be approximately 0.1 the minimum signal, giving an expected signal-to-noise ratio of approximately 10.

5. Experimental Design

The basic design consisted of an electron gun, electrostatic lens, and overlapping collector plates enclosed in a glass envelope which could be evacuated and sealed off from the pumping system. The metal parts were made either of tantalum or nonmagnetic stainless steel, and the spacers were made of glass and porcelain tubing. The electrical connections were made through tungsten wire presses at each end of the glass envelope. The outer surface of the glass envelope was painted with aquadag and connected to ground to reduce the effects of surface leakage and stray capacitances. Figure 4 is a drawing of the assembly.

The electron gun was patterned after one described by Steigerwald [8], and has the virtue of having a long crossover distance which can be controlled over a wide range by varying the bias voltage. The dimensions are given in figure 5.

The electrostatic lens was a symmetrical three electrode system consisting of two identical apertured disks at ground potential with a central apertured disk at negative potential. When operated 50 v below the accelerating potential, the lens had a focal length of 18 cm. The collector plates were placed at 30 cm from the center of the lens. Therefore, to obtain an image on the collector plates, it is found, using the thin lens formula of light optics, that the object distance must be 45 cm. Since the distance from the cathode to the lens was fixed at 25 cm, the beam was made to diverge from a virtual source 20 cm behind the cathode. Under these conditions d (on fig. 2) is 20 cm, and from eq (11a) b is found to be 0.66.

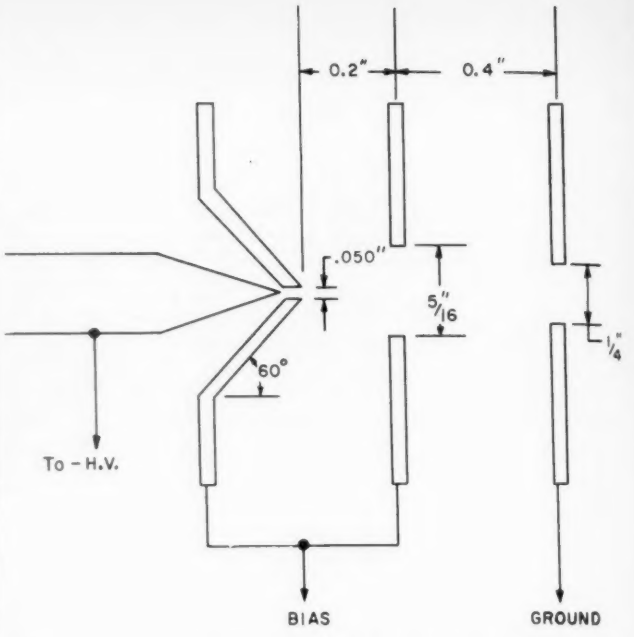

FIGURE 5. *Dimensions in inches for Steigerwald-type electron gun used.*

We have now two changes from the postulated case which will require recalculating the expected current change for a signal. One change is that due to the shift of the object position, and the other is that due to the shorter path (55 cm instead of 100 cm).

If we consider 2.8×10^{-8} oersted (the H calculated for the first case) as the minimum signal we wish to measure, we now get for y_{min}, from eq (11),

$$y_{min}=\frac{(0.15)(0.66)(2.8\times10^{-8})(55)^2}{\sqrt{1{,}000}}=2.61\times10^{-7}\text{ cm}$$

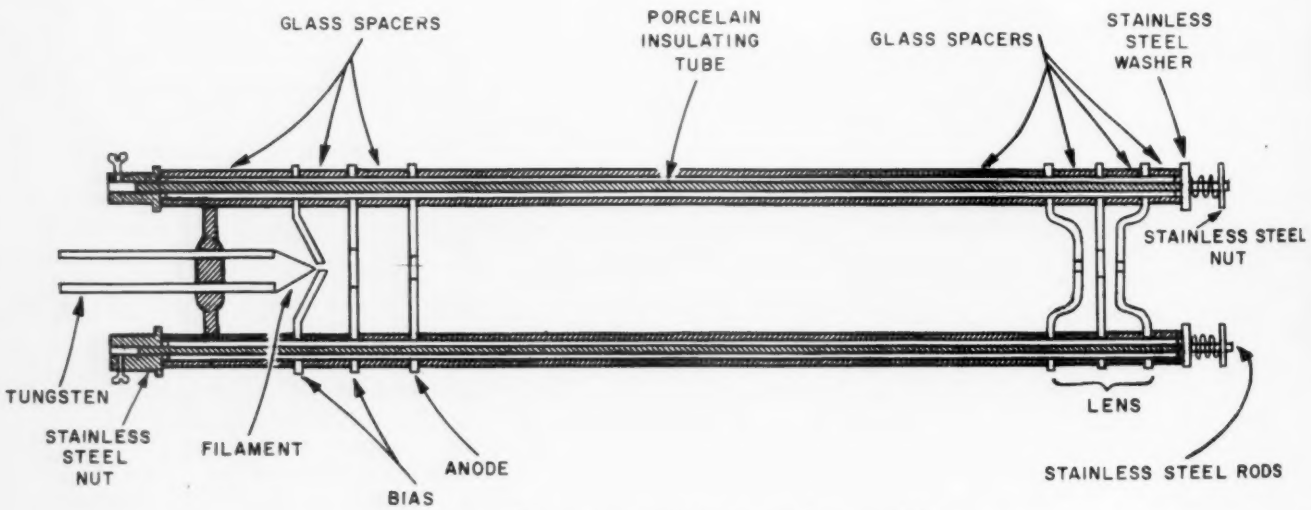

FIGURE 4. *Electron gun and electrostatic lens assembly.*

Electrodes are made of tantalum, and rods, washers and nuts of nonmagnetic stainless steel.

and i_{min} from eq (15) is

$$i_{min}=\frac{(4)(2\times10^{-8})(2.61\times10^{-7})}{(3.14)(0.01)}=6.65\times10^{-13} \text{ amp.}$$

This corresponds to an expected sensitivity of 2.4×10^{-10} amp/γ for 1,000-v acceleration and 2.9×10^{-10} amp/γ for 700 v.

The measuring circuit was required to measure a beam current of the order of 4×10^{-8} amp and, more important, measure differences of the order of 10^{-12} amp or less. The first part, that of measuring the total current, was taken care of by using a millivoltmeter with shunt box which could measure down to 10^{-11} amp. The second, that of measuring a difference of 1 part in 10,000 between two d-c signals at a level of 10^{-8} amps required considerable design effort since no suitable low-level differential amplifiers were available at the time. A satisfactory solution was arrived at by using a modified version of the Nier mass-ratio measuring method [9]. More elegant solutions to this problem are now possible.

Since the most sensitive stage of this differential amplifier was the input tube, the two electrometer tubes and their two hi-meg grid resistors were soldered directly to the collector-plate leads of the magnetometer tube, and the connections to the rest of the amplifier were made with long leads so that the amplifier could be kept at some distance from the magnetometer tube. The electrometer tube assembly was enclosed in a glass "bottle" which was waxed to the end of the magnetometer tube. A stopcock on the bottle made it possible to evacuate it and then seal it off. The bottle was painted with aquadag and grounded to keep the tube light tight and reduce the effect of external capacitances.

The final unit in the magnetometer tube was the collector plate assembly. This was made up of two semicircular phosphor-coated plates overlapping along the straight edges, but electrically separated. They were alined at 90° to the electron beam. It was highly important that these be rigidly mounted since vibration could cause a considerable noise signal. The construction is shown in figure 3. It was also highly important that the resistance between these two plates and between each plate and ground be high compared to the input resistance to the electrometer circuit. A measurement of this gave a value of 1.7×10^{13} ohms.

The circuit for the magnetometer tube is shown on figure 6. The filament was heated with a-c using a variac and transformer. The transformer was specially built with a 2.5-v secondary and insulation for 5,000 v. The electron gun was self-biased as shown. A divider network was placed across the high-voltage supply, and the lens voltage was obtained from this by inserting a banana-plug connection at the position giving the best definition of image. The high-voltage supply consisted of a commercial 5-kv supply with 5 percent regulation and a series tube regulator circuit to bring the stability to 1 part in 13,000.

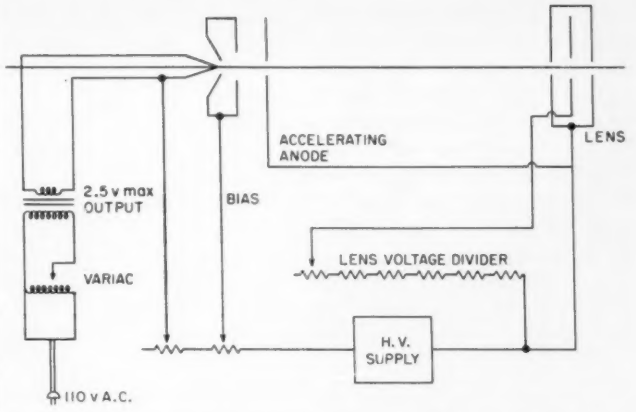

FIGURE 6. *Electrical connections to electron gun and lens.*

The magnetometer was placed at the center of a set of four rectangular coils (with each pair in series) to compensate for the horizontal and vertical components of the earth's magnetic field [10].

6. Experimental Tests

To test the operation of the detector the amplifiers were balanced to give a zero difference with the electron beam off. With the beam on, it was found that zero balance was obtained when the beam was all on one plate and just barely touching the other. Figure 7 shows the current readings on each plate as the beam was moved across the dividing edge by changing the coil current. It was felt that this effect was probably due to ion currents and charging of the glass surface. To correct this a 1-in. wide aquadag ring was printed on the inside of the glass tube 1/8 in. from the collector plates, and a tungsten wire was sealed through the glass so that it was even with the inner surface and making contact with the aquadag. It was found that when this guard ring was grounded or a positive or nega-

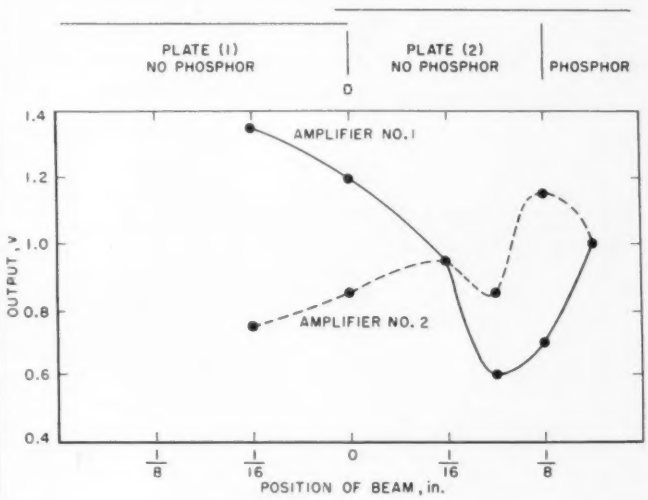

FIGURE 7. *Amplifier-output signal versus beam position relative to detector edge.*

tive voltage was applied the beam could be balanced with what visually appeared to be half the beam on each plate. Figure 8 shows the change in output per plate as the voltage on the guard ring was varied from positive to negative. The position of the beam was adjusted to be half on each plate. Figure 9 shows the current on each plate as the beam was moved across the edge with the guard ring at ground potential and at -5 v and $+5$ v. It is seen that with the guard ring at ground the beam balances on the edge, but as the beam moves more on to one plate the polarity changes. With either a negative or a positive voltage on the guard ring the output was zero for balance position and did not change sign as the beam was moved across the edge.

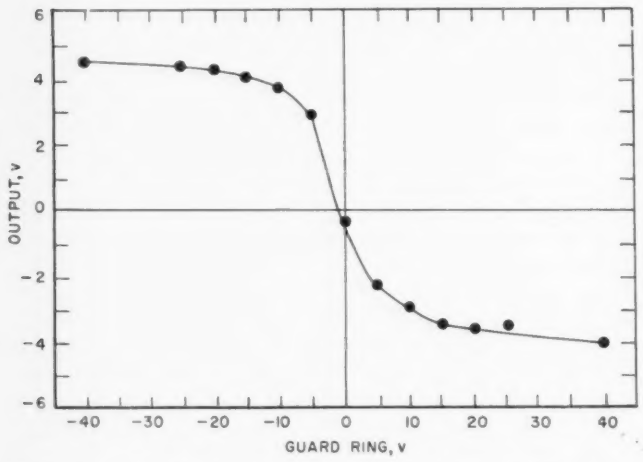

FIGURE 8. *Output signal as a function of guard-ring voltage.* The electron beam was half on each detector plate.

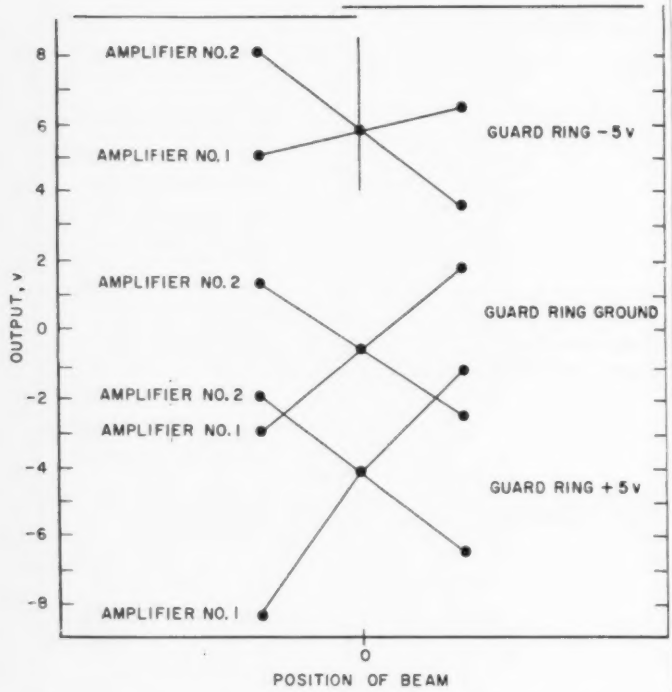

FIGURE 9. *Amplifier-output signal versus beam position for three guard-ring potentials.*

When the beam was centered, the output signal showed a great deal of fluctuation. This, however, appeared to correlate with the movement of automobiles at a distance of about 200 yd from the building in which the tests were being made. To overcome this the entire equipment was moved to Blossom Point Proving Grounds, Md.,[5] and set up in a shack located 5 miles from where other tests were being made. The location chosen was peninsula-shaped and on the land side the nearest building was over 1 mile away. The compensating coils and tube were set up in approximately north-south orientation with the measuring edge of the collector plates in a horizontal position.

7. Experimental Results

The sensitivity was tested by turning on and off a calibrated coil. The coil had an average diameter of 15 cm and produced a field of 11 γ/amp at a distance of 200 cm. Three measurements of sensitivity and stability were made with the center of the coil placed at a distance of 200 cm from the center of the magnetometer tube. The axis of the coil was perpendicular to the tube, parallel to the edges of the collector plates, and midway between the lens and collector plates.

Table 1 gives the results of these three tests. In every case the filament was operated at 1.1 v a-c using a constant voltage transformer. The guard ring was at ground potential. In the second and third tests a laboratory built 2-kv power supply replaced the commercial 5-kv supply used for the accelerating voltage, the bias was increased and the beam recentered. In the third case the accelerating voltage was reduced from 1000 v to 700 v d-c.

TABLE 1

	Test 1	Test 2	Test 3
Accelerating voltage, volts	1000	1000	700
Test field, H_d, γ	0.74	0.80	0.80
Avg change output, mv	56	108	251
Avg change output, amp	0.56×10^{-10}	1.08×10^{-10}	2.51×10^{-10}
Experimental sensitivity, amp/γ	0.76×10^{-10}	1.36×10^{-10}	3.15×10^{-10}
Theoretical sensitivity, amp/γ	2.4×10^{-10}	2.4×10^{-10}	2.9×10^{-10}
Experimental/theoretical	0.3	0.6	1
Noise, mv	21	16	26
N/S	0.375	0.148	0.103
Noise, γ	0.278	0.118	0.086
S/N	2.67	6.75	9.7

The increased sensitivity in the second test was probably the result of increased current density due to increasing the bias. The noise level given above included both instrumental noise and short-term magnetic field variations. A decrease in instrumental noise may have taken place due to the use of a different power supply, but this was not definitely

[5] The Blossom Point Proving Ground, Md., was operated by the Ordnance Development Division of the NBS, which is now the Diamond Ordnance Fuse Laboratories operated by the Dept. of the Army.

established. The improvement in sensitivity in the third case was probably due to the decreased accelerating potential (since the deflection varies as the inverse square root of the accelerating voltage) and increased bias which apparently reduced the spot size.

The experimental to theoretical ratios of 0.3, 0.6, and 1 indicate that the theoretical approach was reasonably accurate, and that even greater sensitivities can be obtained. The discrepancy probably lies in the original estimate of the radius of the image, 0.01 cm, which was selected as a reasonably attainable image size. It would appear from the test results that in the first two cases the spot size was larger than this value, but approximately equal to it in the last case.

8. Conclusions and Suggestions for Improvement

While it was shown that the expected sensitivity was closely approached, further improvements could be made. These would involve increasing the length of the tube, decreasing the spot size, and decreasing the accelerating potential.

If we select parameters $V=600$ v, $L=100$ cm, $M=1$, $T=3{,}000°$ K, $i_i=1\times10^{-8}$, $R=0.05$ mm, and $H=2.8\times10^{8}$ oersted, then from eq (11) we would expect a minimum deflection

$$y_{min}=\frac{(0.15)\,(2.8\times10^{-8})\,(100)^2}{2\sqrt{600}}=0.85\times10^{-6}\text{ cm}$$

and from eq (15) a minimum signal

$$i_{min}=\frac{(4)\,(1\times10^{-8})\,(0.85\times10^{-6})}{(3.14)\,(0.005)}=2.17\times10^{-12}\text{ amp}$$

corresponding to a sensitivity of 7.83×10^{-10} amp/γ.

Another way to obtain increased sensitivity would be to use field emission.[6] Current densities at the cathode as high as 6×10^{9} amp/cm^2 have been obtained, and values of the order of 10^{7} amp/cm^2 are fairly easily obtained. Since the previous calculation calls for only 0.131 amp/cm^2, it is seen that with field emission in place of thermionic emission one can easily obtain a set of conditions to give considerably greater sensitivity with the present basic design of tube.

[6] This was not tried at the time due to the more difficult problem involved and the limited time available.

It is also possible that improvement in image characteristics could be obtained by replacing the electrostatic lens with an aperture and external coil for focusing the beam. This system would have less aberration and, therefore, give a more concentrated image.

In a stationary system one could eliminate the ambient field fluctuation by using a gradiometer arrangement. This would consist of two magnetometer tubes at some convenient distance apart, each surrounded by a set of field compensation coils. A deflection due to a magnetic field change produces a signal in tube 1, which is used to excite both sets of coils. This is done in such a way, using a servosystem, as to bring the beam in tube 1 back to zero. If a gradient exists between tube 1 and tube 2, the feedback will not bring the beam in tube 2 back to zero. This signal would then be an indication of the field gradient over the base distance between the tubes.

The authors acknowledge the assistance of J. A. Simpson for discussions and work done on the theoretical considerations and circuitry, J. J. Madine for the glass work, and L. Mann and A. Dauses for the machine work. The authors also thank the Ordnance Development Division of the National Bureau of Standards (now Diamond Ordnance Fuse Laboratory, U.S. Army) for making available the test location at Blossom Point, Md.

9. References

[1] L. Marton, L. B. Leder, and J. W. Coleman (private communication).
[2] B. G. Cragg, J. Sci. Instr. **32,** 385 (1955).
[3] D. B. Langmuir, Proc. IRE **25,** 977 (1937).
[4] W. Fromm, Advances in Electronics, **4,** 259 (Academic Press, New York, N.Y., 1952).
[5] S. Goldman, Frequency analysis, modulation and noise, pp. 362, 392 (McGraw-Hill Book Co., Inc., New York, N.Y., 1938).
[6] F. E. O'Meara, Rev. Sci. Instr. **22,** 106 (1951).
[7] M. E. Haine & T. Mulway, Electron Physics Symposium, Washington, D.C. (Nov. 1951).
[8] K. H. Steigerwald, Optik **6,** 469 (1949).
[9] A. O. Nier, E. P. Ney & M. G. Ingraham, Rev. Sci. Instr. **18,** 294 (1947).
[10] R. H. Lyddane & A. E. Ruark, Rev. Sci. Instr. **10,** 253 (1939).

Washington, D.C. (Paper 63C1–8)

Journal of Research of the National Bureau of Standards—C. Engineering and Instrumentation
Vol. 63C, No. 1, July–September 1959

A Refined X-Band Microwave Microcalorimeter

Glenn F. Engen

(May 1, 1959)

The microcalorimetric method for evaluation of the efficiency and substitution error of a bolometer mount proposed by Macpherson and Kerns has been the object of further study and refinement at the Boulder Laboratories of the National Bureau of Standards, and an improved instrument based on this technique has been recently placed in operation.

The new microcalorimeter design features are: (1) Greatly improved ambient temperature control, permitting higher sensitivity and resolution; (2) improved d-c instrumentation; (3) improved mechanical construction giving better repeatability; (4) relocation of the thermopile so that it no longer is attached directly to the bolometer mount, thus providing flexibility in the choice of termination; and (5) a more comprehensive treatment of the calorimetric substitution or equivalence error. These features permit the determination of the effective efficiency of a bolometer mount to an accuracy of better than 0.2 percent.

1. Introduction

The bolometric technique, by means of which the heating effect of an unknown amount of rf or microwave power is compared with that of a measured amount of d-c or audiofrequency power through a temperature-sensitive resistive element, is a well-known and extensively employed method in the low-level measurement of microwave power.

In a commonly used arrangement, the bolometer element forms one arm of a Wheatstone bridge, the parameters of which are chosen in such a manner that the bridge is balanced when the bolometer is at its nominal operating resistance. The bolometer is then provided with the required bias power to bring its resistance to this operating value, and the reduction in bias power required to maintain the bridge balance following the application of a microwave signal, is taken as a measure of the microwave power. The measurement of this bolometric or substituted d-c bias power has been the object of refinement until the measurement can be carried out to an accuracy of 0.1 percent [1].[1]

The use of the value thus obtained as a measure of the microwave power involves, however, two well-recognized sources of systematic error. First, the microwave and d-c bias currents take different distributions within the bolometer element, which means that the functional dependence of the bolometer resistance will, in general, be different for the two sources of power, giving rise to a dc—rf substitution error. Second, the bolometric method at best measures only the microwave power dissipated within the bolometer element, whereas one is usually interested in the power dissipated in the entire terminating waveguide structure or bolometer mount. The ratio of these quantities is, by definition, the bolometer mount efficiency. In addition, if the mount is not properly tuned there may be a net reflection of power at its input terminals, but the methods of dealing with this phase of the problem are well-recognized [2] and will not be considered explicitly in this paper.

[1] Figures in brackets indicate the literature references at the end of this paper.

Macpherson and Kerns [3] gave the details of a calorimetric method for the determination of the combined effect of these two sources of error. This technique has been the object of further study and refinement at the Boulder Laboratories, and an improved instrument based on this method was recently placed in operation. A number of calorimetric-type power meters have also been developed [4, 5, 6] in other laboratories which utilize the same general techniques employed by Macpherson and Kerns, but the further development at the NBS has retained the original objective of obtaining a correction factor for the bolometrically-determined power.

2. General Description

The basic theory of operation has been presented in detail in the cited references and need not be repeated here. In brief, however, the instrumentation is such as to permit a calorimetric determination of the total power input to a bolometer mount while a simultaneous bolometric determination is made. The difference between the two measurements is ascribed to the mount efficiency and substitution error. The method, in its present state at least, permits only a determination of the combined effect of these phenomena, referred to as "effective efficiency."

The problem of making a calorimetric determination of power (or energy) may be subdivided as follows: (1) Selection of a calorimetric body or object in which to dissipate the power to be measured, (2) choice of a suitable technique to measure the temperature rise of this body or object, and (3) determination of the proportionality factor or functional dependence of the thermometer response upon the power input. In the microcalorimeter technique, the bolometer mount serves as the calorimetric body or object in which the power is dissipated and whose temperature rise is measured by means of a suitable thermopile, while calibration is effected by observing the thermopile response to a measured amount of d-c power dissipated in the bolometer element.

The thermopile consists of 34 constantan–chromel–P junctions with an approximate senstivity of 2,000 μv/° C. The instrument is designed to yield a nominal output at equilibrium of 100 μv corresponding to a temperature rise of 0.05° C. Since this potential may be measured by the associated instrumentation to an accuracy of a few parts in 10^4, a temperature background which is stable to a few millionths of a degree is indicated for the application.

In order to achieve this background, the twin Joule arrangement is employed as shown in figures 1 and 2, along with a temperature-regulated water bath. The advantage of this method stems from the fact that if symmetry exists with respect to a plane normal to the plane of the illustration as shown, and if no thermal gradients exist within the thermal shields, then the actual temperature of these shields may fluctuate without producing a temperature difference between the bolometer mounts. Thus, by using a triple thermal shield (the innermost one of which is a heavy copper casting), a symmetrical waveguide input system, and suitable thermal shunts, a degree of symmetry is achieved such that the dependence of the temperature difference between the bolometer mounts upon the thermal head existing between the inner thermal shield and the external water bath, is only a factor of approximately one part in 10^4. Since a bath regulation of ± 0.005° C may be obtained with little difficulty, adequate isolation from the bath fluctuations is thus achieved. There still exist in the current model, however, temperature gradients whose origin is yet undetermined such that the thermal background is stable to only 5 to 10 millionths of a degree, but this is satisfactory for the application.

In order to function in the required manner, thermal isolation is required between the bolometer mounts and the remainder of the system. (Isolation is also required between the thermal shields.) This rules out the possibility of using conventional waveguide to convey microwave energy to the bolometer mounts, since this would also readily conduct away the heat generated in the mount. In the earlier instrument, this isolation took the form of choke-flange-air-gap combination, but such an

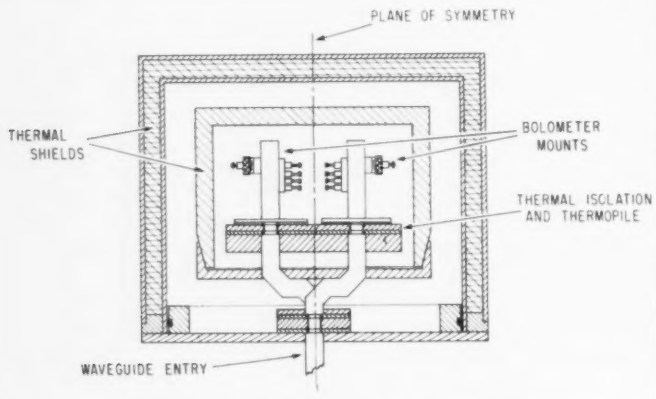

FIGURE 1. *Cross section of microcalorimeter.*

FIGURE 2. *Microcalorimeter and thermal shields.*

arrangement at best is frequency sensitive, and at worst, may introduce systematic errors whose evaluation is quite difficult. In the present model, this isolation is provided by a short section of waveguide, the body or sides of which are fabricated from 0.001-in. copper shim with the addition of suitable plastic to provide the required mechanical rigidity.

A significant increase in the flexibility and operating convenience of the instrument has been realized through relocation of the thermopile. Instead of being attached directly to the bolometer mounts as in the former model, the thermopile is built into the thermal isolation sections in such a way that it senses the temperature difference between the flanges which mate with the bolometer mount flanges as shown in figures 3 and 4. The obvious advantage of this arrangement is that removal of the four screws which hold the bolometer mount in place in the colorimeter also serves to remove the mount from the thermopile assembly, thus permitting flexibility in the choice of termination and enabling the ready duplication or multiplication of the number of bolometer mounts which may be so calibrated.

There are a number of design criteria which the bolometer mounts employed in the calorimeter must satisfy. First, a high degree of stability in those parameters which determine the mount efficiency is obviously desirable, while the ability to tune the mount for an impedance match (no reflection) at the operating frequency is also desirable if comparison with other mounts is anticipated. The choice of the tuning elements which may be employed in achieving this impedance match is severely limited by the necessity of keeping the mass (heat capacity) of the entire mount within prescribed limits. In

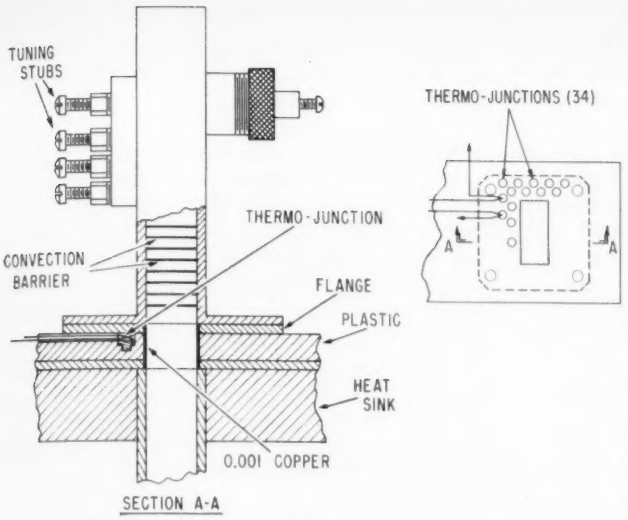

FIGURE 3. *Detail of thermopile construction.*

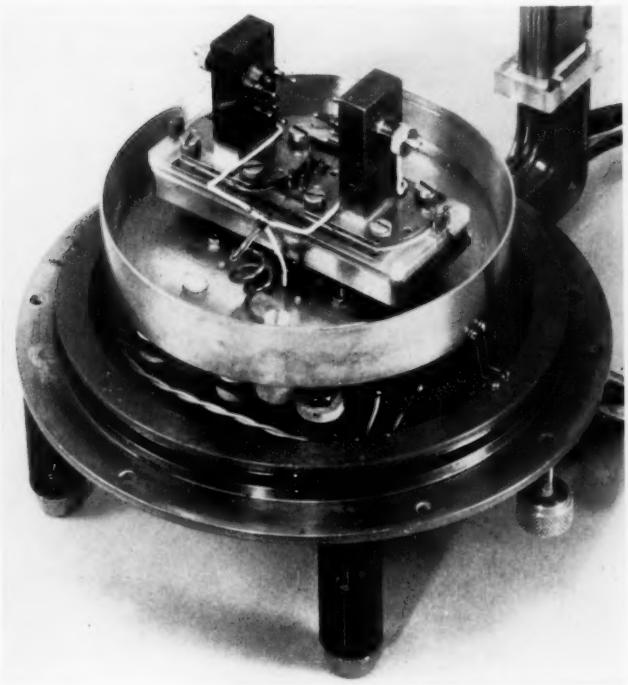

FIGURE 4. *Closeup of microcalorimeter interior.*

addition, while comparatively little is yet known of the distribution of losses within a bolometer mount, many of the commonly employed tuning elements would appear to be potential sources of instability in the mount efficiency.

Another requirement on the mount design is that the calorimetric equivalence error (to be discussed later) be held to a small value; that is, the thermopile response should be essentially independent of the distribution of the heat sources within the mount. This will be true if the mount is of uniform temperature overall, which suggests the use of thick walls and keeping the length short. The design should also provide a high value for the efficiency as this will also reduce the error from calorimetric nonequivalence. Some of these problems will be discussed in greater detail in later sections, but it will be recognized from the present discussion that the design must effect a compromise among a variety of conflicting requirements.

3. Operational Procedure

The operational procedure associated with the instrument is comparatively simple and straightforward. Using the terminology introduced by Macpherson and Kerns [3] an effective efficiency, η_e, may be defined,

$$\eta_e = \frac{\text{Substituted or retracted bias power as measured by the bolometric technique}}{\text{Total microwave power dissipated within bolometer mount}}. \quad (1)$$

In practice the bolometer is operated in conjunction with a selfbalancing d-c bridge [1]. The d-c bias power is first applied and the thermopile response allowed to effectively reach an equilibrium value (which takes 45 min). Microwave power is then applied, d-c power is withdrawn as required to maintain bridge balance, and the thermopile response again permitted to reach equilibrium, at which time the microwave source is removed and the thermopile response to d-c power only once more observed. The procedure thus consists of energizing the bolometer element from the d-c bridge and observing the thermopile response and bridge current, without and with microwave energy present in 45-min intervals. Ideally, only one cycle of microwave power off and on would be required, but in practice averaging the results of two "off" intervals occurring before and after an "on" interval permits further suppression of the thermal background drift. Typical thermopile response curves are shown in figures 5 and 6.

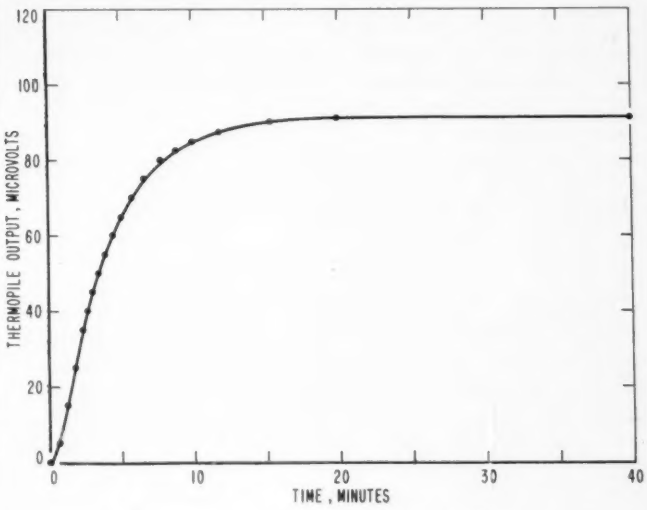

FIGURE 5. *Typical thermopile response.*

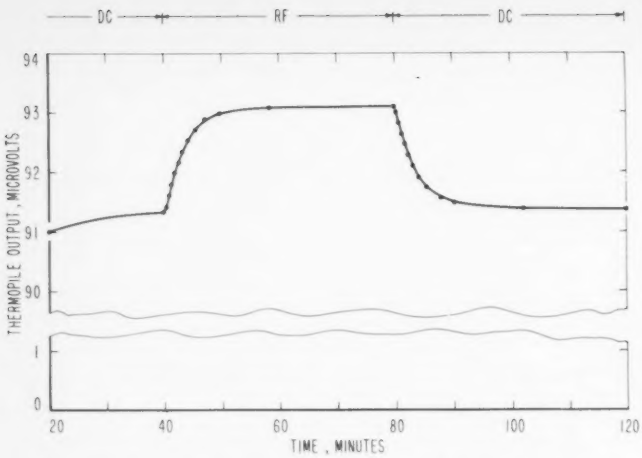

FIGURE 6.—*Response curve for determination of effective efficiency.*

Let i_1 and i_2 represent the bolometer bridge currents without and with microwave energy present in the bolometer and, respectively, e_1 and e_2 the corresponding thermopile responses. Then for the equal arm bridge in common use, the bolometric power is given by the usual formula,

$$P_b=\frac{r_0}{4}\,(i_1^2-i_2^2)$$

where r_0 is the resistance of the bolometer element and bridge arms.

The total power input to the bolometer mount (microwave and d-c) during the microwave "on" interval ideally will be proportional to the thermopile response, e_2, the proportionality factor being $r_0 i_1^2/4e_1$. The microwave power is the difference between this total input and the d-c component, thus

$$P_{rf}=\frac{r_0}{4}\left(\frac{e_2}{e_1}\,i_1^2-i_2^2\right)$$

and

$$\eta_e'=\frac{1-(i_2/i_1)^2}{e_2/e_1-(i_2/i_1)^2} \qquad (2)$$

which gives the effective efficiency (η_e') in terms of the thermopile response and bolometer-bridge currents. The prime is used to indicate that the equation is based on the assumptions that the thermopile response is linear and independent of the distribution of the power dissipation within the mount. The validity of these assumptions will be examined below.

4. Error Analysis

Equation (2) for η_e' has been obtained under certain simplifying assumptions; a more general approach to the problem will now be presented. Within the limits of experimental error (to be discussed below), the thermopile response and cooling mechanisms are both linear, and the thermopile response e_2 is of the form:

$$e_2=k(P_{2_{dc}}+gP_{rf}) \qquad (3)$$

where k and g are constants, and $P_{2_{dc}}$ and P_{rf} are the d-c power dissipated in the bolometer element and the total microwave power dissipated in the bolometer mount, respectively. Equation (3) expresses the fact that a given amount of microwave power will, in general, produce a different thermopile response than an equal amount of d-c power through the factor g.

The constant k may be determined in the manner already discussed so that $k=e_1/P_{1_{dc}}$. Substituting this result and solving eq (3) for P_{rf} gives,

$$P_{rf}=\frac{1}{g}\left(\frac{e_2}{e_1}P_{1_{dc}}-P_{2_{dc}}\right)$$

and

$$\eta_e=g\,\frac{P_{1_{dc}}-P_{2_{dc}}}{\frac{e_2}{e_1}P_{1_{dc}}-P_{2_{dc}}}=g\,\frac{1-(i_2/i_1)^2}{e_2/e_1-(i_2/i_1)^2} \qquad (4)$$

The more complete analysis thus gives a factor g by which the right-hand side of eq (2) is to be multiplied in determining η_e. The error in determining η_e thus consists of the uncertainty in the value of g, and the experimental error in determining the value of this second factor, $\frac{1-(i_2/i_1)^2}{e_2/e_1-(i_2/i_1)^2}$. These will be referred to as the calorimetric equivalence and instrumentation errors, respectively.

The instrumentation error may be evaluated with little difficulty. If the second factor is differentiated with respect to i_1 and i_2, it is found that for typical values of the ratio e_2/e_1; i.e., $1<e_2/e_1<1.05$, the error in η_e is only 5 percent or less of the error in i_1 or i_2. In practice, i_1 and i_2 are measured by a precision potentiometer-standard resistor combination to an accuracy of about 0.03 percent; thus, the total error due to the uncertainty in i_1 or i_2 is only of the order of 0.01 percent and may be neglected.

The error due to the uncertainty in e_2/e_1 may be found in a similar manner, and if the ratio of i_2 to i_1 is ½ or less, the error in η_e is in the range 1.0 to 1.3 times the error in e_2/e_1.

In order for eq (3) to be valid, the thermopile response must be a linear function of the d-c and microwave powers. The error in the ratio e_2/e_1 may conveniently be defined to include, in addition to the instrumentation error in measuring the thermopile output, the error due to nonideal performance of the calorimeter caused by such things as nonlinear thermopile response and cooling, thermal-background drift, etc., which might affect the validity of eq (3). The error in measuring the ratio e_2/e_1 was determined in the following manner. The measurement procedure outlined in the foregoing section was followed except that instead of applying microwave power at the end of the first 45-min interval, the d-c power applied to the bolometer was increased by a nominal 10 percent. In this way the actual operating conditions were simulated, and the measured value of this second d-c power was compared with that predicted on the basis of a linear response from the observation of e_1, e_2 and the first value of d-c power.

In ten measurements of this type, the maximum error observed was 0.04 percent, with an average error of 0.013 percent. A figure of 0.1 percent, corresponding to an error in e_2/e_1 of 0.07 percent, has been arbitrarily assigned as a conservative limit to the error from this source, in which the probable error is perhaps 0.02 percent or less.

With regard to the equivalence error, g is a number which expresses the relative effectiveness of microwave power as compared with d-c power in producing a thermopile response, that is, for a given thermopile output, $g=P_{dc}/P_{rf}$. Ideally, $g=1$ but in practice differs from this value due to the following phenomena:

1. The d-c and microwave powers take different distributions within the bolometer element yielding different thermopile responses.
2. Some of the microwave energy will be dissipated in places other than the bolometer element and the thermopile response will again differ from that produced by an equal amount of d-c power in the bolometer.
3. The thermopile will respond to the dissipation of microwave energy in the waveguide lead-in which does not comprise part of the bolometer mount.

It is just these first and second phenomena, of course, which are responsible for the dc-rf substitution error and mount inefficiency.

With reference to the first of these, the temperature-sensing device in the calorimeter is relatively far removed from the main heat source and it might be estimated conservatively that the error in the calorimetric method due to this phenomena would be at least an order of magnitude or more below the bolometric substitution error which according to the information available [7], does not exceed a few percent.[2]

In order to check the validity of this assumption experimentally, the d-c calibration factor, k, was determined for several different bolometer elements (barretter and thermistor). The initial results of this experiment gave values which differed from one another by as much as 2 percent with a repeatability of 0.1 percent. This anomaly at first appeared to challenge the validity of the above assumption, but further investigation showed that the insertion of a 0.05 in. copper plate at the bolometer-mount input flange (thus blocking the waveguide input), would eliminate this difference. This was interpreted to mean that air convection was playing a significant role in cooling the bolometer capsule (not to be confused with the cooling of the bolometer element within the capsule), and the variations in the value for k were ascribed to the variable role, occasioned by the differences in the capsules associated with the bolometers, played by air convection in conveying this heat from the capsule to the external heat sink via the interior of the waveguide.

By inverting the bolometer mounts such that the closed end was up, it had been hoped that the need for a convection shield or barrier could be eliminated, but these results clearly demonstrated the need for such a shield. In order to provide a convection barrier, in which the microwave dissipation would be negligible, a series of eight 0.002 in. Teflon membranes spaced at 0.05 in. intervals and transverse to the waveguide axis was arranged at the waveguide input. This effectively eliminated the convection problem and gave repeated determinations of k in a refined bolometer mount which agreed to 0.05 percent, which is about the limit of experimental error for this particular measurement. Since the power distributions in the barretter and thermistor are markedly different, it may be safely assumed that the small difference in distribution of the d-c and microwave powers which occurs in practice when the same element is employed, will have a negligible effect.

With regard to the degree of equivalence realized in the thermopile output for power dissipated in the bolometer mount walls as compared with an equal amount in the bolometer element, the problem, once again, is primarily that of attempting to prevent the escape of heat from the mount via air convection. The effectiveness of the convection barrier described in the previous paragraph was demonstrated by temporarily inserting two other heat sources within the mount such that they were in good thermal contact with the side walls. The first of these was located just inside the mount before the teflon barrier, the second on the other side of the barrier, close to the bolometer element as shown in figure 7. The thermopile response for equal amounts of power in the two positions was then compared with that for the bolometer element, and it was found that the heat sources at positions 1 and 2 were approximately 1.5 and 0.5 percent more effective respectively. A conservative figure for the increased effectiveness of the power dissipated in the walls is thus 1 percent with an error of ± 1 percent. It should be noted that this figure applies only to that fraction of the power which is so dissipated. In practice a lower limit of 97 percent may be taken for the efficiency of the mounts designed for use in this calorimeter, which leaves only 3 percent of the energy to be dissipated other than in the bolometer element.

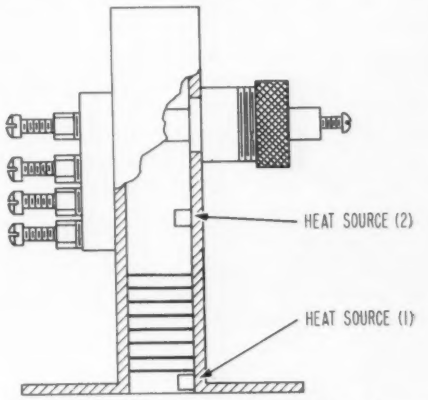

FIGURE 7. *Bolometer mount with auxiliary heat sources.*

[2] Recent advances in the impedance method of measuring bolometer mount efficiency have demonstrated that the substitution error at frequencies near 10 kMc is probably no greater than a few tenths of a percent.

Finally, as noted, the thermopile will respond to the dissipation of microwave energy in the thermal isolation section which is not part of the bolometer mount. If an electrical conductivity of 50 percent of the d-c value is assumed for this ¼ in. length of copper waveguide, the theoretical value of power dissipation will be approximately 0.05 percent, of which the thermopile will probably measure somewhat more than half. A value of 0.04 percent ±0.04 percent thus represents a conservative estimate for this contribution.

The results of this section are summarized in table 1.

TABLE 1

Place of heat dissipation	Total power	Contribution to thermopile response [a]	Error
	%	%	%
Bolometer element	97	97.00	0.00
Waveguide walls	3	3.03	±0.03
Isolation section		0.04	±0.04
Total	100	100.07	±0.07

[a] Compared with an equal amount of d-c power dissipated in the bolometer element.

Rounding off these results gives for g a value 1.001 with a possible error of ±0.1 percent; and this, combined with the instrumentation error of ±0.1 percent, gives for the total error ±0.2 percent.

5. Bolometer Mount Design and Experimental Results

As may be inferred from the foregoing description, the design of the bolometer mounts employed in the microcalorimeter has undergone a series of transitions as required to cope with the various engineering problems encountered in the evaluation of the device. While no claim is made as to the extent of their applicability, certain features of the construction are believed to be of enough interest to merit further description.

The general features of the construction are shown in figures 4 and 7. The mount is machined in two halves from a solid piece of tellurium copper, and the two halves hard-soldered together along the center of the wider side. The brass flange is then attached by soft solder. Except for these two applications, the use of solder has been completely avoided in the construction. The incentive for this method of fabrication was provided by the observation of efficiencies of the order of 85 percent for mounts in which the back plate was fastened with soft solder, while the use of hard solder increased these values to 95—98 percent.

The design employs five tuning stubs as shown, three in front of the bolometer and two at the side. These side stubs provide additional susceptance at the plane of the bolometer element, and thus, over a limited range, serve the same function as a moveable back plate, while the other three stubs serve the usual purpose.

In the five mounts which have been built to this general pattern, effective efficiencies in the vicinity of 98 to 99 percent have been realized. The results of additional measurements to determine the place of this residual dissipation seem to imply that most of it occurs in the plastic capsule surrounding the element and/or in the microwave bypass mechanism, at the d-c lead-in to the bolometer. While additional research will be required to completely resolve these questions, it appears likely, on the basis of present information, that effective efficiences of 99.5 percent and perhaps higher may be realized by proper design and fabrication techniques.

Finally, table 2 shows the results of intercomparisons with commercially available mounts.

TABLE 2

	Model	Effective efficiency
		%
Broadband barretter mount	A	97.7
Broadband barretter mount	B	96.2
Broadband barretter mount	C	95.4
Broadband thermistor mount	D	95.2

The author acknowledges the assistance of Morris E. Harvey, to whose care in making the experimental observations a large amount of credit for the success of this project is due, and extends his thanks to R. W. Beatty and D. M. Kerns for their helpful suggestions in the preparation of the manuscript.

6. References

[1] G. F. Engen, A self-balancing d-c bridge for accurate bolometric power measurements, J. Research NBS **59,** 101 (1957) RP2776.

[2] R. W. Beatty and A. C. Macpherson, Mismatch errors in microwave power measurements, Proc. IRE **41,** 1112 (1953).

[3] A. C. Macpherson and D. M. Kerns, A microwave microcalorimeter, Rev. Sci. Instr. **26,** 27 (1955).

[4] M. Sucher and H. J. Carlin, Broad-band calorimeters for the measurement of low and medium level microwave power. I. Analysis and design, IRE Trans. on Microw. Theory Tech. **6,** 188 (1958).

[5] A. V. James and L. O. Sweet, Broad-band calorimeters for the measurement of low and medium level microwave power. II. Construction and performance, IRE Trans. on Microw. Theory Tech. **6,** 195 (1958).

[6] W. M. Sharpless, A calorimeter for power measurements at millimeter wavelengths, IRE Trans. on Microw. Theory Tech. **2,** 45 (1954).

[7] H. J. Carlin and M. Sucher, Accuracy of bolometric power measurements, Proc. IRE **40,** 1042 (1952).

BOULDER, COLO. (Paper 63C1–9)

Selected Abstracts of Recent Publications by the National Bureau of Standards Staff

Interferometer for large surfaces, J. B. Saunders and F. L. Gross, *J. Research NBS* **62,** *137–139 (April 1959) RP2943.*

An interferometer is described that permits the testing of large areas, such as layout plates. The extension to large areas is obtained by causing a collimated beam of light to reflect from the specimen at a large angle of incidence. The resultant fringe pattern is a contour map of the surface relative to an arbitrarily chosen plane and the contour interval is a function of wavelength and angle of incidence.

Absolute light-scattering photometer: I. design and operation, D. McIntyre and G. C. Doderer, *J. Research NBS* **62,** *153–159 (April 1959) RP2946.*

A new light-scattering photometer has been designed and built for determining the absolute scattering from polymer solutions. The instrument is also capable of performing as a research instrument for making measurements at very low and very high angles, and at very low and very high intensities of scattered light. The instrument scans the angular scattering either manually or automatically while measuring continuously the ratio of the scattered light to the incident light.

Design and performance of a block-type osmometer, D. McIntyre, G. C. Doderer, and J. H. O'Mara, *J. Research NBS* **62,** *63–66 (Feb. 1959) RP2931.*

A block-type osmometer has been designed and constructed utilizing several new features which enhance the precision of the osmotic-pressure measurement and allow simpler manipulative techniques. The details of the construction as well as a discussion of the design and performance of this osmometer are included in the paper.

Infrared high-resolution grating spectrometer, E. K. Plyler and L. R. Blaine, *J. Research NBS* **62,** *7–9 (Jan. 1959) RP2922.*

An infrared grating spectrometer which can be used as a single- or double-pass instrument has been built and set in operation. The collimating mirror has a focal length of 235 centimeters and the instrument has the highest resolution from 1,600 to 3,500 cm^{-1}. In order to have flexibility in scanning the spectra at different speeds, a special drive mechanism has been built which is made of spur gears and worm gears. The speeds range from 2.5 to 200 minutes of time per degree of rotation. Examples of the spectra resolved by the instrument are given. Lines separated by 0.05 cm^{-1} are completely resolved and two lines separated by 0.025 cm^{-1} are partially resolved.

List of other Publications by the National Bureau of Standards Staff

Bureau Publication*

Selected bibliography on building construction and maintenance, E. R. Meggers, *BMS140 (3d edition) 30 cents.*

Non-Bureau Publications

Recent theoretical studies of the propagation of long waves, J. R. Wait, (Abstract) *Congres International sur la Propagation des Ondes Radi-Electriques, Liége (6–11 October 1958).*

An on-off temperature control for electrically heated filaments, R. E. Little and J. D. McKinley, Jr., *Rev. Sci. Instr.* **29,** *No. 12, 1143 (1958).*

A method for measuring the directivity of directional couplers, G. E. Schafer and R. W. Beatty, *IRE Trans. on Microwave Theory Tech.* **MTT–6,** *No. 4 (1958).*

Low-temperature microcell for infrared study of condensed gases, J. E. Stewart, *Anal. Chem.* **20,** *2073 (1958).*

Some properties of flameproof fabrics, M. W. Sandholzer, *Am. Dyestuff Reptr.* **48,** *No. 2, 37 (1959).*

The riometer—a device for the continuous measurement of ionospheric absorption, C. G. Little and H. Leinbach, *Proc. IRE* **47,** *315 (1959).*

The night airglow, F. E. Roach, *Proc. IRE* **47,** *267 (1959).*

A method for measuring the directivity of directional couplers, G. E. Schafer and R. W. Beatty, *IRE Trans. on Microwave Theory Tech.* **MIT–6,** *419 (1958).*

A modulator for microwave mixers, G. E. Schafer, *IRE Trans. on Microwave Theory Tech. (Letter)* **MIT–6,** *333 (1958).*

Cryogenic engineering, R. B. Scott (*D Van Nostrand Co., Inc., New York, N.Y., 1959).*

The day-to-day coordination of IGY observations, A. H. Shapley, *Proc. IRE* **47,** *323 (1959).*

Local standards laboratories, A. T. McPherson, *Instr. and Automation* **32,** *92 (1959).*

New standards for science and industry, A. T. McPherson, *Am. Soc. Quality Control (Fourth Annual Quality Control Symposium, Southern Methodist Univ., Dallas, Texas, Mar. 1959).*

*See also page 85.

Systematic research, A. V. Astin, *Ordnance* **43,** *No. 233, 741 (Mar.–Apr. 1959).*

Unscrambling of gamma-ray scintillation spectrometer pulse-height distributions, J. H. Hubbell and N. E. Schofield, *IRE Trans. Nuclear Sci.* **NS–5,** *No. 3, 156 (1958).*

The theory of extreme values, J. Mandel, *ASTM Bul. No. 236, 29 (1959).*

Charge-storage pulse-height analyzers for use with pulsed accelerators, L. Costrell and R. E. Brueckmann, *Nuclear Instr.* **3,** *350 (North-Holland Publishing Co., Amsterdam, 1958).*

Mechanical properties of high polymers, H. Leaderman, *Ann. Rev. Phys. Chem.* **9,** *(1958).*

Viscoelasticity phenomena in amorphous high polymeric systems, H. Leaderman, *Chapter I in Rheology; Theory and Application Vol. II (edited by F. R. Eirich, Academic Press, New York, N.Y., 1958).*

Microwave double-sweep method for analysis of time-dependent cavity characteristics, S. Ruthberg, *Rev. Sci. Instr.* **29,** *No. 11, 999 1958).*

RF voltmeter calibrating consoles, M. C. Selby, L. F. Behrent, and F. X. Ries, IRE *Convention Record* **6,** *Pt. 5, 251 (1958).*

The program of training and graduate instruction in dental materials at the National Bureau of Standards, W. T. Sweeney, *J. Dental Educ.* **22,** *217 (1958).*

Conductivity of plasmas to microwaves, P. H. Fang, *Phys. Rev.* **113,** *No. 1, 13 (1959).*

Strains in beams having diagonal cracks, D. Watstein and R. G. Mathey, *J. Am. Concrete Inst.* **30,** *No. 6, Title No. 55–46 (1958).*

False negative permanent strains observed with resistance wire strain gages, C. J. Newton, *ASTM Bul.* **235,** *42 (1959).*

Patents

(The following patents have recently been granted on NBS inventions and, except as noted, are assigned to the United States of America as represented by the Secretary of Commerce.)

No. 2,867,382. January 6, 1959. **Maneuvering loads accelerometer.** Preston R. Weaver (Navy).

No. 2,870,436. January 20, 1959. **Electronic analogue-to-digital converter.** Milton L. Kuder.

No. 2,871,042. January 27, 1959. **Supporting and heat insulating means.** Bascom W. Birmingham, Edmund H. Brown, Russell B. Scott, and Peter C. Vander Arend (AEC).

No. 2,871,351. January 27, 1959. **Balance detector used in electronic analogue-to-digital converter.** Milton L. Kuder.

No. 2,871,356. January 27, 1959. **Frequency-stabilized oscillator.** Peter G. Sulzer.

No. 2,871,432. January 27, 1959. **Automatic tracking proximity gage.** Louis A. Marzetta.

No. 2,871,669. February 3, 1959. **Radiation shield circulation system for large liquefied gas storage containers.** Douglas Mann and John Macinko (Navy).

No. 2,872,538. February 3, 1959. **Inertia arming switch.** William B. McLean (Navy).

No. 2,872,867. February 10, 1959. **Ordnance construction.** Robert D. Huntoon (Navy).

No. 2,877,452. March 10, 1959. **Telemetering transmitter for a projectile.** Allen V. Astin (Navy).

No. 2,879,001. March 24, 1959. **High-speed binary adder having simultaneous carry generation.** Arnold Weinberger and John L. Smith.

No. 2,879,409. March 24, 1959. **Diode amplifier.** Arthur W. Holt.

No. 2,879,455. March 24, 1959. **Miniature radar subassembly.** Robert K–F Seal (Navy).

No. 2,879,657. March 31, 1959. **Combination locks.** Robert L. Eichberg.

No. 2,880,378. March 31, 1959. **Shaped processed circuitry.** Clinton O. Lindseth (Navy).

Section A. Physics and Chemistry, Volume 63A, No. 1, July-August 1959. ***Approximate issue date, August 3, 1959.***

Description and analysis of the first spectrum of iodine. C. C. Kiess and C. H. Corliss.

CH in the solar spectrum. Charlotte E. Moore and Herbert P. Broida.

Infrared studies in the 1- to 15-micron region to 30,000 atmospheres. C. E. Weir, E. R. Lippincott, A. Van Valkenburg, and E. N. Bunting.

Phosphinoborine compounds: mass spectra and pyrolysis. Leo A. Wall, Sidney Straus, Roland E. Florin, Fred L. Mohler, and Paul Bradt.

Experimental and theoretical study of kinetics of bulk crystallization in poly (chlorotrifluoroethylene). John D. Hoffman, James J. Weeks, and W. M. Murphey.

Section B. Mathematics and Mathematical Physics, Volume 63B, No. 1, July-September 1959. ***Approximate issue date, September 8, 1959.***

Relations between summation methods and integral transformations. Werner Greub.

Uniform asymptotic expansions for Weber parabolic functions of large orders. F. W. J. Olver.

On a modification of Watson's lemma. F. Oberhettinger.

Principal submatrices of a full-rowed non-negative matrix. K. Goldberg.

Zeros of certain polynomials. A. J. Goldman.

Tables of transport integrals: A supplement. William M. Rogers, William J. Hall, and Robert L. Powell.

Lens design: A new approach. Orestes N. Stavroudis.

Analytical integration of the differential equation for water storage. Vujica M. Yevdjevich.

Compressible turbulent boundary layers with heat transfer and pressure gradient in flow direction. Alfred Walz.

Section D. Radio Propagation, Volume 63D, July-August 1959. ***Approximate issue date, July 13, 1959.***

Preliminary results of the National Bureau of Standards radio and ionospheric observations during the International Geophysical Year. David M. Gates.

Origin of [0I] 5577 in the airglow and the aurora. Franklin E. Roach, James W. McCaulley, and Edward Marovich.

Comparison of absolute intensities of [0I] 5577 in the auroral and subauroral zones. F. E. Roach, J. W. McCaulley, and C. M. Purdy.

Origin of "very low-frequency emissions." R. M. Gallet and R. A. Helliwell.

Climatology of ground-based radio ducts. Bradford R. Bean.

Power requirements and choice of an optimum frequency for a worldwide standard-frequency broadcasting station. A. D. Watt and R. W. Plush.

Measurements of phase stability over a low-level tropospheric path. M. C. Thompson, Jr. and H. B. Janes.

System loss in radio wave propagation. Kenneth A. Norton.

Mode expansion in the low-frequency range for propagation through a curved stratified atmosphere. H. Bremmer.

Transmission and reflection by a parallel wire grid. Martin T. Decker.

Synoptic variation of the radio refractive index. B. R. Bean and L. P. Riggs.

Low-frequency propagation paths in arctic areas. A. D. Watt, E. L. Maxwell, and E. H. Whelan.

UNITED STATES
GOVERNMENT PRINTING OFFICE
DIVISION OF PUBLIC DOCUMENTS
WASHINGTON 25, D.C.

OFFICIAL BUSINESS

PENALTY FOR PRIVATE USE TO AVOID PAYMENT OF POSTAGE, $300 (GPO)

National Bureau of Standards, Journal of Research
C. Engineering and Instrumentation

Vol. 63C, No. 1

July–September 1959

Contents

	Page
Creep of cold-drawn nickel. William D. Jenkins and Carl R. Johnson.	1
Friction and endurance of prelubricated and unlubricated ball bearings at high speeds and extreme temperatures. Hobart S. White.	19
Effect of light and water on the degradation of asphalt. L. R. Kleinschmidt and H. R. Snoke.	31
Current and potential relations for the cathodic protection of steel in a high resistivity environment. W. J. Schwerdtfeger.	37
A tilting air-lubricated piston gage for pressures below one-half inch of mercury. U. O. Hutton.	47
Compact multi-anvil wedge-type high pressure apparatus. E. C. Lloyd, U. O. Hutton, and D. P. Johnson.	59
A coulometric-titration coulometer. Stanley W. Smith and John K. Taylor.	65
Electron beam magnetometer. L. Marton, Lewis B. Leder, J. W. Coleman, and D. C. Schubert.	69
A refined X-band microwave microcalorimeter. Glenn F. Engen.	77
Selected abstracts and other recent publications by National Bureau of Standards staff.	83

For sale by the Superintendent of Documents, U.S. Government Printing Office, Washington 25, D.C. Price 75 cents (single copy)
Subscription price: $2.25 a year; 50 cents additional for foreign mailing.

UNITED STATES GOVERNMENT PRINTING OFFICE, WASHINGTON : 1959